

Flexible and Printed Electronics



TOPICAL REVIEW

Review of digital printing technologies for electronic materials

OPEN ACCESS

RECEIVED
13 February 2020

REVISED
26 June 2020

ACCEPTED FOR PUBLICATION
9 November 2020

PUBLISHED
15 December 2020

Original content from this work may be used under the terms of the [Creative Commons Attribution 4.0 licence](https://creativecommons.org/licenses/by/4.0/).

Any further distribution of this work must maintain attribution to the author(s) and the title of the work, journal citation and DOI.



Kye-Si Kwon^{1,2} , Md Khalilur Rahman^{2,3}, Thanh Huy Phung¹, Stephen D Hoath⁴, Sunho Jeong⁵ and Jang Sub Kim⁶

¹ Department of Mechanical Engineering, Soonchunhyang University, 22, Soonchunhyang-ro, Asan city, Chungnam 31538, Republic of Korea

² Department of Electronic Materials and Devices Engineering, Soonchunhyang University, 22, Soonchunhyang-ro, Asan city, Chungnam 31538, Republic of Korea

³ Department of Physics, Comilla University, Cumilla 3506, Bangladesh

⁴ Emeritus Fellow, Wolfson College, Cambridge, United Kingdom

⁵ Department of Advanced Materials Engineering for Information and Electronics, Kyung Hee University, 1732 Deogyong-daero, Giheung-gu, Yongin-si, Gyeonggi-do 17104, Republic of Korea

⁶ School of Electronics and Electrical Engineering, DanKook University, Yongin, 16890, Republic of Korea

E-mail: kswon@sch.ac.kr

Keywords: inkjet printing technology, inkjet print-head, printing method, jet dispenser, display applications, conductive ink, printed electronics

Abstract

Direct printing methods have been used as manufacturing tools for printed electronics applications due to their cost effectiveness. In this review, the piezo-driven inkjet is discussed in detail since it is a mature technology and suitable for the production printing of printed electronics. In addition, other printing methods are considered for using higher viscosity ink and for producing smaller printed feature size. Various direct printing methods are compared in terms of jet mechanism, printing algorithm, and their applications. In particular high resolution printing methods using high viscosity inks, such as electrohydrodynamic jet, aerosol jet and micro-plotter are reviewed. To understand the recent status of industrial printing applications, display (liquid crystal display and organic light emitting diode) materials and printing issues are discussed. Finally, a brief overview of nano-particle metal based conductive inks is included because these inks have been widely used for printed electronics applications.

1. Introduction

Digital printing technologies use bitmap images or computer-generated patterns to deposit ink onto target substrates, and digital printing has been widely used for decades for printing graphics and documents. The recent developments in printing technologies are mainly related to production printing through the implementation of low cost, fast (high frequency jetting) and high-resolution methods. Along with recent advances, there has been a lot of effort to use digital printing for direct deposition of functional materials. Direct printing technologies can have advantages over conventional photolithographic manufacturing processes, since the associated manufacturing costs can be significantly reduced due to its additive manufacturing features [1–3]. Even though the same printing technology could be used for different purposes, the requirements are quite different in terms of print-heads, inks and printing algorithms

for use in different applications. In this review, we will assess the nozzle-based printing technologies for printed electronics applications. Throughout this paper, five key printing components will be discussed, including: (a) dispensing head, (b) printing equipment, (c) substrate, (d) pre (post) process and (e) functional ink.

Among various printing technologies, the inkjet printing method has been a main interest to industry because it can easily be scaled up for mass production [2]. The inkjet print-head has high throughput capability [4] because thousands of high-density nozzles designed into modern print-heads that can be used for printing. The number of nozzles used for printing can be increased further by the array layout of inkjet print-heads. High throughput features of inkjet technology were developed for graphics printing first. These features are now being adapted for printed electronics applications. So, it is worthwhile to review recent advances in inkjet printing technologies for

graphics printing and also discuss any additional or different features of inkjet technologies required for printed electronics applications. In section 2, we will review recent inkjet printing technologies from hardware component and process point of view.

In order to use inkjet technology as a manufacturing tool, the ink should be continuously supplied to the print-head. For this purpose, recent inkjet print-head systems for industrial purposes have an automatic ink supply system with ink level sensors. In addition, recent print-heads have capabilities of continuous ink circulation through the print-head manifold. By using an ink circulation system, jet reliability could be increased significantly by removing air bubbles and increasing ink suspension stability. Recent development of ink supply systems for industrial purposes are discussed in section 2.2.

In most printed electronics applications, the accuracy requirement for drop placement tends to be higher than in graphics printing [5]. Droplet placement could deviate from the target position due to various causes, including the hardware alignment and jet directionality [6–8]. As the production printing speed and jetting frequency increase, additional printing accuracy issues arise [9–11]. High speed printing usually requires high frequency jetting. A recent print-head development trend is to maximize jet printing capabilities beyond 40 kHz, though jetting performance tends to depend significantly on jetting frequency. To increase printing uniformity without respect to jetting frequency, waveform design methods have been proposed [5] to suppress residual pressure waves inside the print-head, as discussed in section 2.3. In addition, it should be noted that high printing speed could result in deviation of drop placement unless the relative movement of print-head with respect to substrate is considered. Air flow between print-head and substrate could also cause non-straight jetting and smaller ink droplets such as ‘satellites’ could fly away rather than deposit on the substrate. In addition, inkjet print-head nozzle plates can sometimes be wetted due to unsteady motion of satellites [12]. There have been efforts to investigate how air flow affects jet directionality, as discussed in section 2.7.

Proper jetting performance from the inkjet print-head is the critical and first step for inkjet printing implementation. In order to obtain proper jetting from the inkjet print-head, the functional material (ink) should have specific properties [13]. To ensure a reliable inkjet process, the jetting conditions should be optimized. Vision measurement methods have been commonly used in order to evaluate the jetting performance [10]. Recently, there have been efforts to standardize the vision measurement methods [14] and the current status is discussed in section 2.4.

There has been increasing concern regarding jetting reliability of print-heads having many nozzles [15]. To ensure reliable printing process, there have

been demands for jetting status monitoring of all nozzles. Pre-determined patterns can be printed for vision inspection and identification of missing dots due to misfiring nozzles. However, these earlier methods were not based on real-time monitoring. Recently, real-time monitoring methods based on piezo self-sensing have been developed and a recent study showed that inkjet print-heads with more than 1000 nozzles can be monitored within a few seconds [16], which could potentially increase the reliability of the inkjet printing process for mass production. Inkjet jetting monitoring issues are discussed in section 2.5.

In some printed electronics applications, printing of fine patterns with a characteristic feature size of a few micrometers is required, which is beyond capability of conventional piezo inkjet print-heads [17]. For example, display electronics often requires conductive patterns with width of less than 5 μm , which are invisible to the human naked eye. However, in practice, printed dot sizes less than 30 μm are difficult to achieve using conventional inkjet printing without proper surface treatment of a substrate [18]. In addition, recent applications require the deposition of high viscosity material for better functionality [19]. The use of ink with higher viscosity is recommended since more solid contents remain even after solvent evaporation. The additional advantages of using higher viscosity inks are that the printed patterns are less affected by the substrate conditions. As alternative methods for inkjet printing, we discuss other types of dispensing methods in section 3, including different types of dispenser for high viscosity ink, aerosol jet printing (AJP), microplot printing, and electrohydrodynamic (EHD) jetting. For proper use of printing methods for specific applications, it is important to understand the advantages and limitation of each method. Our review study aims at increasing the understanding of the current status of printing methods so that researchers as well as printing process developers can select proper printing methods for their specific application.

The printing software for printed electronics manufacture is discussed in section 4. In graphics applications, the raster image processor (RIP) has been used to generate printing information based on the half-tone algorithm. In this way, the color and grayscale image can be converted to a binary image for printing. However, the half-tone algorithms are not intended for line connection or area coating of electronics materials. Most graphics printing algorithms are intended to produce scattered dots for better human eye perception. However, in most printed electronics applications, exact dimensions and precise droplet placement on the target location are critical requirements [20]. In order to meet these requirements, computer aided design (CAD) tools are commonly used to design patterns. The additional advantage of using CAD information is that

the layer information in CAD software can be effectively used when patterns of different materials need to be assigned to each layer. The CAD designed patterns can be effectively converted into bitmap images, which has desired dimension information. The designed dimensions in the bitmap images could be defined by the physical dimension of one pixel in the printed image. Alternatively, instead of using bitmap images, vector information from CAD can often be used in case of single nozzle head systems such as EHD and other dispensing systems.

The primary differences between printed electronics and graphics are in the printing materials used: functional ink and substrate [21]. It is beyond the scope of this work to review all kinds of functional inks and substrates as this review is mainly focused on the digital printing methods, including dispensing heads and printing equipment, in relation to functional ink properties. For functional inks and their applications, two examples are given in this review study: metal inks and functional inks for display devices. In section 5, the recent progress of inkjet printing technologies for the display application is discussed. In section 6, the status of conductive ink development is overviewed.

2. Inkjet printing technology for printed electronics

2.1. Development of inkjet print-heads

Inkjet printing is a mature technology in the field of graphics and marking applications. Low-cost inkjet printers are readily available in the market for home and office uses. Recently, inkjet technology has attracted closer attention from a variety of fields because of the advantages of deposition of exact amounts of functional material on the required place. It is a type of additive manufacturing method, which can reduce production costs by using directly printed computer-generated patterns instead of physical pattern masks.

It is well-known that continuous inkjet (CIJ) and drop-on-demand inkjet (DOD inkjet) are two main types of inkjet printing [2]. Although using CIJ has been considered for printed electronics applications [22], most of its applications are still limited to conventional applications such as marking on commercial products. Most printed electronics applications are based on DOD inkjet. Thermal and piezo inkjet print-head technologies have both been commonly used for DOD printing. For printed electronics applications, piezo-driven inkjet printing (lead zirconate titanate (PZT) inkjet) has been the more widely used technology because it can print various solvent based inks [23].

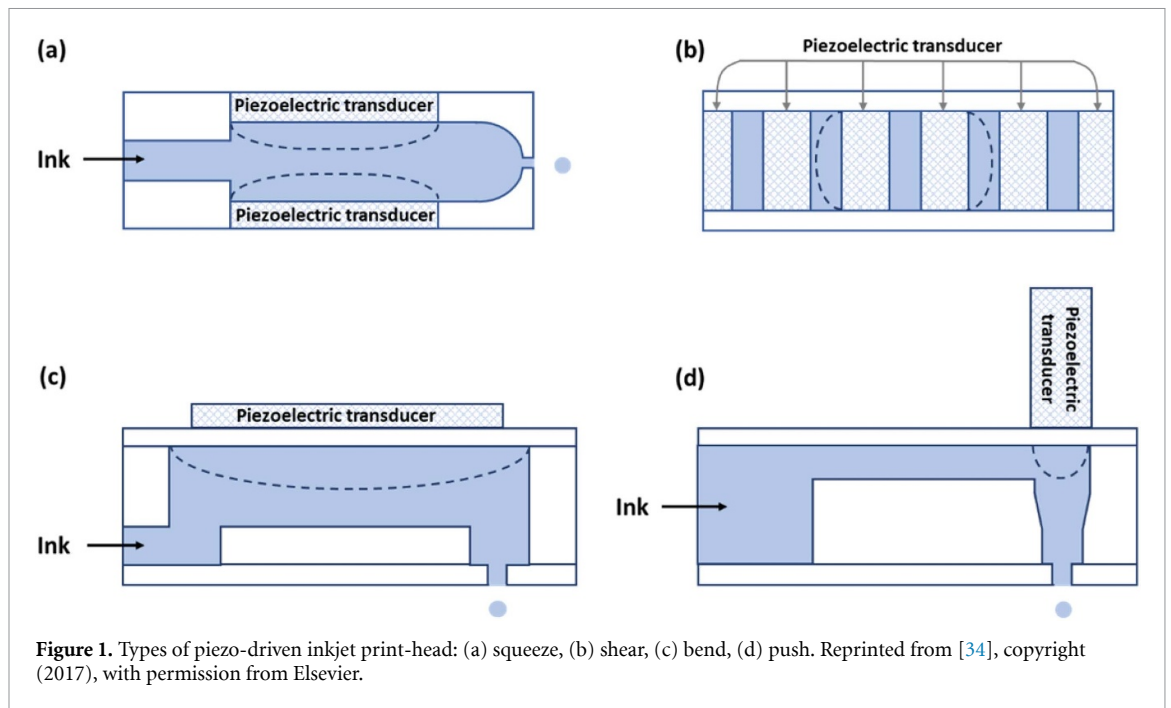
Figure 1 illustrates several types of PZT inkjet print-head. The piezo-driven type inkjet print-head designs differ according to manufacturer in order to meet specific feature requirements. Recent inkjet

Table 1. Recent available inkjet print-heads.

Typical commercially available print-head from different maker	Features
<i>Konica Minolta</i> (Konica KM1024)	<ul style="list-style-type: none"> • Maximum jetting frequency: 45 kHz, with built-in heater. • Print width: 72 mm. • Drop volume: 13 pl. • Resolution: 360 dpi (Single pass printing). • Number of nozzles: 1024 [29].
<i>Fujifilm Dimatix</i> (Starfire SG1024)	<ul style="list-style-type: none"> • Maximum jetting frequency: 30 kHz. • Print width: 64.96 mm. • Droplet volume: 12–33 pl. (Nominal) • Resolution: 400dpi (Single pass printing) • Number of nozzles: 1024 [30].
<i>Trident</i> (Trident 256JET, 768JET, 384 JET) <i>Kyocera</i> (Kyocera KJ4B-1200)	Custom design print-head Repairable parts [31] <ul style="list-style-type: none"> • Maximum jetting frequency: 64 kHz. • Print width: 112.44 mm Drop volume: 1.5–5 pl • Resolution: 1200 × 1200 dpi (single pass) • Number of nozzles: 5312 [32].
<i>Xaar</i> (Xaar 5601)	<ul style="list-style-type: none"> • Maximum frequency: 100 kHz. • Print width: 116 mm. • Drop volume: 3–21 pl. • Resolution: 1220 dpi. (single pass) • Number of nozzles: 5680 [33].

print-heads have high density nozzles (more than 1024), which are capable of single pass printing with high resolution of 1200 dot per inch (dpi) [24, 25] at jetting frequency of 40 kHz and greater. The droplet volume produced by some inkjet print-heads can be adjusted from 1 pl to 80 pl [26, 27]. Table 1 shows typical recent inkjet print-heads commercially available and their features. To increase nozzle density, recent print-heads are often made by MEMS technology using thin film actuators [27, 28].

Some print-heads are equipped with a heater for use with thermal phase-change materials with relatively high viscosities at room temperature [26]. Note that the viscosity of most inks can be reduced by increasing the ink temperature [20]. Moreover, a nozzle (print-head) heater can be useful in stabilizing the ink properties in the presence of changing ambient conditions.



Prototyping (printing) for research and development (R&D) purposes should always be carried out for establishing the feasibility of inkjet implementation. As inkjet applications diversify, new functional materials should be tested for jetting. Since electronic materials are expensive, the early stage of ink development requires frequent jetting evaluation and printing tests using a minimum amount of ink prior to using the ink in large quantity for commercial inkjet print-heads. For this R&D purpose, inkjet print-heads with single or a few nozzles are commonly used as shown in table 2. Their range of jettable ink properties is comparable to those handled by most recent commercialized inkjet print-heads and by using them the functional ink can be verified for scaling up for mass production.

The single-nozzle inkjet print-head from Micro-fab has a squeeze type PZT nozzle, which combines a glass capillary tube and a cylindrical piezo actuator. Due to the glass nozzle tip, the meniscus motion and ink sedimentation can be monitored [35–37] as shown in figure 2, which is a useful feature for ink and process development. Note that the squeeze type single nozzle print-head has stronger jetting force than that of the commercially available multi-nozzle inkjet print-head. As a result, a wider range of ink can be jetted (ink with viscosity less than 20 mPas and surface tension range of 20–70 mN m⁻¹) while most commercial inkjet heads have a narrower jettable range of 10–12 mPas and surface tension of 20–40 mN m⁻¹ [38]. Note that inks that are jettable in the squeeze type inkjet print-head does not always have good jetting characteristics in commercial multi-nozzle inkjet print-heads.

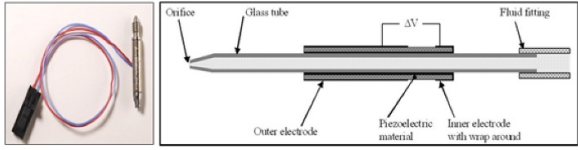
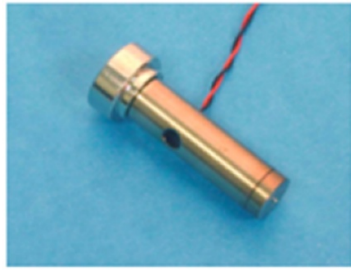
2.2. Ink supply system for inkjet print-head

In inkjet printing systems, a means to supply ink to the print-head is required. The simplest ink supply systems use bottles or syringe barrels to hold the ink, where regulated air pressure is often used to manipulate ink supply and maintain proper pressure for the print-head.

In production systems, ink should be continuously supplied to the print-head without running out of ink during the inkjet process. Moreover, in printed electronics applications, many inks include particles, which may result in frequent problems of nozzle blocking due to sedimentation and conglomeration. In order to solve these issues, ink recirculation systems are often used in industry. Figure 3 shows a simple recirculation system equipped with ink level sensors to maintain the ink supply to the print-head [16]. For the re-circulation and continuous ink supply to the head, more than two reservoirs are commonly used, which are indicated as R1 and R2 in figure 3(a). Note that there should be negative pressure applied in the reservoir (R1), which is connected to the inkjet print-head, to hold the meniscus without dripping ink from the nozzle. The circulation system could be extended to the case of more than one inkjet print-head as shown in figure 3(b) [39].

An ink supply system with re-circulation capability has the added advantages of increasing jet reliability due to its self-maintaining characteristics. For example, one of the most commonly occurring jet failures is due to particulate ink drying at the inkjet nozzle. Researchers have shown that inkjet drop speed depends significantly on non-jetting time, especially if the amount of circulated ink is small [40, 41]. As shown in figure 4, if the non-jetting time increases,

Table 2. Inkjet print-heads for research purposes.

Maker	Research purpose print-heads	Features
Microfab	<ul style="list-style-type: none"> • Print-Head for low temperature purpose  <ul style="list-style-type: none"> • Print-Head for high temperature purpose  <p>(source: www.microfab.com)</p>	<p>Single squeeze type inkjet nozzle. Transparent nozzle with monitoring capability of nozzle tip. High temperature capability, up to 240 °C for liquid metal (adhesives, waxes, polymers and liquid metals)</p>
Fujifilm Dimatix	 <p>(source: www.fujifilmusa.com/)</p>	<p>Sixteen nozzles with DPN (drive per nozzle) capabilities Minimize material waste (1.5 ml) Disposable print-head</p>

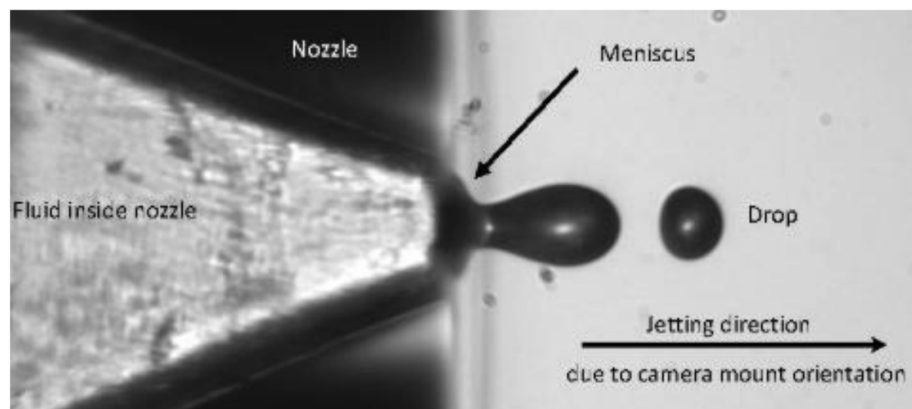


Figure 2. Meniscus and drop ejection process monitoring. Reproduced from [35] with permission of IS&T: the Society for Imaging Science and Technology sole copyright owners of Printing for Fabrication 2016 (NIP32) 32nd International Conference on Digital Printing Technology.

the jetting speed reduces. In worst cases, the nozzle may become blocked. However, when the recirculation is working, the advection of concentrated ink near the nozzle tip to the circulation path reduces the high concentration at the nozzle, which can avoid serious blockage.

A further advantage of using a re-circulation system is its effectiveness in removing air bubbles entrapped in the inkjet manifold, which potentially

cause jetting failure [26]. In addition to recirculation, a pulsed voltage to the piezo actuator can be used to agitate the highly concentrated ink near the DOD inkjet nozzle in order to increase jet reliability [41].

In most inkjet re-circulation systems, ink recirculates through inkjet print-head manifolds. However, there can be different designs, in which the ink circulates through the actuator channels near the

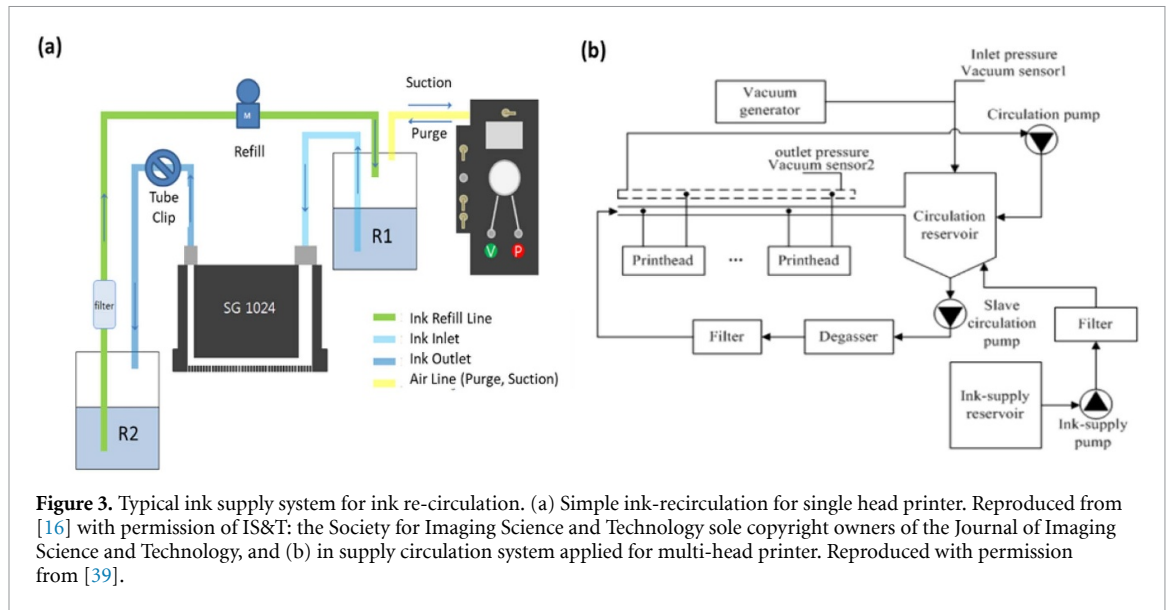


Figure 3. Typical ink supply system for ink re-circulation. (a) Simple ink-recirculation for single head printer. Reproduced from [16] with permission of IS&T: the Society for Imaging Science and Technology sole copyright owners of the Journal of Imaging Science and Technology, and (b) in supply circulation system applied for multi-head printer. Reproduced with permission from [39].

nozzles, which can be effective to increase reliability by removing air bubbles and debris near the nozzle, as shown by the ink flow direction in figure 5(b). There have been reports that ink re-circulation is not only effective for preventing jet failures but also effective for recovering the jetting status of individual nozzles in presence of jet failures [42].

2.3. Driver and driving waveform for inkjet print-head

2.3.1. Driver electronics

Once ink is supplied to the inkjet print-head nozzles, driving voltage shapes (a *waveform*) should be applied to the piezo actuators to stimulate pressure waves to produce jetting. For this purpose, electronic drivers are required to control jetting by applying proper driving voltage to each nozzle. There are two types of inkjet print-head drivers: (a) drive per nozzle (DPN); (b) shared driver. DPN type drivers can apply driving voltage independently to each nozzle: it is effective to equalize the jetting performance from all the nozzles by adjusting each driving voltage. However, the cost for the driver could be high and it may take considerable time to adjust all driving voltages for each nozzle. The shared driver has been more commonly used in industry because of its cost effectiveness. Here, a single driver is used for driving groups of nozzles, say 128 or 256 nozzles, and on-off control of each driving voltage will be controlled by on-off switches [44].

The requirement for the inkjet print-head layout and the number of inkjet print-heads can differ according to the application. The firmware for the driver and the software are often customized. To meet specific customer requirements, third party inkjet print-head drivers (GIS, METEOR, DPS, AMICA, etc) are often used [45, 46]. There are also several system integrators, who use commercially available inkjet print-heads and 3rd party drivers to

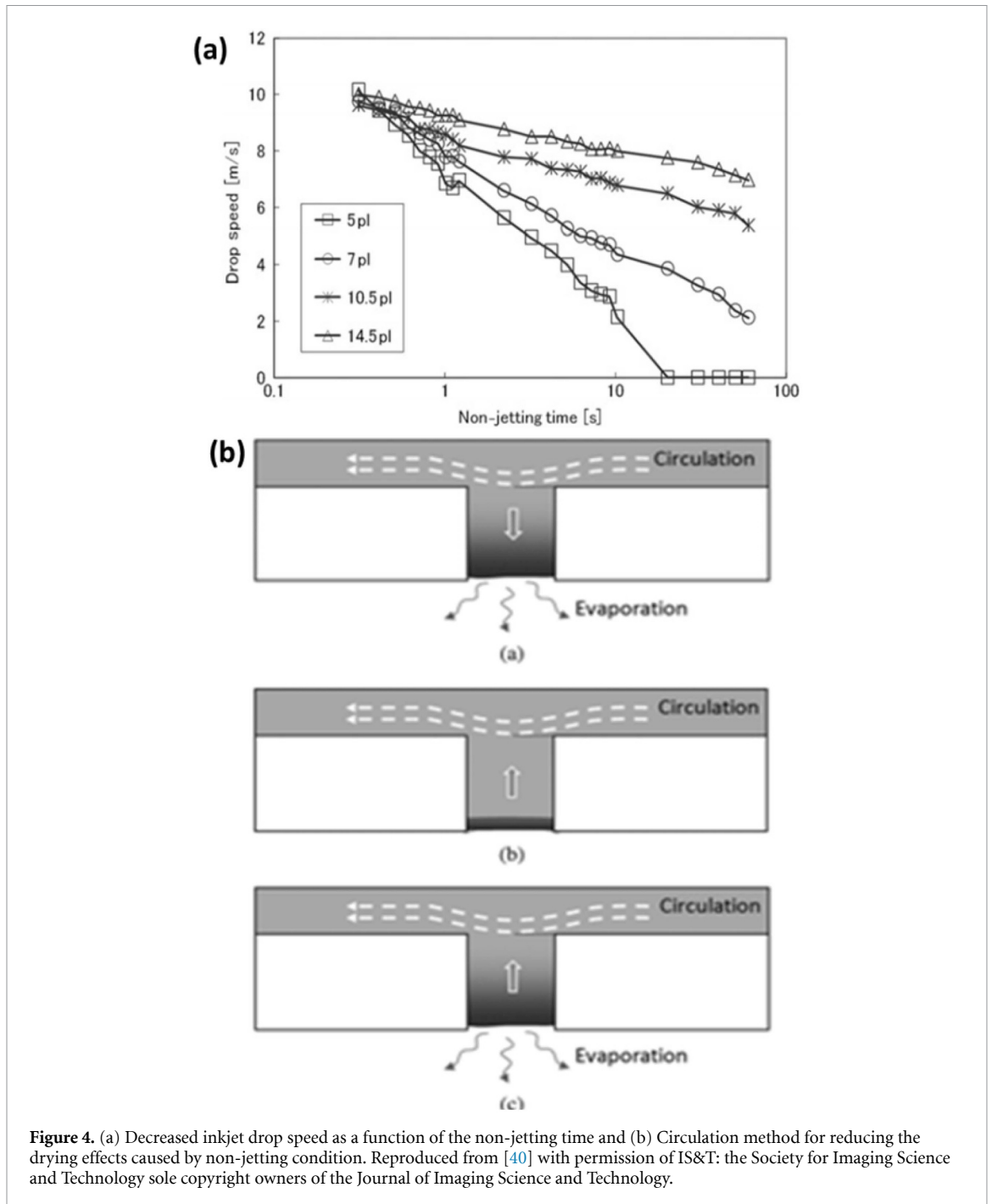
build printing machines for a specific purpose (for example, Unijet, Gosan Tech, STI, SMES, Kateeva, Shibaura etc)

2.3.2. Driving waveform voltage for enhancing jetting performance

The waveform voltage needs to be designed properly to produce desired droplet jetting from a piezo inkjet print-head. Visualized jet images are commonly used for the design of the driving waveform [13]. Figure 6 shows the basic waveform with four control parameters: rising time, falling time, dwell time and voltage amplitude. In general, rising and falling time are usually set to fixed values considering the driver slew rate and driving current specifications. In most commercialized inkjet print-heads, rising and falling times of $2 \mu\text{s}$ and $3 \mu\text{s}$ are used. Therefore, in order to control jetting performance, the dwell time and voltage amplitude are commonly used [13, 47]. The dwell time is determined to maximize the pressure wave inside of the print-head for efficient jetting. In other words, the dwell time should be adjusted to maximize the jetting speed of the droplets. For this purpose, the jetting speed plot with respect to dwell time is commonly used [48].

Alternatively, empirical methods could be used to select the optimal dwell time by comparing a series of jetting images, taken at the same time after a jet trigger, obtained by varying the dwell times. For example, in the case of the experimental results shown in figure 7, the dwell time of $5 \mu\text{s}$ was found to maximize the jetting speed. Here, the lowest droplet position indicates the fastest jetting speed.

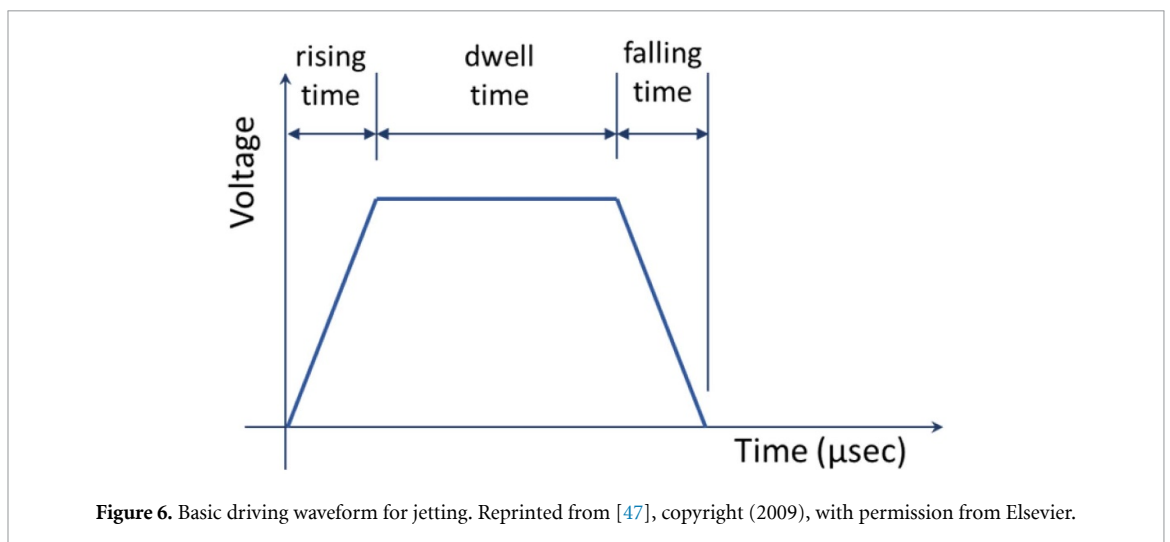
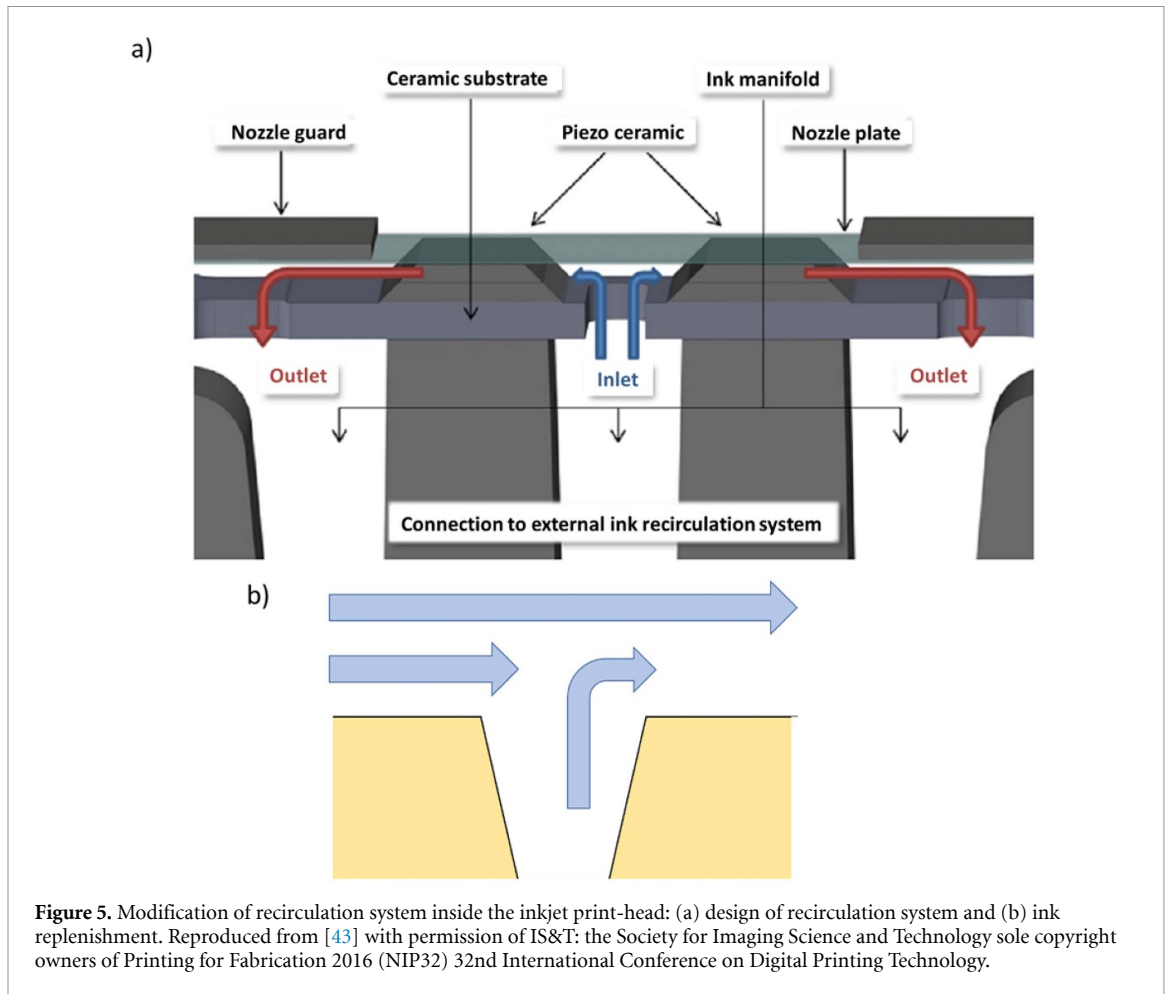
After selecting the optimal dwell time, the magnitude of the jetting voltage is adjusted to obtain the target droplet speed and volume. Furthermore, the driving voltage for each nozzle could be adjusted to obtain equalize the droplet volume from all nozzles



as depicted in figure 8. For this purpose, the DPN method could be used as the inkjet print-head driving method [48].

After jetting, a residual pressure wave from this drive waveform design remains for a while, which could result in frequency dependent jetting characteristics [10, 49]. As shown in figure 9, even though the same voltage waveform was applied, the jetting speed and drop formation can be affected at higher jet frequencies. Recent applications require faster printing speeds based on high frequency jetting. To ensure printing uniformity, the residual pressure waves should be damped out immediately prior to

consecutive jetting. For this purpose, the use of an additional cancel pulse voltage closely following the basic jetting waveform has been used in order to suppress the residual pressure waves [42, 49]. Figure 10 compares the pressure wave behaviors from two different waveforms: a basic trapezoidal waveform (figure 10(a)), and a waveform with a cancel pulse (figure 10(b)). With a suitable cancel pulse voltage, jetting performance could be made more uniform irrespective of jetting frequency as shown in figure 10(c). For the effective design of waveforms with cancel pulses, the use of the piezo self-sensing method has been proposed [49].



2.3.3. Grayscale printing

Most inkjet print-heads use binary images for printing information, though recently designed print-heads are capable of grayscale printing by depositing different droplet volumes on target locations. For grayscale printing, the number of droplets on the target location are controlled (mainly by firmware in the print-head) to produce different amounts

of ink as shown in figure 11. In the case of printed electronics, this could be a useful function [50–52] because the amount of jetted ink can be varied at specific locations. However, the maximum allowable jetting frequency could be reduced accordingly, since longer durations of waveform (or series of waveforms) may be needed to produce bigger droplets, as shown in figure 11.

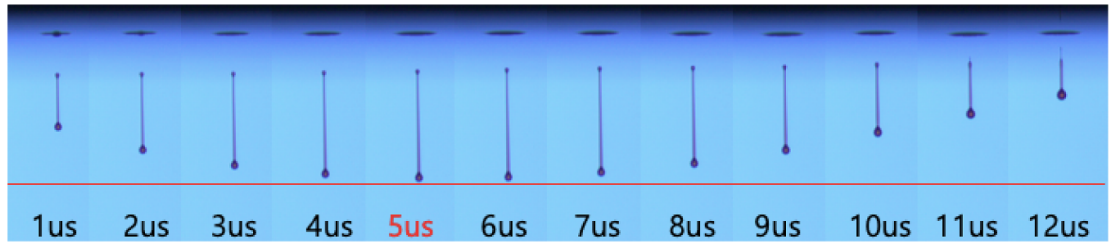


Figure 7. Jetting speed changes according to the chosen dwell time. This figure was adapted from authors' own work.

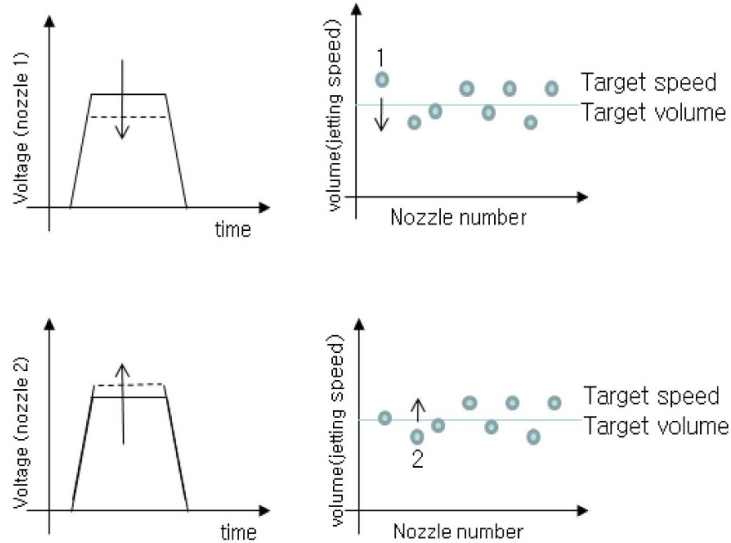


Figure 8. Voltage adjusting method for uniform jetting across inkjet print-head nozzles. Reprinted from [48] John Wiley & Sons. (Wiley-VCH Verlag GmbH & Co. KGaA 2012).

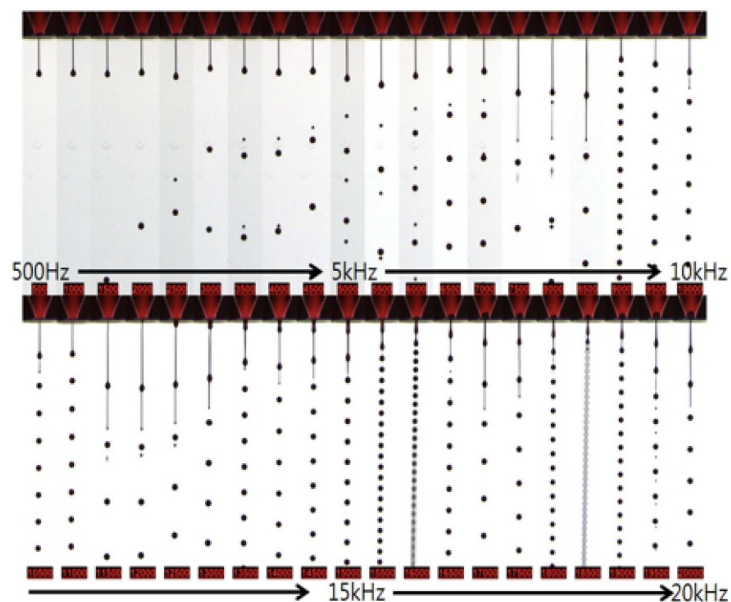
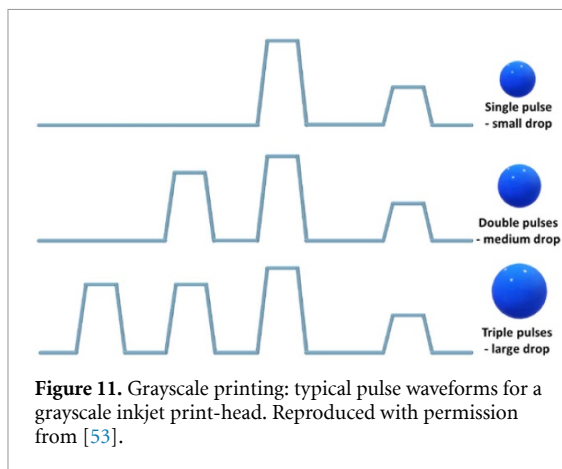
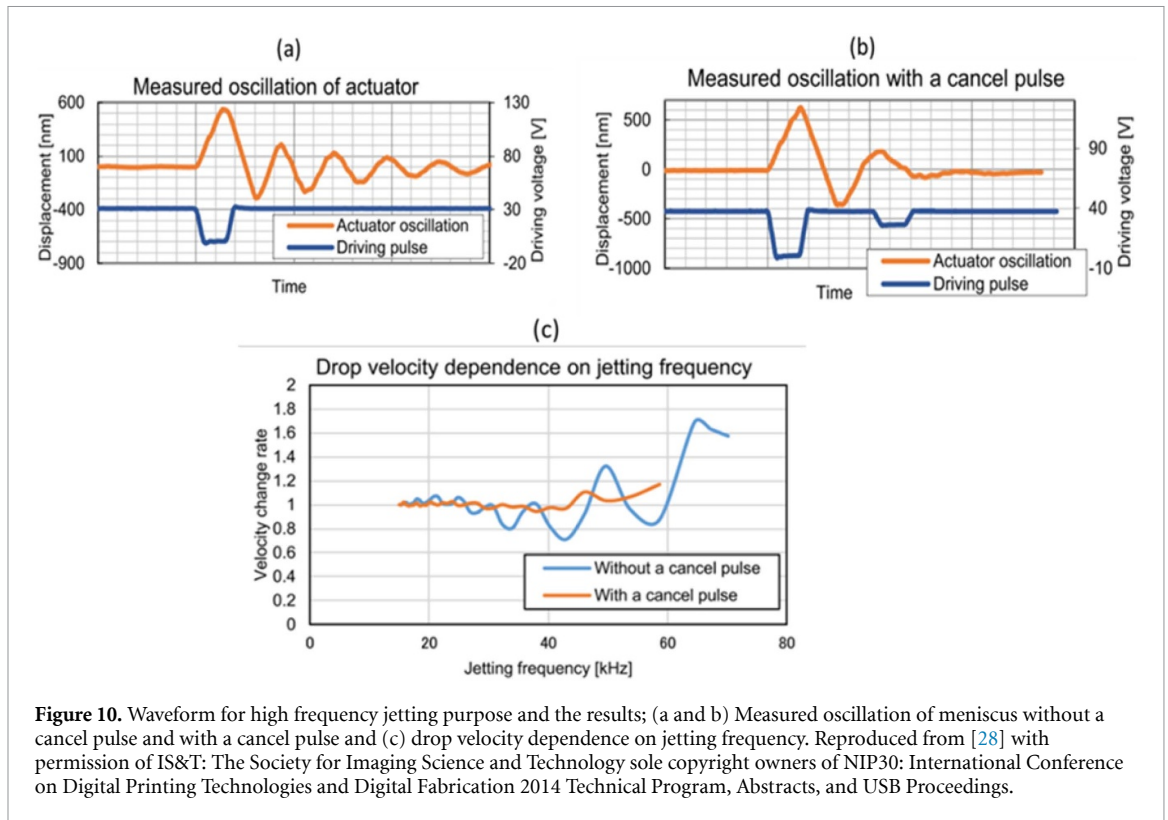


Figure 9. Jetting behavior with respect to jetting frequency. Reprinted from [10] with the permission of AIP Publishing.

2.4. Standardization of drop visualization for inkjet printing

To evaluate and optimize the jetting performance of inkjet print-heads, drop visualization methods

have been used widely. For this purpose, the drop visualization system based on strobe light emitting diodes (LEDs) has often been used, as shown in figure 12. From the visualized images, the drop



jetting speed and droplet volume are commonly measured [14].

Projects on standardization of drop visualization by the International Electrotechnical Commission (IEC) have recently provided a traceable methodology for inkjet printing equipment used in printed and flexible electronics. The published IEC standards gain ISO status after ratification. The first of these IEC standards cover measurement of drop speed [14] (IEC 62 899–302-1), droplet volume [54] (IEC 62 899–302-2) and that on jetted drop direction is nearing completion [55] (IEC 62 899–302-3). Another standard, on the measurement of inkjet-printed drop position accuracy, is at the new project stage [56] (IEC-4).

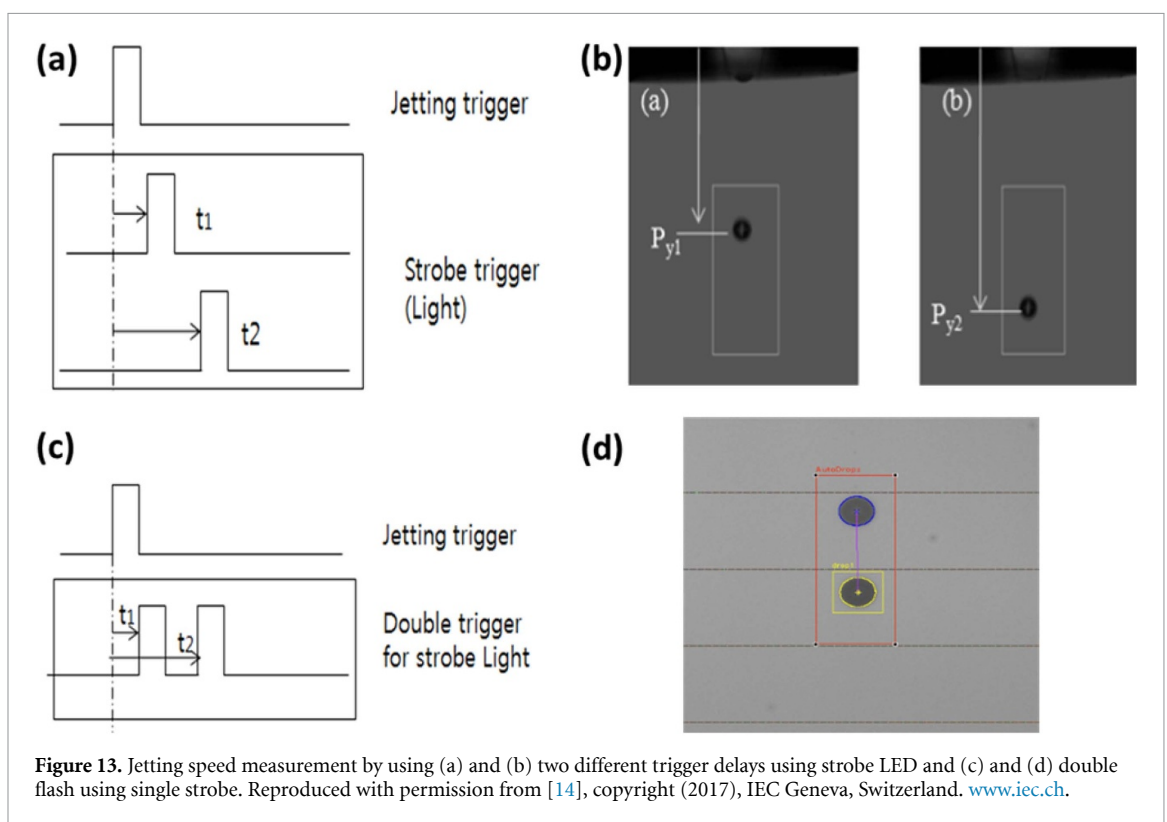
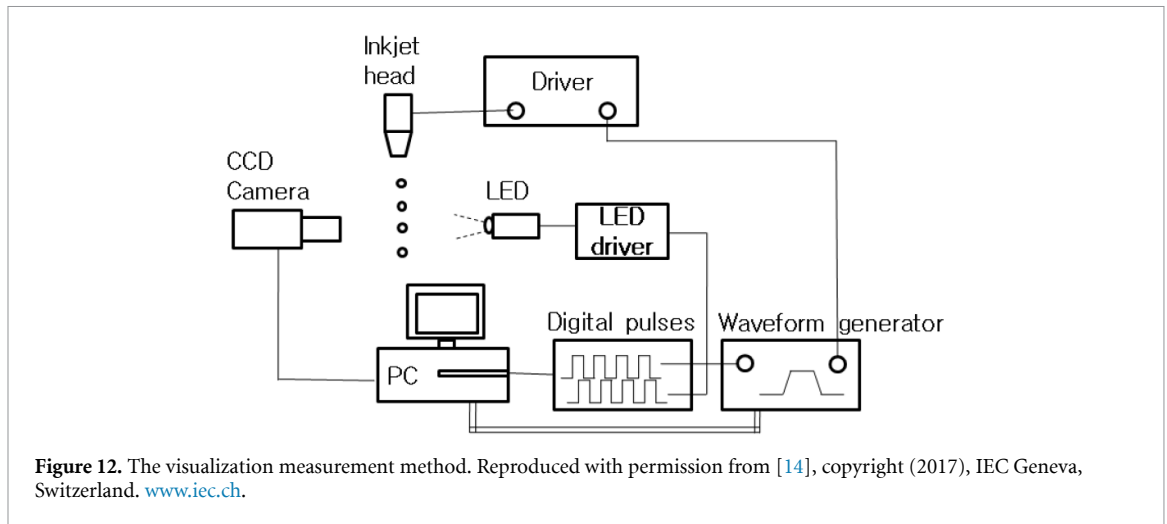
The first published standard [14] deals with drop jetting speed, and various drop watcher flash techniques are presented such as single flash, double flash and strobe flash, as shown in figure 13.

The standard for drop speed presents several methods for measuring the jetting speed. The most commonly used method for measuring the jetting speed can be calculated by the travel distance of a droplet during the two times of interest [14] as:

$$V = \frac{\sqrt{(Py2 - Py1)^2 + (Px2 - Px1)^2}}{t2 - t1},$$

where P_x , P_y are the centers of the droplet position in the image plane. In addition, the standard (IEC 62 899–302-1) also provides alternative methods that can be used. For example, the jetting speed measurement method of high frequency jetting and the drop formation measurement methods are included. In this way, the procedures are designed to measure drop speed consistently in spite of speed variation during drop formation [14].

Standard (IEC 62 899–302-2) presents procedures (methods) to measure the volume of a flying droplet [54]. In case of volume measurement, there has always been an issue of measurement accuracy. Drop visualization system (drop watchers) using high resolution images can typically yield 0.1% level errors for drop speed. However, the same jet image rarely yields better than 2% and 3% absolute errors for inkjet drop volume. The published method provides the accurate measurement procedure for the droplet volume for a



spherical drop as well as volume estimation method for non-spherical droplet with long ligament.

2.5. Jetting status monitoring for a multi-head nozzle

Figure 14 shows the approximate number of jets (nozzles) in commercially available production printers. Recently, most production printer systems use thousands of nozzles in order to meet the requirements for throughput. To increase the number of nozzles for printing, arrays of inkjet print-heads are commonly used, where a number of the inkjet print-heads should be accurately aligned [57].

As a large number of nozzles are used for high throughput process, jetting reliability is a critical issue. In order to ensure jetting reliability, there

have been two conventional monitoring methods: (a) scanning of the jetting status of every nozzle via drop visualization; (b) quality investigation of printed patterns.

For a large number of nozzles (such as more than 10 000), it could take a long time to scan the jetting status of every nozzles by using drop visualization. Moreover, the printing process could be greatly delayed to accommodate the inspection [16].

Alternatively, standard patterns can be printed on a substrate such as paper for inspection purposes. Then, an in-line automated inspection process can be performed to find out any missing printed patterns [50], and thereby, non-firing nozzles could be found. Figure 15 shows typical printing patterns for the inspection of non-firing nozzles. After identifying

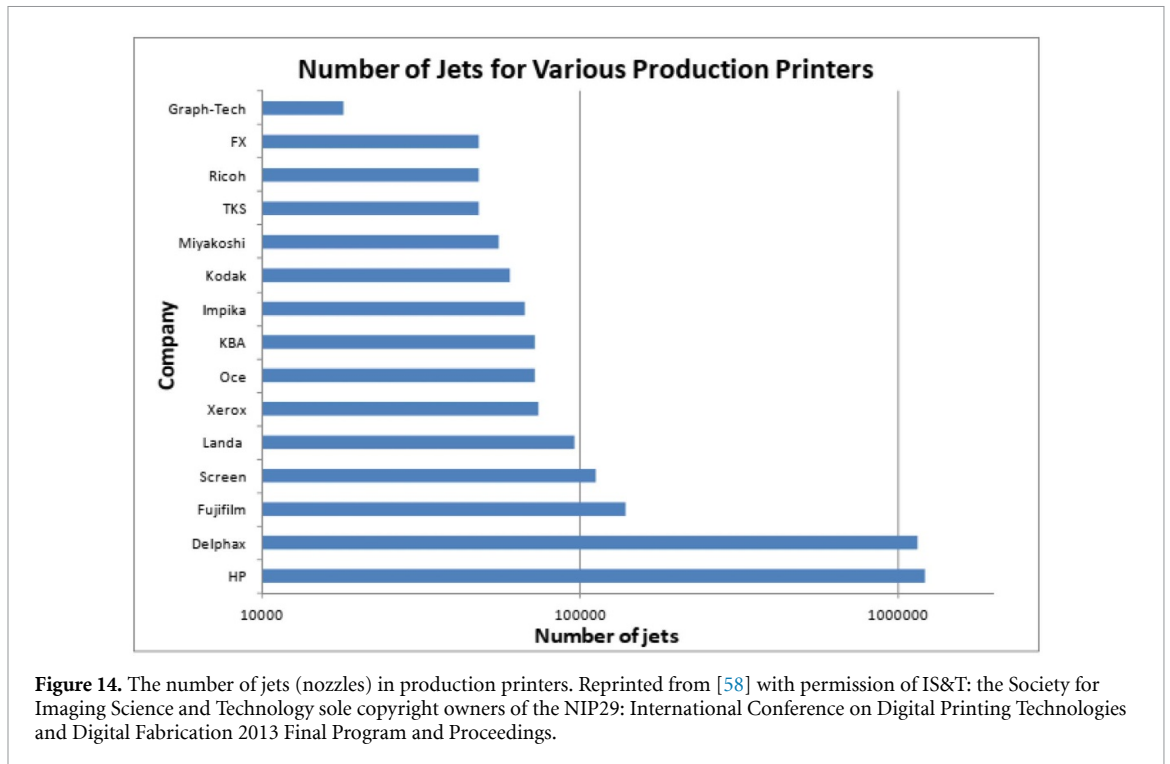


Figure 14. The number of jets (nozzles) in production printers. Reprinted from [58] with permission of IS&T: the Society for Imaging Science and Technology sole copyright owners of the NIP29: International Conference on Digital Printing Technologies and Digital Fabrication 2013 Final Program and Proceedings.

the missing jet, the non-printed part can be printed via redundant neighboring nozzles [58].

The quality inspection method can be effectively used for inspection of nozzle jetting status prior to production printing. However, this is only available when printing with inks that contrast with a substrate. For example, the method cannot be available with transparent inks or in applications that substrates are not available, i.e. 3D printing. Furthermore, jet failures could still occur during the printing process.

In the case of applications where jetting reliability is important, real-time instant nozzle scanning is required without additional process of inspection of standard patterns. Ideally the inspection should not interrupt the printing process. The inkjet print-head using piezo actuator has inherent sensing capabilities that can monitor the pressure wave inside the print-head. When a jetting failure occurs, the pressure wave will deviate from that of the normal jetting condition. The principle of using the actuator as a sensor is known as the 'self-sensing method' and it is based on electrical current measurement of the piezo actuator without requiring any additional sensors [49, 60]. However, it has several issues of scanning time, cost and accuracy of detection when the method is applied to practical inkjet printing systems.

For implementation in real-time inkjet monitoring, low-cost and high-speed measurement methods have been proposed in [16, 61, 62]. The monitoring time required for scanning 1024 heads can be as short as a few seconds including the reporting of analyzed results on a computer screen. Figure 16 shows a screen captured software display after detection of jet failures using such a system [16]. Note that the method could

be extended to monitor more than one print-head by using parallel sensing methods. However, the self-sensing signal might require averaging of the signals in order to increase the signal to noise ratio for better detection of jet failures.

2.6. Droplet placement: accuracy issues in inkjet

For printed electronics applications, the requirement for droplet placement accuracy is more demanding compared to that of graphics applications. In printed graphics, the resulting image or text may still look acceptable even if several ink drops are misplaced or missing. However, in electronics, it may cause a short circuit among conductive traces or an open circuit, which causes complete device failure. Sometimes, undesired/uncontrolled conductive resistances can be obtained, which can be even more troublesome. The printing defects can directly affect the yield since defective parts or the entire printed substrate should be discarded.

The required drop placement accuracy might differ according to applications. For example, the display industry requires precision placement accuracy of droplets, in order to deposit ink droplets within the pixel boundary (black matrix or pixel define layer (PDL)) as shown in figure 17. Note that printing defects often result from combined effects of droplet wetting characteristics on the substrate and jet directionality from the inkjet print-head. The effects of substrate surface energy (wettability) on printing defects are beyond the scope of this review.

The drop placement errors can result from numerous causes such as the printer's mechanical assembly accuracy, motion stage control accuracy and

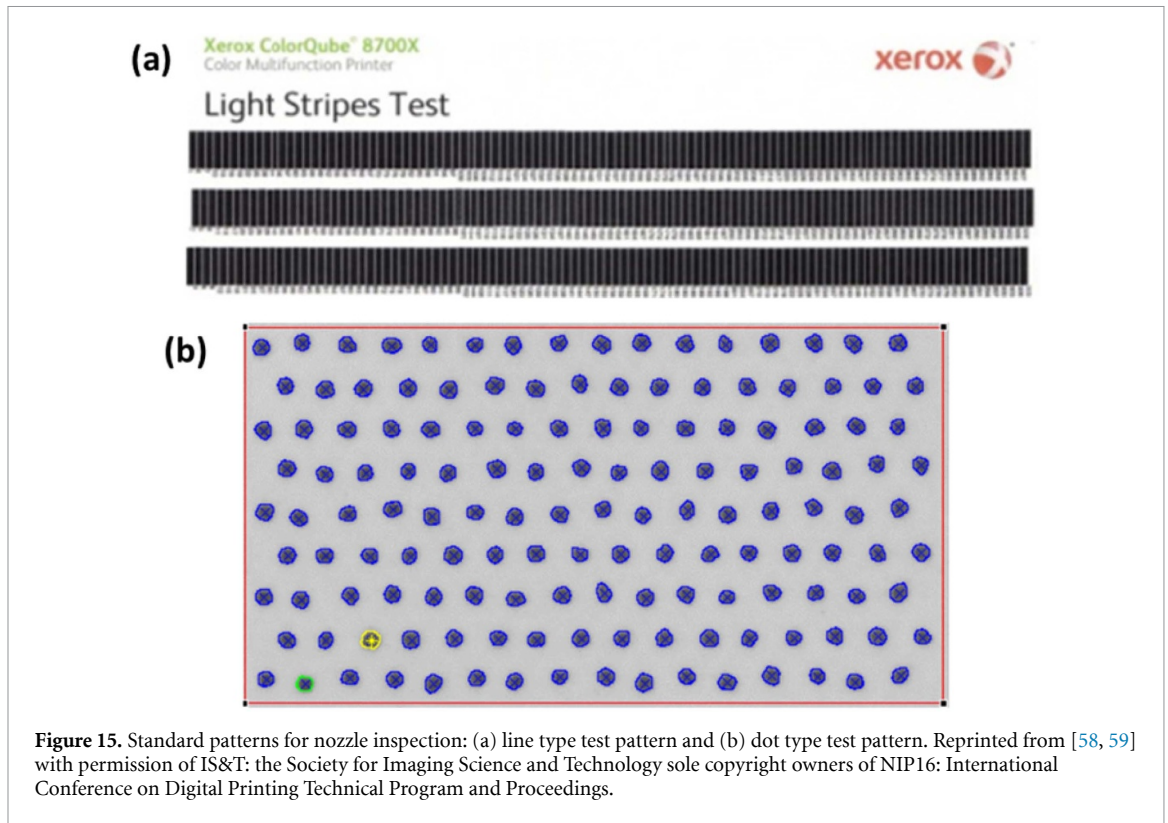


Figure 15. Standard patterns for nozzle inspection: (a) line type test pattern and (b) dot type test pattern. Reprinted from [58, 59] with permission of IS&T: the Society for Imaging Science and Technology sole copyright owners of NIP16: International Conference on Digital Printing Technical Program and Proceedings.

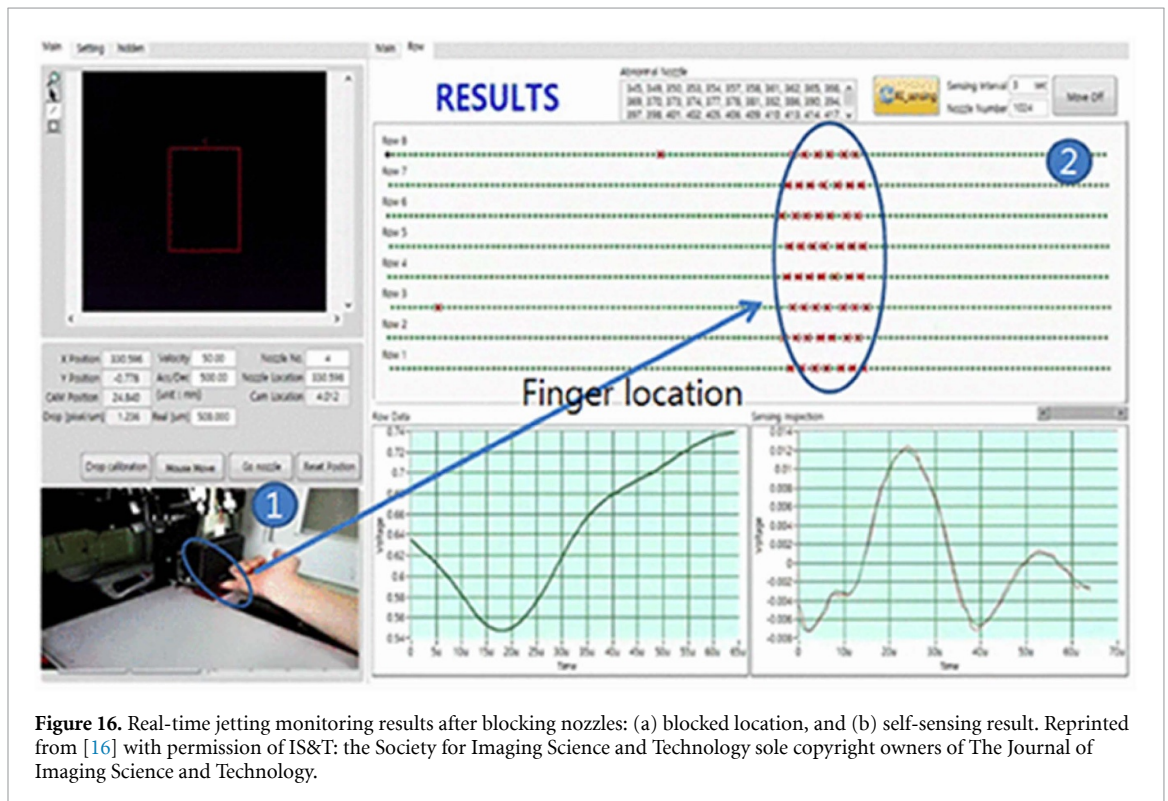
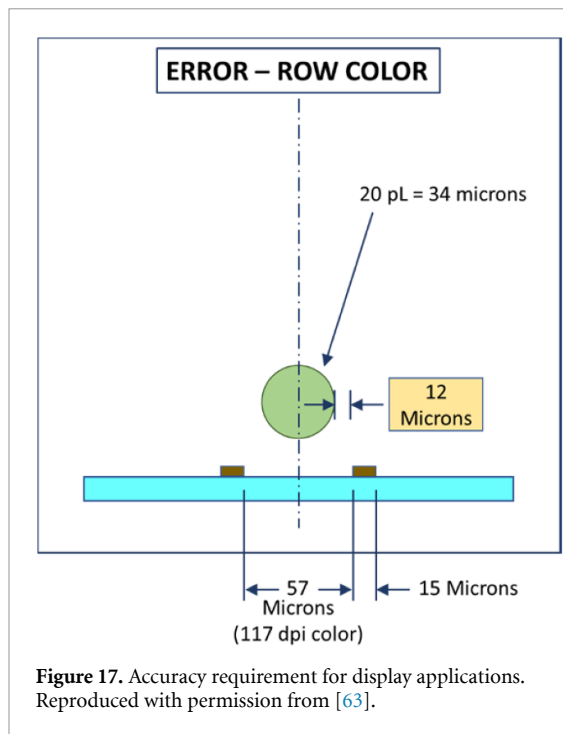


Figure 16. Real-time jetting monitoring results after blocking nozzles: (a) blocked location, and (b) self-sensing result. Reprinted from [16] with permission of IS&T: the Society for Imaging Science and Technology sole copyright owners of The Journal of Imaging Science and Technology.

jet straightness. As the printable area increases, many print-heads are used in order to reduce the number of printing passes. In such case, small misalignments in the print-head array assembly could result in large drop placement errors. Nevertheless, measurable and repeatable errors, such as motion control errors or misalignment of the assembly sometimes

can be corrected and compensated. However, there can be non-repeatable and unpredictable causes for placement inaccuracy such as poor jet directionality from nozzle plate wetting, partial fluid clogs inside or outside of the nozzle and air bubble entrapment in the print-head system. To prevent poor jet straightness, it is important to maintain good jetting conditions



during the whole printing process. Figure 18 shows an example of good and bad directionality from an inkjet print-head nozzle before and after nozzle flooding [17].

The achievable placement accuracy using inkjet printing is about $\pm 10 \mu\text{m}$. Note that the required accuracy is related to droplet size. In general, smaller droplet size requires higher accuracy in droplet placement since printing resolution is related to dot size.

There are several simple methods for increasing placement accuracy. For example, the jet straightness could increase as the jetting speed becomes higher. Note that the jet directionality of the droplet could be easily affected, in cases of lower jetting speed and small droplet volume, by external environmental factors such as local air flow and nozzle wetting, which could lead to unwanted jetting failures. The jetting speed can be easily controlled via the print-head driving voltage amplitude. However, high jetting speed could produce unwanted long ligament or satellites as shown in figure 19. Note that the satellite droplet formation is also related to ink properties as well as driving waveform shape [13]. Despite the possible presence of satellite droplets, a high jetting speed more than 5 m s^{-1} is recommended in most printing applications.

Alternatively, placement errors caused by poor jetting directionality as well as adverse effects of satellites could be reduced by reducing stand-off distance between nozzle and substrate. In practice, a stand-off distance less than 0.5 mm is preferred to reduce such placement errors.

Recent inkjet printing processes require high printing speed to enable high throughput for mass production. As the printing speed increases, other

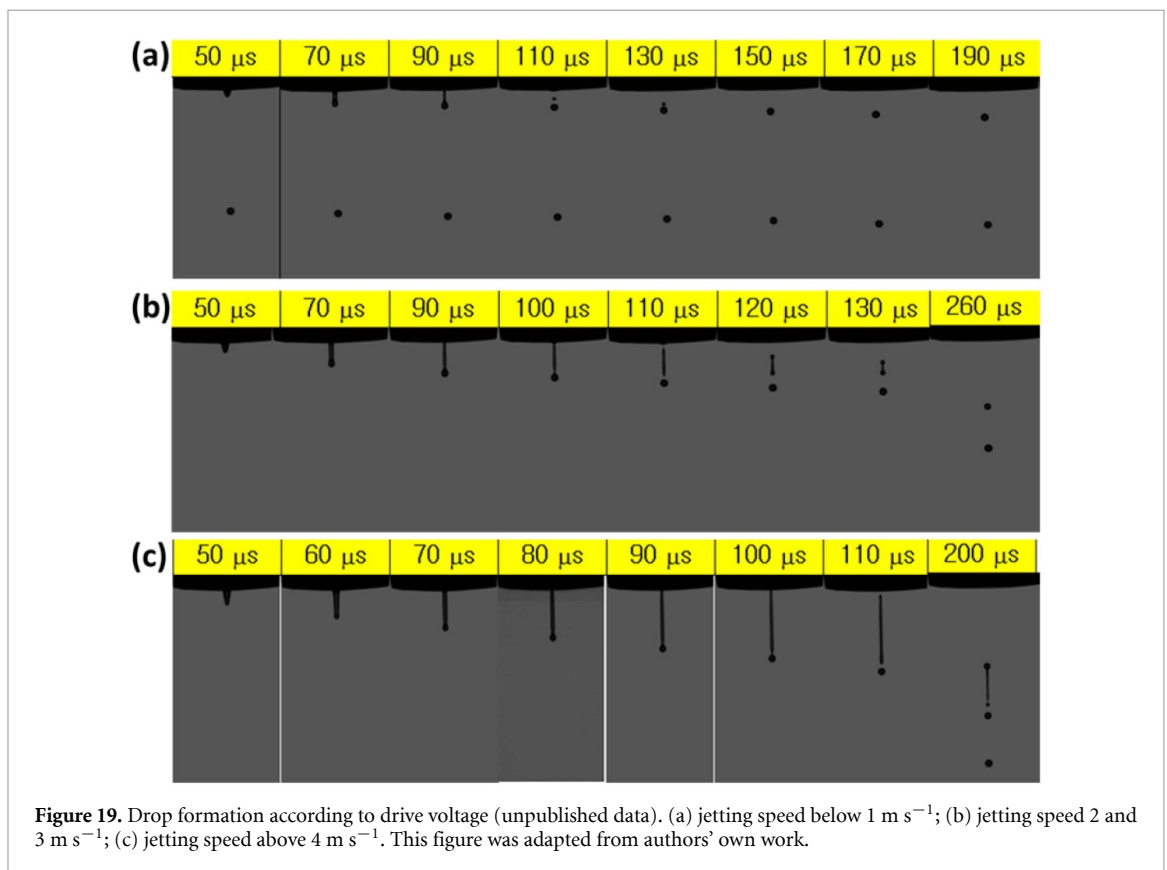
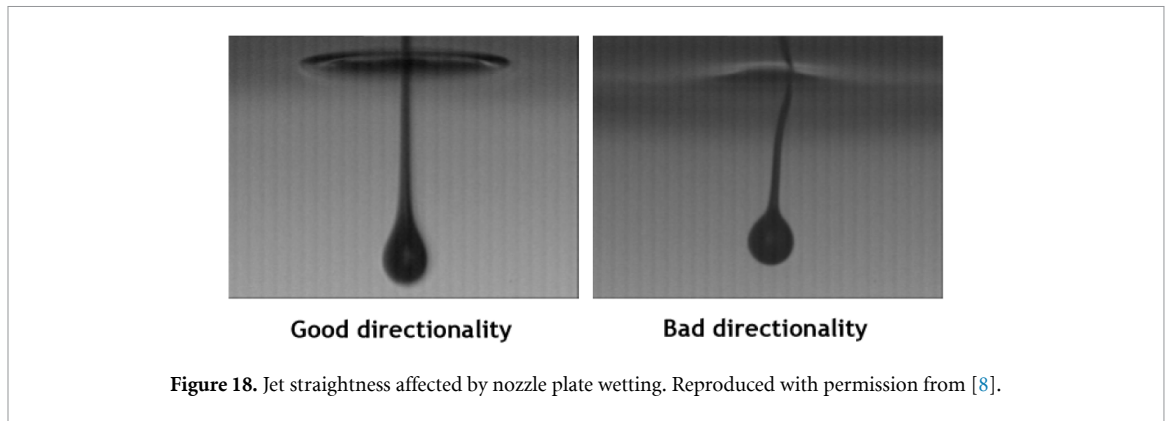
types of printing placement errors occur. For example, air flow effects in the gap between print-head and substrate could affect jet straightness [64]. Effects of air flow effects on jet straightness will be discussed later in section 2.7.

In addition to air flow effects, drop placement can be deviated due to the relative movement between inkjet print-head and substrate [7]. This deviation error could be proportional to the printing speed if it not corrected properly. The firing signal for the inkjet print-head is coming from the substrate motion counter that counts the number of encoder (position) signals based on pre-determined patterns. After firing an ejection waveform, the droplet needs to travel a certain distance before reaching the substrate. Even if the jetting speed (more than 6 m s^{-1}) is much higher than the relative speed of print-head and substrate (less than 1 m s^{-1}), the printing speed effect cannot be ignored. However, this is a predictable error that can be compensated for via the printing software algorithm. The commonly used correction method is to add a speed-dependent offset distance along the substrate (indicated in figure 20) in order to compensate for the errors. To effectively use the compensation method, it is commonly practice to use constant substrate speed motion, which excludes the distances it takes to accelerate and decelerate the relative motion.

There are often cases when the jetting speeds from individual nozzles are unequal, as shown in figure 21. Variations in ejector to ejector jetting speeds could result in placement errors. These errors are difficult to compensate for via software. The jetting speed of a specific nozzle could vary unpredictably during the printing process according to jetting condition variation. The best method for reducing the placement errors is to reduce either the stand-off distance or the printing speed (relative movement of substrate with respect to print-head). Alternatively, DPN drivers can be used to adjust driving voltage independently for each nozzle, in order to equalize the jetting speed across all the nozzles as discussed in figure 8.

2.7. Single pass printing

In the past, multiple pass printing was a common practice to print desired patterns since inkjet print-heads had a limited number of nozzles. While multiple pass printing could increase the print resolution, it has limitations in reducing the printing time (takt time). As discussed in previous sections, recent inkjet print-head development is targeting single pass printing with high density nozzles. Indeed, the single pass printing method has been developed for either a 'web' (where the continuous substrate is mounted on rollers, known as roll-to-roll or R2R) or a 'sheet' (individual pieces of substrate on a moving transport system). The primary benefit of single pass printing is higher production speed and therefore increased productivity. In most printing applications, the printing



substrate width (area) is wider than that of the print-head. To implement single pass printing, an array of print-heads might be needed.

Since the assembly accuracy could affect drop placement errors, a lot of effort needs to be made to align each inkjet print-head. Recently, actuators have been used to place individual inkjet print-heads into the print bar with an accuracy of $\pm 10 \mu\text{m}$ as shown in figure 22 [58].

Note that initial design of web-based printing was targeted for paper-based printing, for example, graphics and document applications. Recently, the concept of web printing has been extended to printed electronics applications. In this case, low cost flexible substrates can be effectively used and the feasibility of web-based printing has been explored [66]. To use the web printing mechanism for printed electronics, the

droplet placement accuracy has been one of important issues. For example, in order to minimize air flow and vortex effects on jet directionality, a guide plate was proposed to avoid air circulation near nozzles as shown in figure 24.

One of the commonly used single pass printing methods is web-based printing as shown in figure 23. By using the web-based printing, the printing process can be made continuous at high speed.

Web-based printing systems require flexible substrates. During the feeding of substrate, the substrate might vibrate or some part of the stand-off distance could vary, as shown in figure 25(a). To place the droplet accurately, it is important to maintain the target stand-off distance. For this purpose, the use of a vacuum chuck was proposed to keep the stand-off distance constant as shown in figure 25(b) [66].

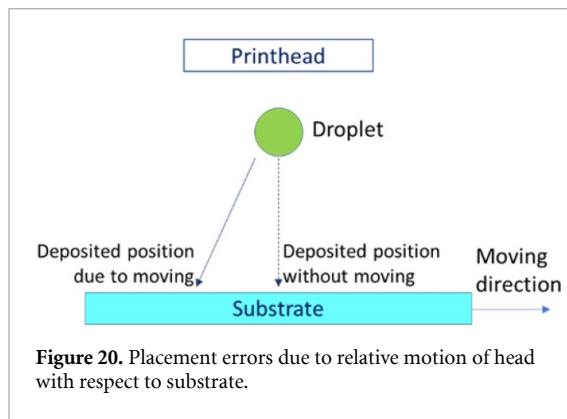


Figure 20. Placement errors due to relative motion of head with respect to substrate.

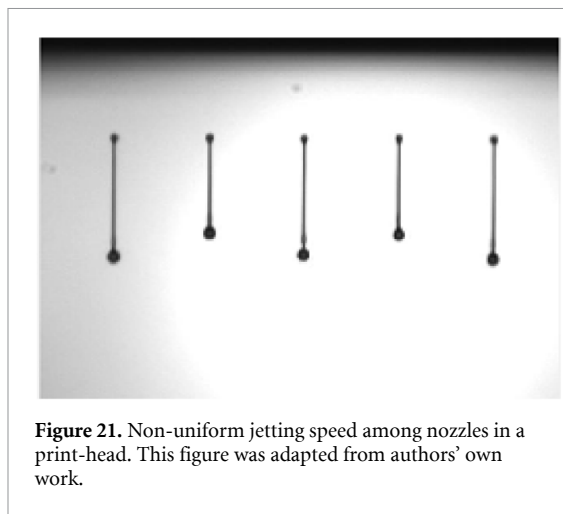


Figure 21. Non-uniform jetting speed among nozzles in a print-head. This figure was adapted from authors' own work.

Most web manufacturing processes are based on the continuous feed of a flexible substrate. Most printed electronics applications require the printing of multiple layers requiring highly accurate registration. In order to reduce the substrate registration error, web-based printing may require image compensation (figure 26). For this purpose, the substrate may have alignment marks for real-time compensation of position error as shown in figure 26.

2.8. Drying and morphology of printed patterns

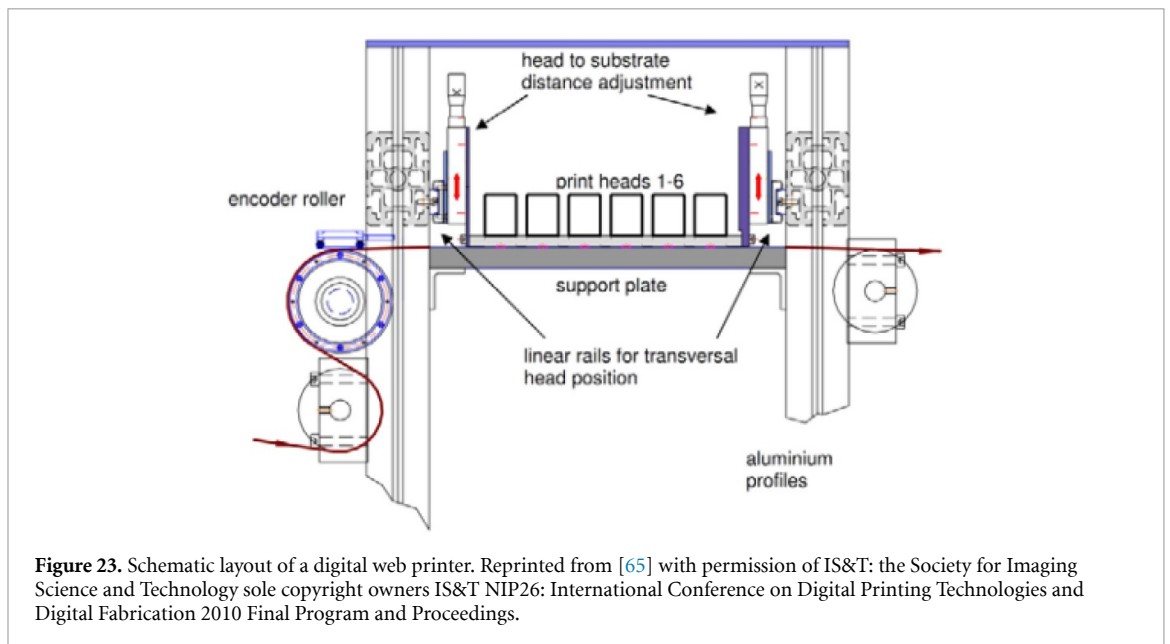
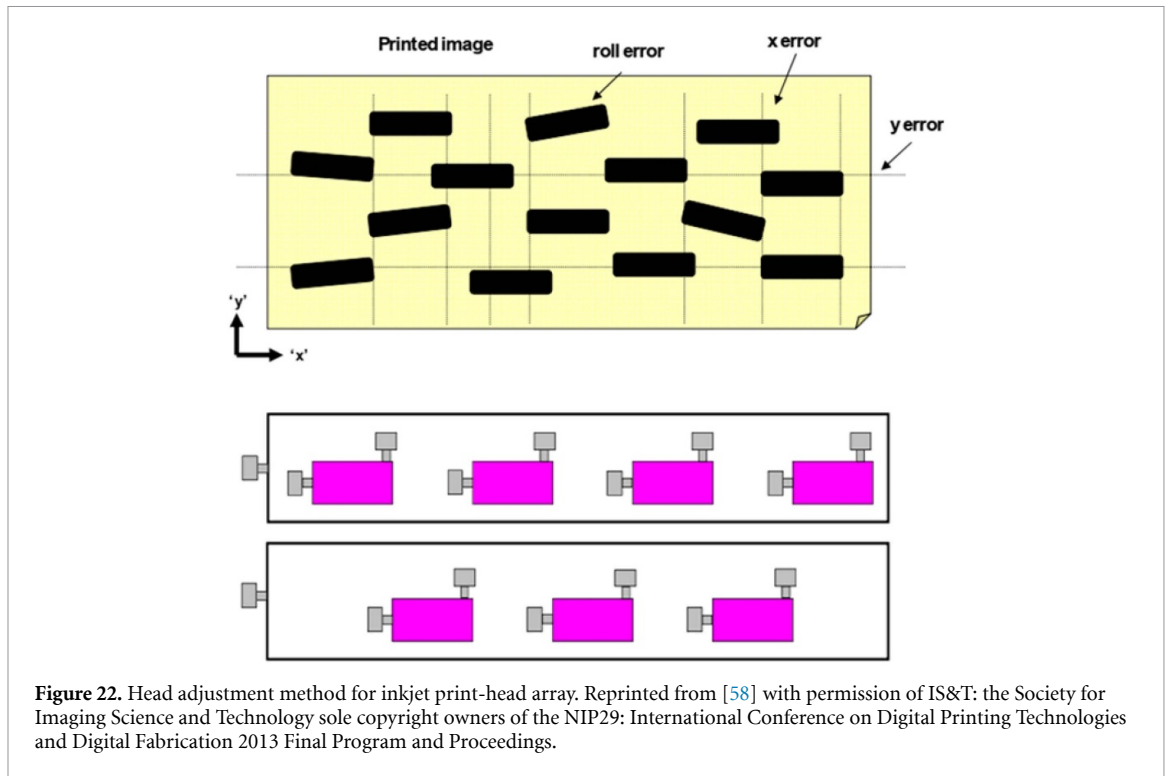
Since inkjet uses low viscosity inks, it could contain a large proportion of the carrier liquids such as water or organic solvents [38], which should evaporate to leave the final solidified patterns on the substrate. For printed electronics applications, the individual droplets may need to be connected to form lines or areas. In such cases, the drying characteristics of deposited droplets are important to form uniform patterns. Figure 27 shows typical line behavior with respect to drop spacing and drop delay (time interval between two consecutive drops) [67]. Here, the drop delay could be used to control the evaporation degree of deposited droplet prior to jetting of consecutive droplet. Note that when the evaporation degree is too low, there can be bulging and non-uniform lines as shown in figure 27(d). In addition to drop delay, the

evaporation can be accelerated further if the substrate is heated. However, fast evaporation could cause the pattern that appears as stacked coins [67]. Note that in the cases of using UV curable inks [68] (inks that could be cured by using ultra-violet light) or phase-change materials [26], the forming of the patterns can be improved significantly by using UV irradiation [68]. In practice, printed patterns using UV curable ink should be cured instantly for pattern uniformity, and even 3D structures can be printed via instant curing [69, 70].

After the deposition of solvent-based ink droplets on a substrate, there can be non-uniform particle distribution in the dried patterns. For example, the particles often are accumulated near the edge of the droplets or patterns as shown in figure 28. This phenomenon is well-known as coffee-ring effect, or coffee-stain effect. Deegan [71] explained that during the evaporation, the contact line is pinned to the substrate, and the evaporating liquid at the edge must be replenished by the liquid from the center. As a result, a capillary flow is formed, which transfers the particles to the edges. Fischer developed a model to explain that convection flow in the droplet could transfer the solute to the outer edge [72]. Marangoni effects may also influence local fluid flows along the edges due to local temperature change during evaporation [73, 74].

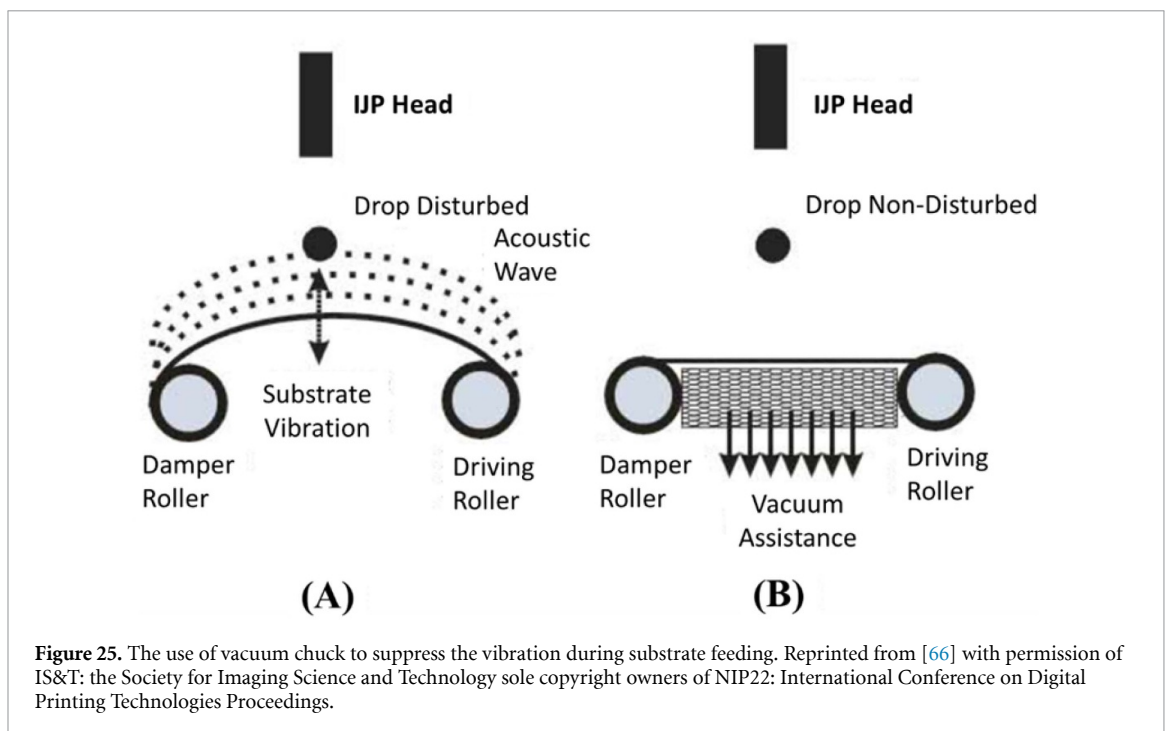
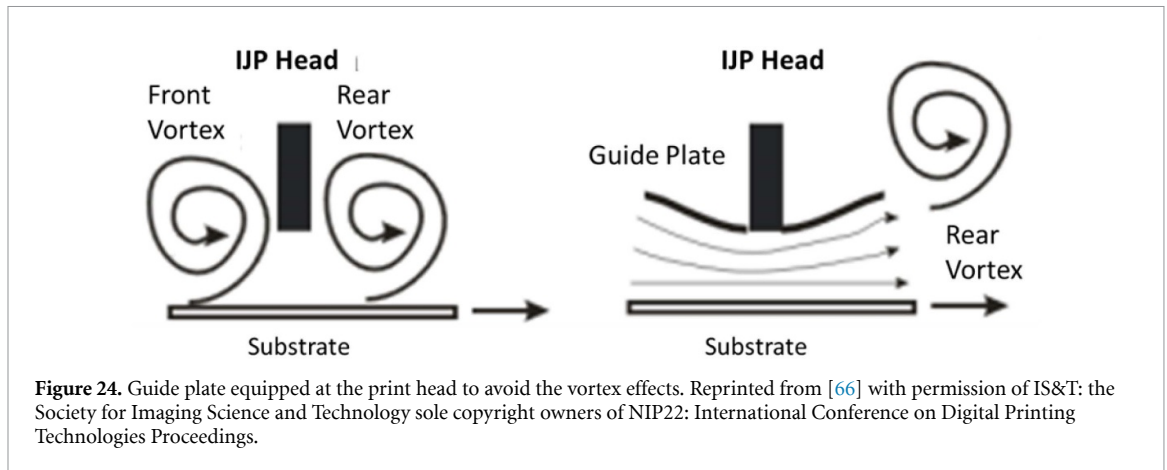
In most inkjet applications for printed electronics, the coffee-ring effect should be avoided because the non-uniformity could affect the devices performance [67, 75, 76]. In order to suppress the effect, several methods have been proposed. One popular method is based on substrate heating in order to accelerate solvent evaporation. If the evaporation is faster than the outward convection flow, the coffee ring effect could be avoided [77]. Substrate heating could also influence droplet spreading, drying and sintering efficiency of printed patterns [78, 79]. However, the use of excessively high heating temperature could result in damage the printed devices [80].

Alternatively to substrate heating, different methods have been explored to reduce the coffee ring effects, such as substrate modification, ink modification and multi-jetting methods. Substrates with hydrophobic surfaces or low contact angle hysteresis could be used to prevent the coffee ring by reducing contact line pinning [81–85]. Ink can be modified in order to suppress the coffee ring effect via a reverse process, which can transfer particles from the edge to the droplet center. By using proper solvent mixtures [86], or adding surfactants in to the ink [87, 88], a Marangoni flow can transfer the particles toward the droplet center. Drying and evaporation of droplets in alcohol vapor environment could result in similar effects [89]. Goto *et al* [90] proposed the use of mixing solvent to control the strength of the interaction between the substrate surface and



molecules in semiconductor crystal solution, which can reduce the outward flow of particles. In addition, the shape or size of particles could affect coffee ring effects. For example, in the case of specific solutions such as graphene oxide [75] and colloidal solution of polystyrene beads [77], the size of the particles should exceed thresholds in order to reduce the coffee ring effects. Alternatively, Yunker [91] found that adding anisotropically-shaped particles can significantly reduce the coffee ring effect. Multi-jetting with different materials could be another useful method for suppressing the coffee ring effect [76, 92]. For example, subsequent printing of ink B (solution ink) right after printing of ink A (antisolvent ink) could

grow single-crystal semiconducting film on the top of droplet, as described in figure 29. Due to this film, evaporation could be very slow, which could help forming smooth printed pattern on the substrate [92]. Recently, a different multi-jetting approach was proposed by Karam *et al* [76] to obtain uniform particle distribution in the printed pattern. In their method, supporting droplets (mainly solvents) were deposited prior to jetting of a so-called ‘wetting droplet’ onto it. Due to the surface tension effects of supporting droplets, the particles in the wetting droplet could be kept uniformly distributed during the solvent evaporation process as shown as shown in figure 30.



It should be noted that the coffee ring effect can be useful in some cases, especially in printed electronics. By controlling the coffee ring effect, patterns with high aspect ratio (thickness: width) could be obtained [82]. For example, it can be used to create invisible conductive patterns by concentrating particles on the outer part of pattern, leaving empty holes in the center. The coffee ring could connect the lines as shown in figure 31 with rim of 10 μm , which is almost invisible to the naked eyes [93]. This could be used for transparent electrodes or transparent conductive films in display applications.

3. Other printing technologies for high resolution printing using high viscosity ink printing

Even though the conventional inkjet printing method is widely used for printed electronics applications due to its capability of scale-up for mass production, there

are also limitations to expanding its applications further due to the requirement of the low viscosity of printable inks. The droplet deposition based on low viscosity inks (<10 mPas) might lead to patterns with less remaining material after evaporation. The use of low viscosity materials often leads to non-uniform widths and thicknesses depending on substrate conditions or evaporation behavior of ink as discussed in section 2.8. In addition, recent applications demand printing methods using high viscosity ink or printing fine patterns with only a few micrometers in width, which is generally beyond the capability of conventional inkjet printing method. In this section, we will review these other printing methods, which overcome some of the limitations of inkjet printing methods.

3.1. Dispensing methods for high viscosity ink

To obtain better electronics characteristics of printed patterns, the required ink viscosity should be very high, more than 1000 mPas, in order to increase

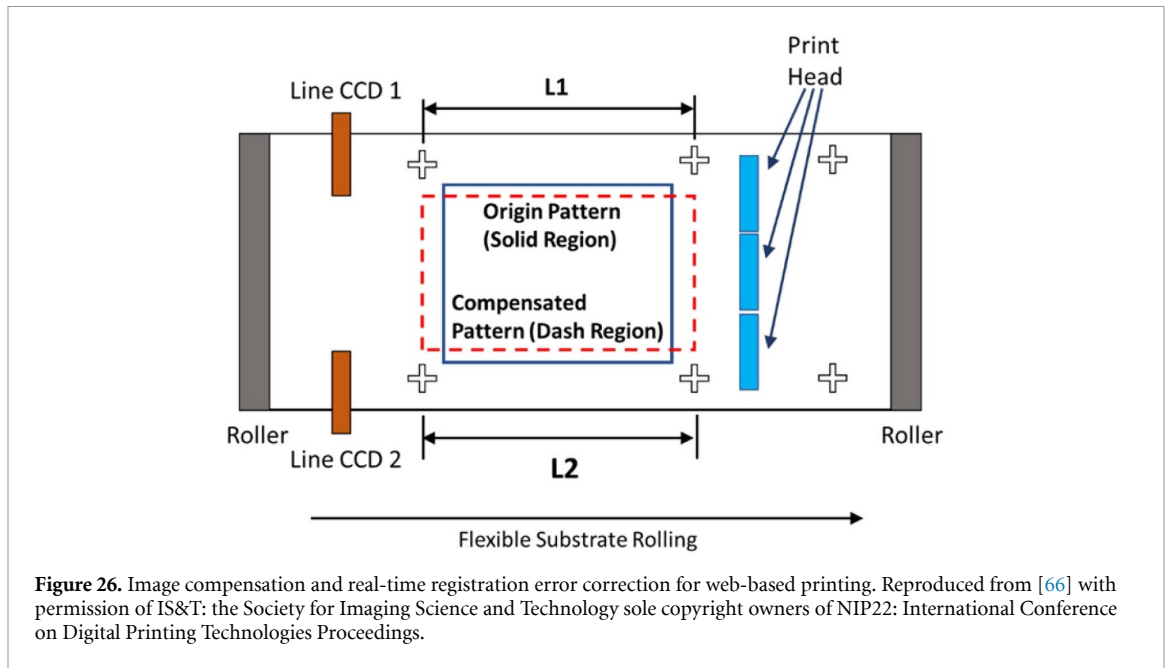


Figure 26. Image compensation and real-time registration error correction for web-based printing. Reproduced from [66] with permission of IS&T: the Society for Imaging Science and Technology sole copyright owners of NIP22: International Conference on Digital Printing Technologies Proceedings.

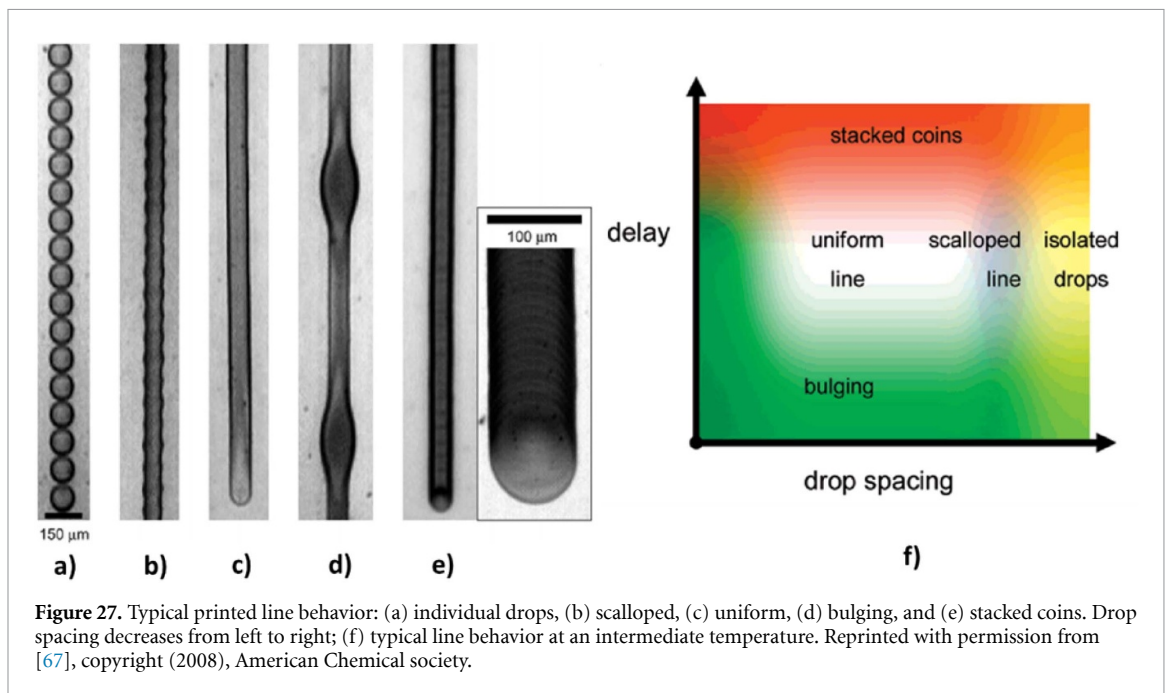


Figure 27. Typical printed line behavior: (a) individual drops, (b) scalloped, (c) uniform, (d) bulging, and (e) stacked coins. Drop spacing decreases from left to right; (f) typical line behavior at an intermediate temperature. Reprinted with permission from [67], copyright (2008), American Chemical society.

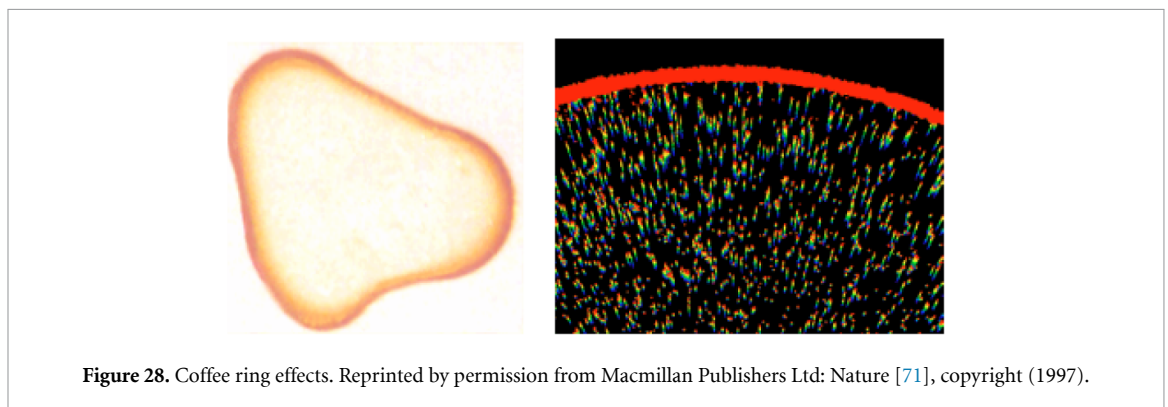
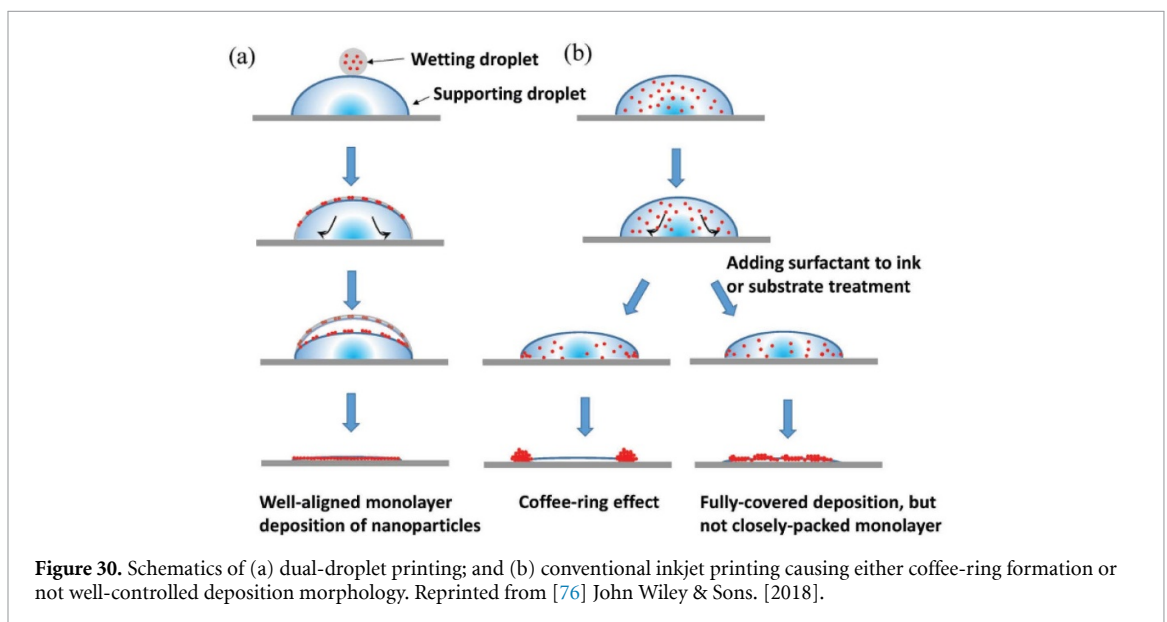
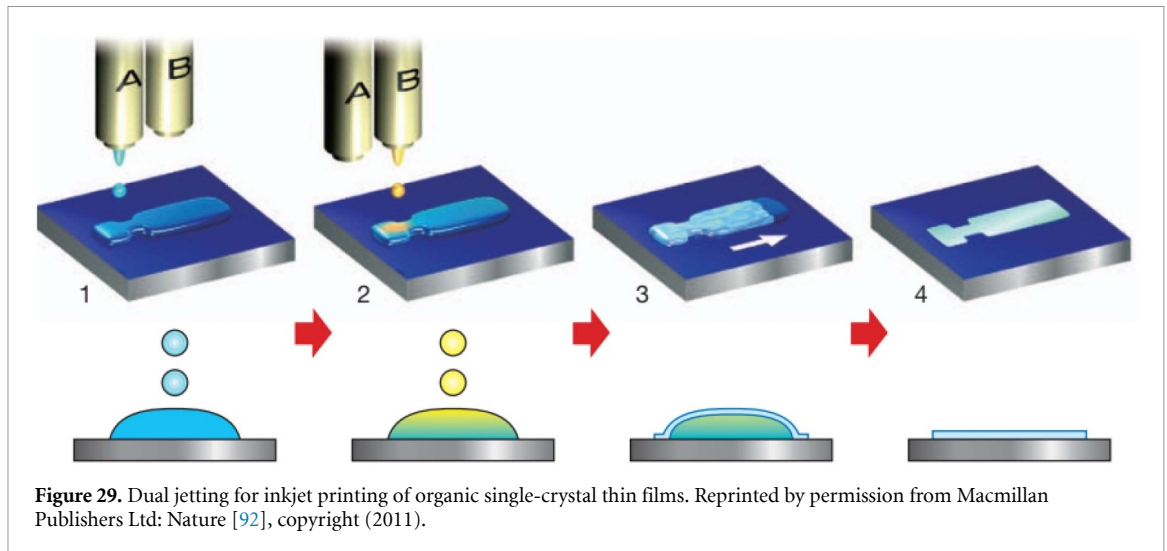


Figure 28. Coffee ring effects. Reprinted by permission from Macmillan Publishers Ltd: Nature [71], copyright (1997).



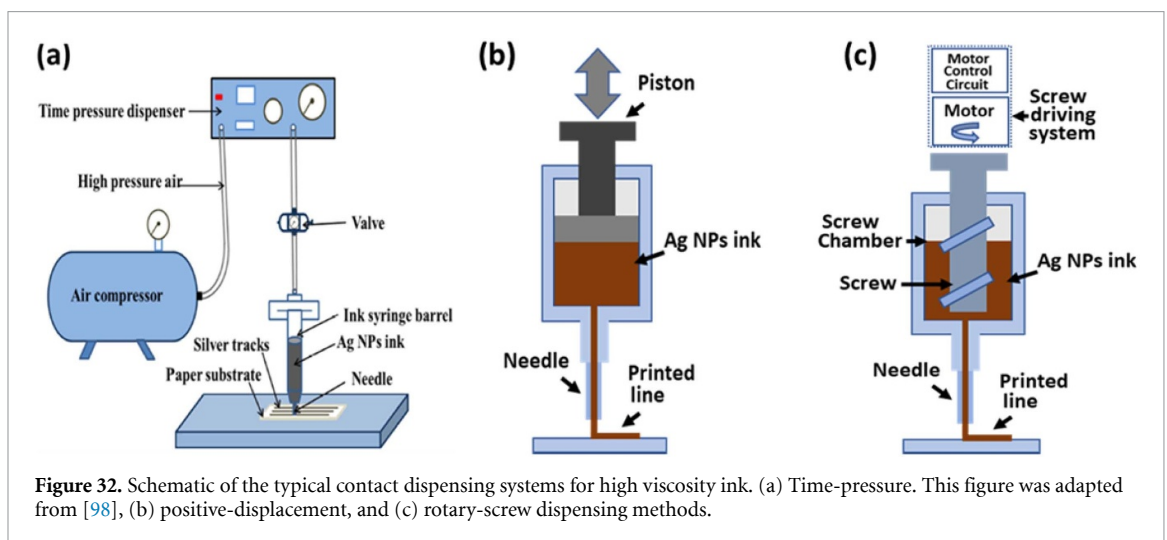
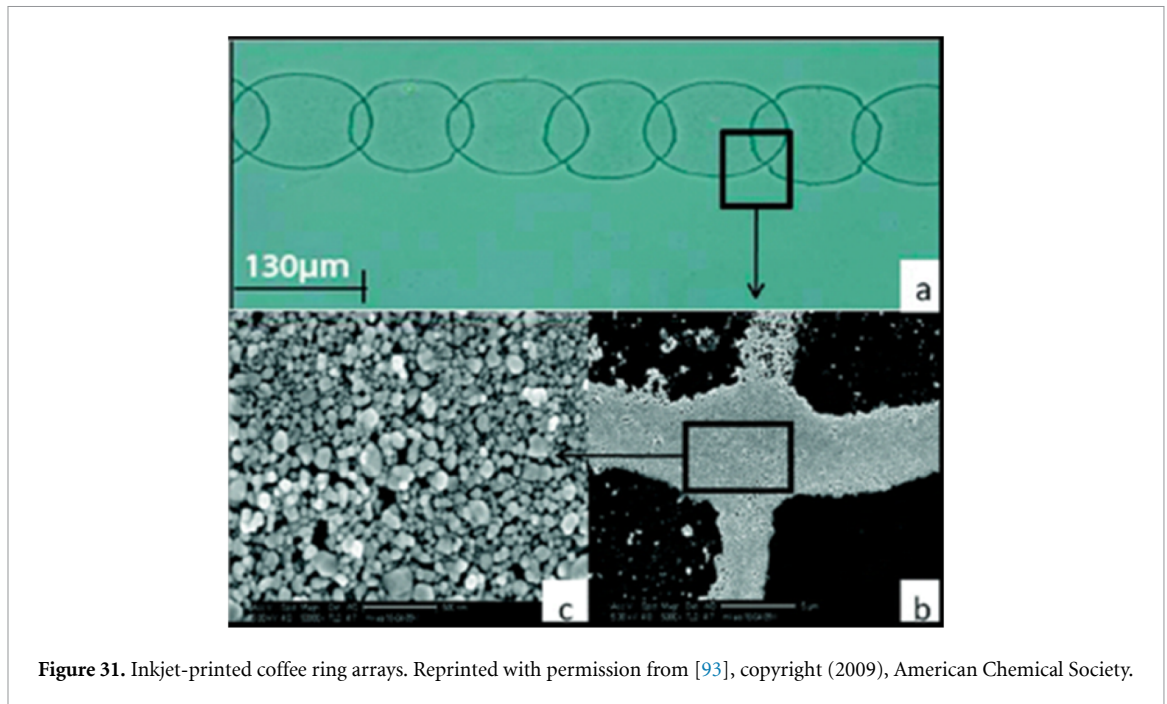
the solid (≥ 80 wt%) loading. When using ink with higher viscosity, the printed patterns become less affected by the surface condition of the substrate. For this reason, dispensers for high viscosity ink have been widely used for industrial processes. Dispensing methods can be classified as contact and non-contact (jet) dispensing methods according to the dispensing mechanism [94].

3.1.1. Contact type dispenser

Figure 32 shows the typical contact type dispensing methods for high viscosity ink, including time-pressure, positive-displacement, and rotary-screw dispensing methods. Here, the widely used dispenser is based on the time-pressure method shown in figure 32(a). In the time-pressure dispensing method, air pressure is applied to the syringe barrel to push the ink out of the nozzle tip. The applied pressure and duration should be controlled to determine the amount of dispensed ink. To print continuous lines, pressure should be applied for a long duration,

whereas pressure pulses should be used to deposit single dots on the substrate (dot-based printing). Note that dot-based printing normally involves point contact at specific printing spots via z -direction motion control. However, it should be noted that the ink viscosity could be affected by the ambient temperature or caused by high rate pressure pulses, which can change the ink flowrate during the dispensing process [95–97].

The positive-displacement method uses a piston to push ink stored inside the syringe barrel instead of air pressure, as shown in (figure 32(b)). Here, the volume of the deposited ink or flowrate of the ink is related to the displacement of the piston inside the syringe barrel. To control the displacement of the piston, a stepper motor is usually used. In case of positive-displacement method, the ink flowrate (or dispensing speed) and amount of dispensed ink is related directly to the rate of piston displacement regardless of the ink viscosity [97]; and the printable viscosity of the ink depends on the power of the



driving motor and mechanical system. Nonetheless, ink properties such as compressibility and viscoelasticity could affect the ‘true’ volume and flowrate of dispensed ink [99]. Note that due to the ink compressibility, the ink flow response could be delayed when the motor starts or stops.

Another dispensing method is based on a rotary-screw mechanism, and is often known as auger pump, spiral pump or Archimedes’ pump (figure 32(c)). When the screw rotates during operation, it creates a shearing force, forcing the fluid flows along the threaded groove to be dispensed [97]. Normally, a supply pressure should be pre-applied to supply the ink into the injection chamber. The rotary-screw dispenser may be more complex in terms of mechanism than other dispensing methods but can provide better control of deposition in case of using shear-thinning fluids.

Time-pressure, positive-displacement and auger pump dispensing methods can be used for very high viscosity liquid, up to the order of 10^6 mPas [100], if the power (or pressure) of the system is high enough. However, the use of ink with low viscosity should be avoided since proper printing is not possible due to ink dripping or excessive ink flows from the nozzle.

The use of the correct size of the nozzle inner diameter is important since it is directly related to pattern width or dot size. The nozzle inner diameter for fluids with very high viscosity such as adhesives and solder paste could range from about hundreds of micrometers to several millimeters [94, 101–103]. For dispensing of dots or lines with feature size less than $250 \mu\text{m}$, the nozzle size could be down to $50 \mu\text{m}$ [104]. Note that the nozzle selection is closely related to ink viscosity, the smaller nozzle inner diameter is suitable for ink with lower viscosity and vice versa.

Although contact dispensing methods can be used for very high viscosity materials, their applications may be limited because the nozzle position should be maintained close to the substrate during dispensing process. As a result, the needle cannot reach narrow spaces for printing. Dispensing on uneven surfaces may also become difficult without proper 3D motion control [105, 106].

Contact based dispensers use the transfer of extruded viscous ink from the nozzle tip onto the substrate. The delivery speed or flowrate of the ink is usually slow due to the pressure loss during ink flow through the nozzle. As the results, the whole manufacturing process could be very slow. The methods are suitable for printing continuous lines rather than dot-based printing. In the case of dot-based printing, where single dots are deposited on the substrate, the nozzle needs to move down from the initial (non-contact) position to close to the substrate for dispensing the ink. Then, the nozzle moves back to the initial position. The dot printing process could require considerable operation time, as shown in (figure 33). In the case of dot printing process, the ink breakup behavior from the substrate is likely to have significant influences on the dispensed shape and volume on the substrate [107]. In general, the dot size and dot volume are difficult to control. The repeatability is also another issue to consider, which might be affected by the compressibility of air and ink, and the precision of mechanical system (motor and screw).

3.1.2. Non-contact (jet) type dispensers

To overcome problems of contact type dispensing methods, non-contact dispensing systems have drawn attention. The most commonly used non-contact jet dispensing systems are based on the motion of a needle inside an injection chamber. Figure 34 depicts the basic principle of the method. As shown in figure 34, there are several steps of needle movement. At the initial stage, the needle covers the nozzle to prevent the ink flow from the nozzle. To form jetting, the needle is moved up and then pushed back to cause collision on needle seat, which can produce high pressure for jetting. The inner diameter of the nozzle used in non-contact type dispensers could vary from 50 μm to more than 200 μm [108].

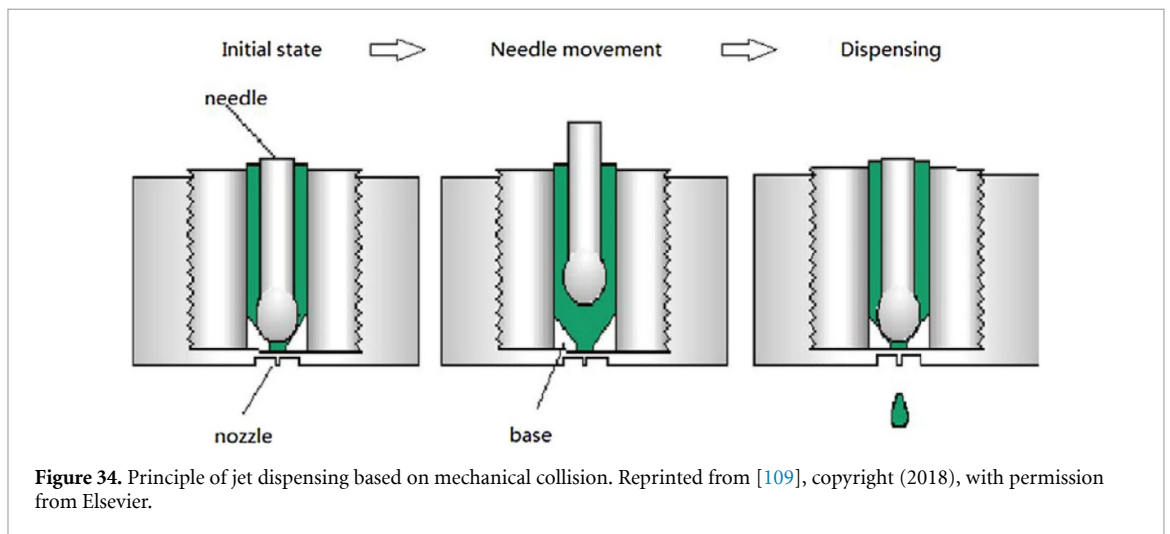
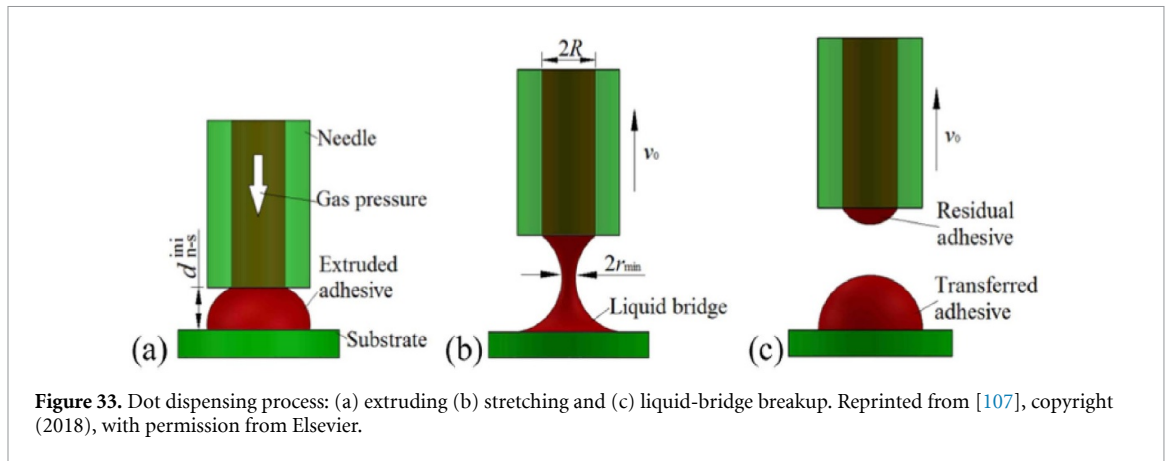
Several methods could be used to control the needle motion for jet dispensing as shown in figure 35. Air pressure has been widely used to control the motion of the needle. Figure 35(a) shows a typical jet dispensing system using air pressure [110]. When the dispenser operates, the air pressure is supplied to lift the needle. Then, as the air pressure is removed, the restoration force from spring pushes back the needle to produce jetting. In order to control the on-off air pressure and motion of the needle, a solenoid micro-valve is usually used [108, 110]. The control parameter effects on jetting have been discussed in [110].

When using air pressure to lift the needle, a pneumatic valve is used for on-off control of jetting. However, the pneumatic valves have relatively short lifespan, and the maximum jetting frequency could be relatively low (typically ~ 100 Hz) [110, 113]. For these reasons, the piezoelectric (PZT) driven non-contact dispensing method is emerging as an alternative method due to its high efficiency, fast response, and high precision actuation [114]. Figure 35(b) shows a schematic of the typical piezoelectric needle-collision jetting dispenser. In the PZT driving dispensing system, a piezostack actuator is used as the driving component, which is attached to a displacement amplifier. The method has the advantage of controlling the amount of fluid material ejected out of the orifice accurately. However, the achievement of proper stroke of needle is an important issue of the dispenser. To get a displacement of the needle up to 0.3 mm or above, two different type displacement amplifiers are commonly used as shown in figure 36. The basic working principle of these dispensers is quite similar to those using pneumatic valves, except in the actuation mechanism used in order to generate the needle motion.

Recently, C. Zhou and his co-worker [106, 112] proposed a new type of non-contact dispenser, giant magnetostrictive and magnifier (GMM) for a glue injector. The GMM jetting dispenser's working principle is based on the properties of ferromagnetic materials that causes them to change their shape or dimensions during the process of magnetization. Similar to PZT driving dispensers, the displacement of the needle driven by the GMM rod may not be enough for producing jetting. A beam is used for magnifying the displacement as shown in figure 35(c). It is reported that this dispensing process can jet glue with viscosity of 1500 mPas steadily at room temperature conditions. It can deliver 250 dots of glue per second by using the GMM combining with the magnifying structure [105].

In the case of using jet (non-contact type) dispensers, operating conditions such as needle motion, back pressure, working temperature and stand-off distance should be optimized in order to dispense droplets with the desired volume. In piezo-driven dispensers, the driving voltage for the piezostack is important, while for the pneumatic valve dispenser, the lift pressure and valve open time should be carefully selected. When using high-viscosity inks as the jetting material, the nozzle heater is commonly used to reduce the ink viscosity. Note that the thermal insulation can be important in the case of piezo-driven dispensers because the piezostack should be protected from high temperature heating [114].

Although non-contact dispensing systems can have many advantages compared to the contact dispensing systems, the contact dispensing methods cannot be completely displaced by them. For example, the pressure caused by collision of the needle



is limited. As a result, the printable viscosity ranges of jet dispensing systems could be lower than that of contact dispensing methods. Table 3 shows the summary of dispensing methods and their characteristics for comparison purposes.

3.2. Micro-plotter

In general, the printed pattern size is generally correlated to the deposition nozzle diameter. In order to reduce the printed feature size, the nozzle inner diameter should be reduced accordingly. However, the ink viscosity should be low considering the pressure loss by ink flow through the nozzle with small inner diameter. To overcome the limitation, the so-called micro-plotter could be one of the enabling technologies to dispense relatively high viscosity ink through the fine nozzle. The dispensing mechanism is based on the ultrasonic pumping action at the core of the micro-plotter head. The mechanism is capable of depositing ink droplets with dot size of less than $5\ \mu\text{m}$, which is much smaller than inkjet system [123, 124] by using relatively high viscosity solution up to 450 mPa·s [131]. Besides, this printing method is able to dispense novel materials that other dispensing systems might struggle with, such as carbon nanotubes (CNTs) and graphene solutions [131]. The

working mechanism of the micro-plotter is fundamentally different from that of inkjet printers or other piezoelectric-based fluid dispensers. The piezo actuator in the micro-plotter generates ultrasonic vibrations, which will cause fluid to be ejected from the tip of the micropipette. Note that conventional inkjet print-heads use pressure waves (or pressure) of ink caused by the contraction (or expansion) action of the piezo actuator for droplet jetting [123, 132].

There are two different printing methods for micro-plotter dispensing systems depending on the ink loading method: (a) ink supply from the wide end of the micropipette; (b) dipping of the sharp end of the micropipette into a solution well. A continuous fluid supply is useful for a larger deposition quantity using a single fluid, whereas dipping the micropipette tip into fluid is useful for depositing multiple fluids (dip-pen mode).

Figure 37 shows the schematic layout of the micro-plotter. For dispensing ink, AC current is applied to a piece of PZT piezoelectric attached to the micropipette. Here, the PZT causes the micropipette to vibrate along its axis [124, 133]. In order to dispense the droplet solution on a target location, the dispenser tip is lowered to the substrate by controlling a precision positioning stage based on the surface

Table 3. Comparison of various printing methods for printed electronics.

Method	Impact type	Printing mechanism	Printable fluid characteristic	Feature jet amount/Dot-line size	Printing throughput
<i>Piezo driven inkjet printing</i>	Non-contact printing	When a waveform is applied, deformation of piezoelectric transducer causes a pressure wave to eject the droplet from the nozzle.	Viscosity in range of 1–50 mPas, typically of 10–20 mPas and surface tension of 20–40 mN m ⁻¹ . [38, 115]	Drop volume varies from pl several to tens of pl. Normally, $D_{\text{dot}} > 10 \mu\text{m}$ depending on droplet size and surface energy of substrates	Tens of kHz jetting. Multi nozzle, multi-head system could be implemented for single pass printing. (Table 1, section 2.7).
<i>Time-pressure dispensing</i>	Contact dispenser	High pressure is applied during a period of time to disperse the liquid.	Ink viscosity up to 10 ⁶ mPas [100, 116] depending on the applied pressure. Effective viscosity range: 500–20 000 mPas [94]		Less than 25 000 dots h ⁻¹ [94], or less than 25 $\mu\text{l sec}^{-1}$ [117]. Required duration of air pressure pulse >50 ms [11]
<i>Positive displacement dispensing</i>	Contact dispenser	A piston is used to push the liquid inside syringe barrel. The volume of dispensed liquid is controlled precisely via piston's displacement. The piston displacement can be controlled by air pressure or a motor.	Ink viscosity range: 1–5 000 000 mPas [94, 100, 118]		Less than 36 000 dots h ⁻¹ [94] or less than 250 $\mu\text{l sec}^{-1}$ [117]
<i>Auger pump dispenser (Archimedes screw dispenser)</i>	Contact dispenser	A motor is used to rotate the screw (Auger pump). Liquid follow the screw to be dispensed.	Effective ink viscosity range: 15 000–600 000 mPas, possibly up to 10 ⁶ mPas [100] depending on supply pressure and screw structure.	Typically, $D_{\text{dot}} > 200 \mu\text{m}$ [14]. Normally $D_{\text{dot}} > 2 \cdot ID$ of the nozzle [117]	Less than 40 000 dots h ⁻¹ [94] or less than 50 $\mu\text{l sec}^{-1}$ [117]
<i>Air-valve jet dispensing</i>	Non-contact jet dispenser	Air pressure is used to lift the needle. The needle strikes the nozzle seat to produce jetting.	Typically, in medium viscosity range (20–300 mPas) [99, 108, 119] Some dispensers can jet high viscosity ink, up to 100 000 mPas. [94, 108]	$D_{\text{dot}} > 100 \mu\text{m}$ [120]. Drop size ~ 1.5 –2.5 times of nozzle size [108]	Typically, 100 dots s ⁻¹ [110].
<i>Piezo jet dispensing</i>	Non-contact jet dispenser	Piezo actuator is used to lift the needle. The needle strikes the nozzle seat to produce jetting.	Typically used for ink with medium viscosity (50–300 mPas). Some dispenser can jet high viscosity ink, up to 500 000 mPas. [121]	$D_{\text{dot}} > 100 \mu\text{m}$ [120].	Up to 500 dots s ⁻¹ [122]
<i>Magnetic jet dispenser</i>	Non-contact jet dispenser	Magnetic field is used to lift the needle. The needle strikes the nozzle seat to produce jetting.	Able to jet ink with viscosity up to 1500 mPas.	$D_{\text{dot}} > 1.2 \text{ mm}^*$ [106]	Less than 250 dots s ⁻¹ [106]

(Continued)

Table 3. (Continued).

Method	Impact type	Printing mechanism	Printable fluid characteristic	Feature jet amount/Dot-line size	Printing throughput
<i>Micro-plotter</i>	Contact printing	The piezo actuator generates ultrasonic vibrations to push the fluid out from the nozzle.	Viscosity up to 450 mPas. Able to print graphene or CNT inks.	$D_{\text{dot}} \leq 5 \mu\text{m}$ [123, 124]	Typical printing speed: $\sim 1 \text{ mm s}^{-1}$ to form continuous lines. [123, 124]
<i>Aerosol jet printing</i>	Non-contact printing	Ink is atomized and transferred to the nozzle by N_2 . At the nozzle tip, a second N_2 stream is used to focus the atomized ink on the substrate.	Ink viscosity range: 1–2500 mPas. [100, 125, 126]	$D_{\text{dot}} < 5 \mu\text{m}$, [100, 125, 126]	Printing speed about tens of mm s^{-1} [125, 126]
<i>EHD printing</i>	Non-contact	Ink is pushed to nozzle to form extruded meniscus. Then, high voltage (electrical field) is applied at the nozzle to produce Taylor cone jet.	DOD EHD: 1–100 mPas, NFES: more than 1000 mPas. [127]	Down to 100 nm. [128]	DOD EHD jet frequency: up to several kHz [128–130] Maximum printing speed of NFES: more than 500 mm s^{-1} [127].

* Authors testing conditions

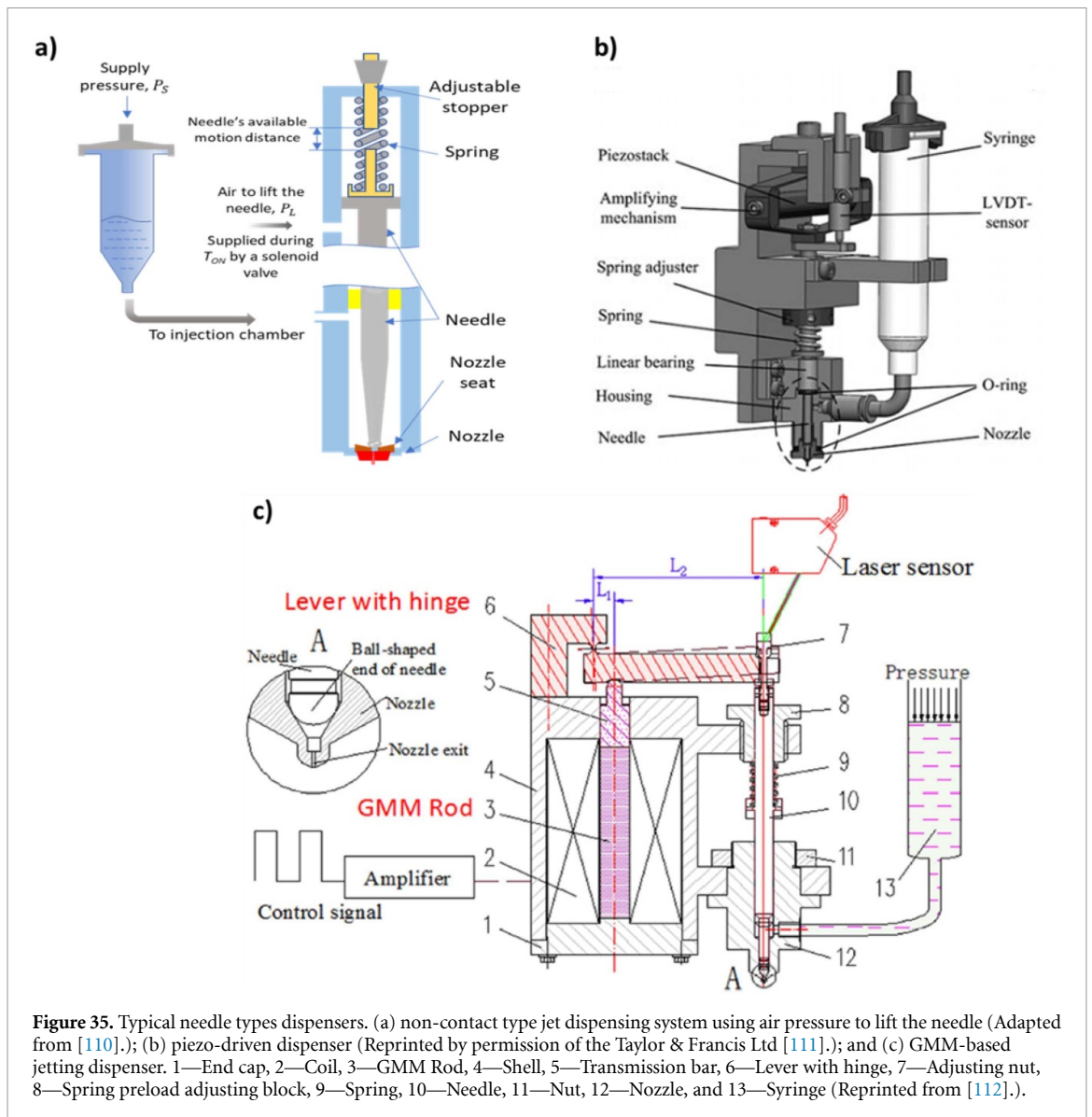


Figure 35. Typical needle types dispensers. (a) non-contact type jet dispensing system using air pressure to lift the needle (Adapted from [110].); (b) piezo-driven dispenser (Reprinted by permission of the Taylor & Francis Ltd [111].); and (c) GMM-based jetting dispenser. 1—End cap, 2—Coil, 3—GMM Rod, 4—Shell, 5—Transmission bar, 6—Lever with hinge, 7—Adjusting nut, 8—Spring preload adjusting block, 9—Spring, 10—Needle, 11—Nut, 12—Nozzle, and 13—Syringe (Reprinted from [112].).

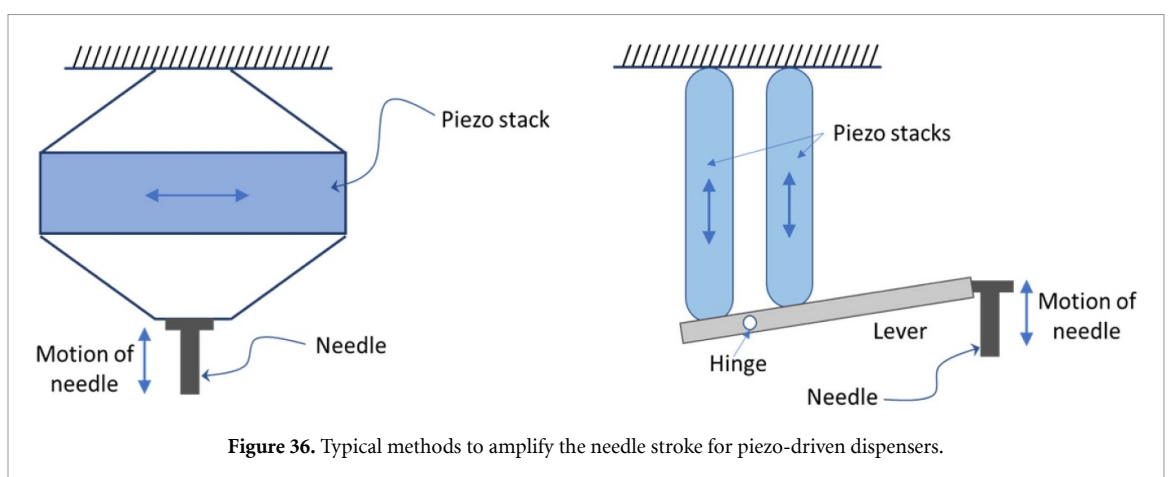
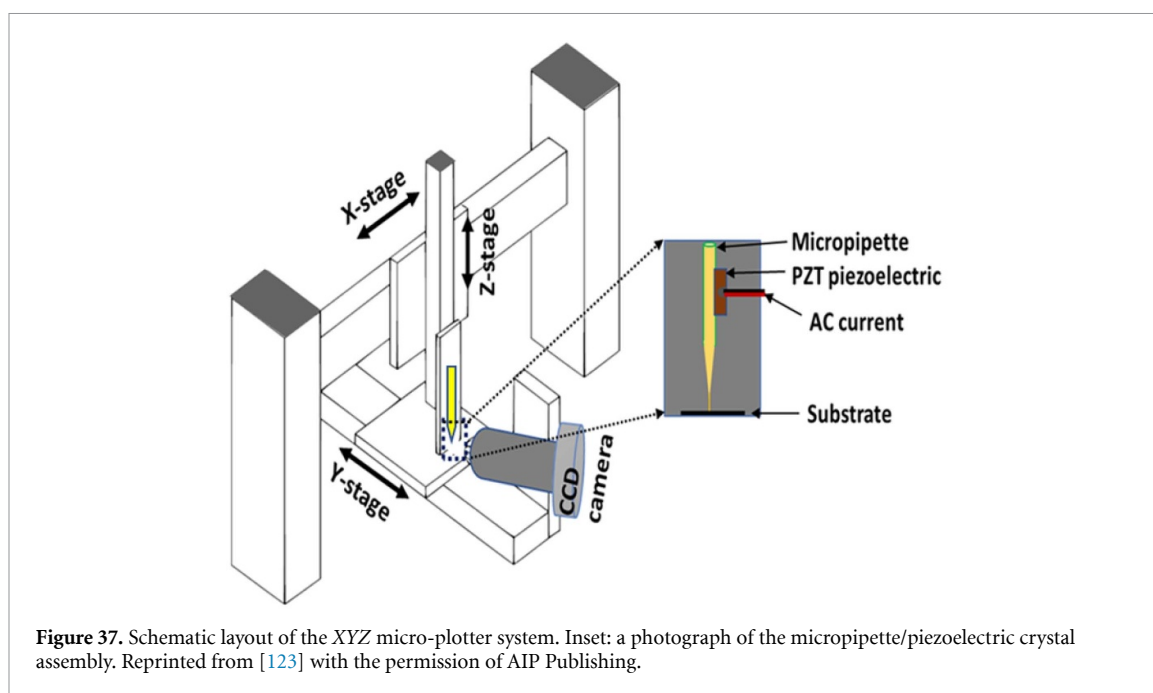


Figure 36. Typical methods to amplify the needle stroke for piezo-driven dispensers.

height information. The optimal stand-off distance ($\sim 2 \mu\text{m}$) between the micropipette tip to substrate surface should be maintained in order to properly deposit the droplets [124].

The frequency of AC driving voltage for the piezo actuator is in the range 400–700 kHz with 1–4 V

peak-to-peak driving voltage. Then, the ultrasonic vibration causes the fluid in the tip (inner diameter, ID, ranging from $1 \mu\text{m}$ to $100 \mu\text{m}$) to wick out onto the surface. In general, smaller micropipette IDs produce smaller dots on the substrate. The size of the deposited droplets can also be controlled by raising



or lowering the amplitude of the peak-to-peak amplitude of AC voltage. Since micro plotters can dispense ink with high viscosity as well as high particle concentration, it can fabricate patterns with high aspect ratios. After completing the printing of continuous features such as lines or arcs, the AC driving signal for the piezo actuator is shut off and the micropipette dispenser tip is raised.

The deposition speed about 1 mm s^{-1} was considered to be optimal to print desired patterns with uniform line width. Note that the thickness of a printed line could be increased by using a lower printing speed. However, excessive ink deposition could lead to non-optimal drying conditions or flowing of the deposited ink on substrates [133, 134].

3.3. Aerosol jet printing

The AJP method is a non-contact direct-writing method, which allows the deposition of various functional materials with a wide range of viscosities (1–2500 mPas) [135]. This non-contact process enables printing over non-flat surfaces with less than $10 \mu\text{m}$ feature size. A schematic of the AJP method illustrating its working principle is shown in figure 38. As shown in figure 38, the ink is stored in a reservoir and ‘atomized’ into a fine mist of material having droplets of different sizes. For the atomization, dry nitrogen gas (N_2) as a carrier gas was applied over the ink surface in a pneumatic atomizer while an ultrasonic atomizer is used as an additional atomization power source. Here, generated droplets bigger than $5 \mu\text{m}$ returned back into the ink reservoir due to the force of gravity. The finer droplets with dimension less than $5 \mu\text{m}$ are propelled by the N_2 gas stream towards the deposition nozzle. Before reaching the deposition nozzle, a device called virtual impactor

removes the excess carrier gas and increases the density of the aerosol stream to enhance the deposition as shown in (figure 38). At the deposition nozzle, a second flow of dry N_2 gas (the sheath gas) surrounds and compresses the aerosol stream as it passes through the nozzle. This results in focusing of the jet stream, thereby reducing the spray-over. The stream of ink particles is then deposited onto the substrate, and is capable of forming fine features ($<10 \mu\text{m}$) [125, 136, 137]. Since it is based on a continuous jet, a mechanical shutter is used for on-off control of the jet [135]. Since, the deposited material is not in the form of liquid but has the form of an atomized jet, the printed patterns could have high aspect ratios [138].

In order to obtain printed lines with high-resolution and high-aspect ratio, the focusing ratio (FR), (the ratio of sheath gas flow rate and carrier gas flow rate) plays important roles [125, 139–141]. The required ranges of FR also depend on the ink formulation. In general, the printed line width decreases with increasing the FR and printing speed, or vice versa [139, 140].

In order to obtain fine patterns, over-spraying conditions should be avoided. The inner diameter of the nozzle should be used in range of 100 and $300 \mu\text{m}$ and the stand-off distance should not exceed more than 5 mm to avoid overspray of the deposited droplets [139, 141]. Note that improper temperature of the heated substrate holder often affects the jet stream and could cause overspray. It has been reported that the temperature should be limited in the range of $40\text{--}80 \text{ }^\circ\text{C}$ in order to avoid overspray [125, 141]. The overspray effect was also observed in the case of fast drying of the aerosol droplets by sheath gas. To reduce such drying effects, low volatile cosolvent (tetralin) (about 10%) can be added in the ink formulation [137, 140].

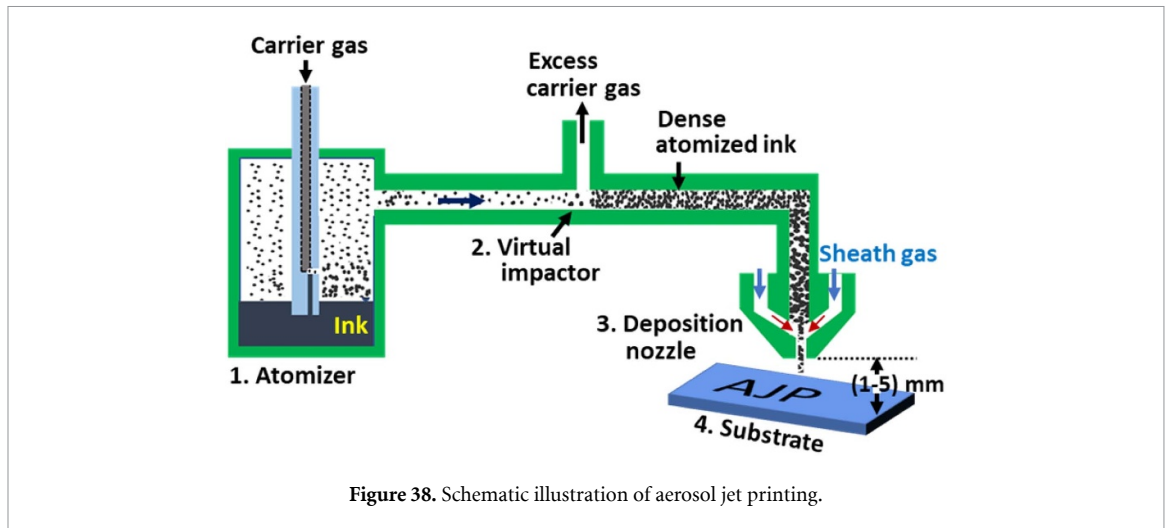


Figure 38. Schematic illustration of aerosol jet printing.

Since this technique is based on non-contact aerosol jet deposition, it can print complex patterns on non-planar substrate as it is less affected by substrate conditions. Recently, complex conformal surfaces (3D printed electronics) printing have been demonstrated by controlling the position in z-direction of the writing head over the substrate [142, 143]. Various materials (conductive polymers, organic semiconductors, dielectrics, novel materials, bio-materials) can be deposited by using an aerosol jet [144, 145]. However, the printing parameters may need to be changed and adjusted for finding optimal jet conditions if any new inks are considered for printing [137]. In general, equipment for AJP is far more expensive compared to other direct writing printing systems because of the additional units required for the generation of the droplet mist and the focused carrier gas stream [145].

3.4. EHD jet printing

The EHD jet printing method has been drawn attention because it could produce very small patterns or dots (less than a few micrometers) for various applications [18, 146]. The EHD method uses electrostatic forces to extract (or ‘pull down’) the jet from the nozzle tip for DOD and continuous jet printing as shown in figure 39, while conventional inkjet printing methods rely on thermal or acoustic energy to ‘push’ the droplet out of the nozzle [146–148].

Using conventional inkjet printing, a jetted droplet with a less than 0.1 pl might not reach the substrate since its kinetic energy can often be too small. For example, a jetted small droplet with a few micrometer diameter (for example, satellite droplets) could float in the air (or fly away from the target position) instead of being directly deposited on the substrate. However, EHD uses a pull down mechanism via electrical field and very tiny droplets can be placed on a target location of the substrate.

The EHD jet printing method can be divided into two methods: (a) drop on demand printing;

Table 4. Comparison of drop on demand (DOD) EHD jet and NFES printing methods.

Method	DOD EHD jet	Near field electrospinning (NFES)
<i>Ink supply to nozzle tip</i>	Air pressure (constant pressure) or syringe pump (constant flow rate)	Syringe pump (constant flow rate)
<i>Driving voltage</i>	Pulse superposed by DC voltage	DC voltage only
<i>Nozzle size (inner diameter)</i>	Less than 50 μm (Typically, few micrometers)	More than 100 μm
<i>Ink viscosity</i>	Up to 100 mPas	More than 1000 mPas (Normally polymer with high molecular weight can be added.)
<i>Printing speed</i>	Typically, less than 1 mm s^{-1}	More than 200 mm s^{-1} (continuous jet)
<i>Dot based printing</i>	Possible	Impossible

(b) continuous jet printing based on near field electrospinning (NFES) [127, 147, 148] as shown in figure 39. The basic principles for these two modes of EHD are similar, but the fluid system, driving voltage, nozzle requirement and ink viscosity differ according to the printing modes as shown in table 4.

For DOD EHD jet printing, the pulse driving voltage is applied either on a nozzle part or the substrate in order to generate one droplet per pulse voltage as shown in figure 39(a). Air pressure is often used for supplying ink to the nozzle tip while a constant flow rate using a syringe pump can be used in case of ink with higher viscosity. However, it should be noted that a continuous ink supply using a syringe pump may not be suitable for DOD printing methods.

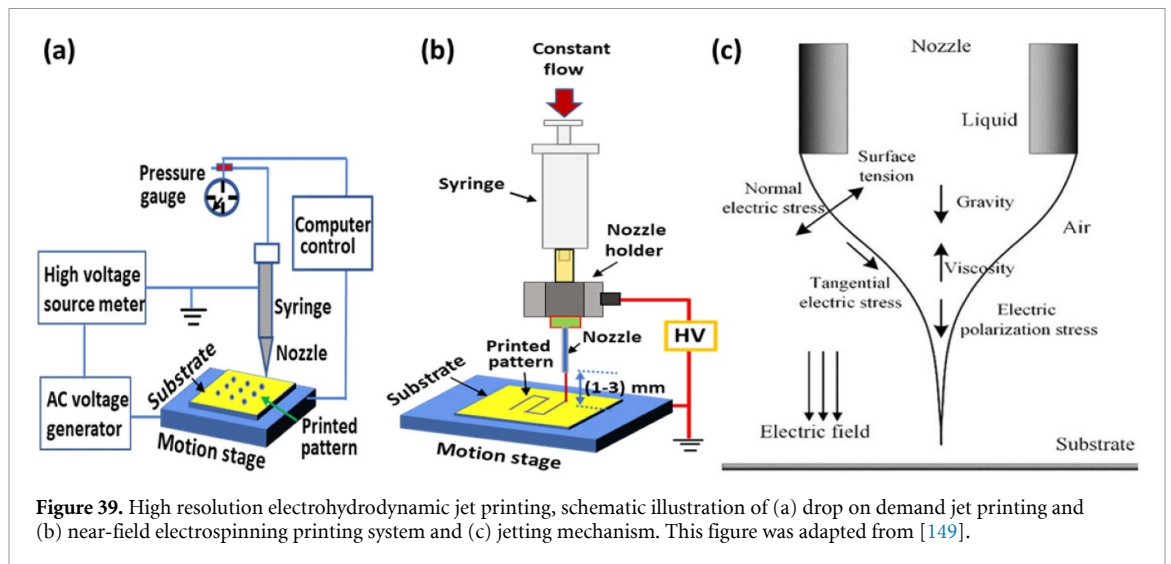


Figure 39. High resolution electrohydrodynamic jet printing, schematic illustration of (a) drop on demand jet printing and (b) near-field electrospinning printing system and (c) jetting mechanism. This figure was adapted from [149].

Drop on demand EHD jet uses relatively low viscosity ink (less than 100 mPas) for producing single droplet jetting per pulse voltage [129]. However, the use of ink with high viscosity has been of interest in the various fields of research and industry. The implementation of DOD jetting using ink with high viscosity (more than 100 mPas) is still challenging for most applications.

On the other hand, NFES printing uses high viscosity ink, which contains polymer with high molecular weight. The proper mixing ratio of polymer and functional ink is important to obtain a stable continuous jet for printing. For straight line printing, printing speed should be fast with a few millimeters stand-off distance. In fact, the method is called NFES due to the relatively short stand-off distance in contrast with conventional electrospinning. In conventional electrospinning, the charges from the deposited pattern will generate repulsive force resulting in irregular patterns, as shown in figure 40 [150].

To obtain the desired patterns using NFES printing, a masking method has been used to remove the unwanted part after the printing process, as shown in figure 41 [127]. Note that the low printing speed region due to acceleration and deceleration of motion should be discarded because of the irregular patterns.

The line width is related to flow rate, nozzle size, ink properties, electrical field intensity and printing speed. Figure 42 shows the typical printed results according to flow rate.

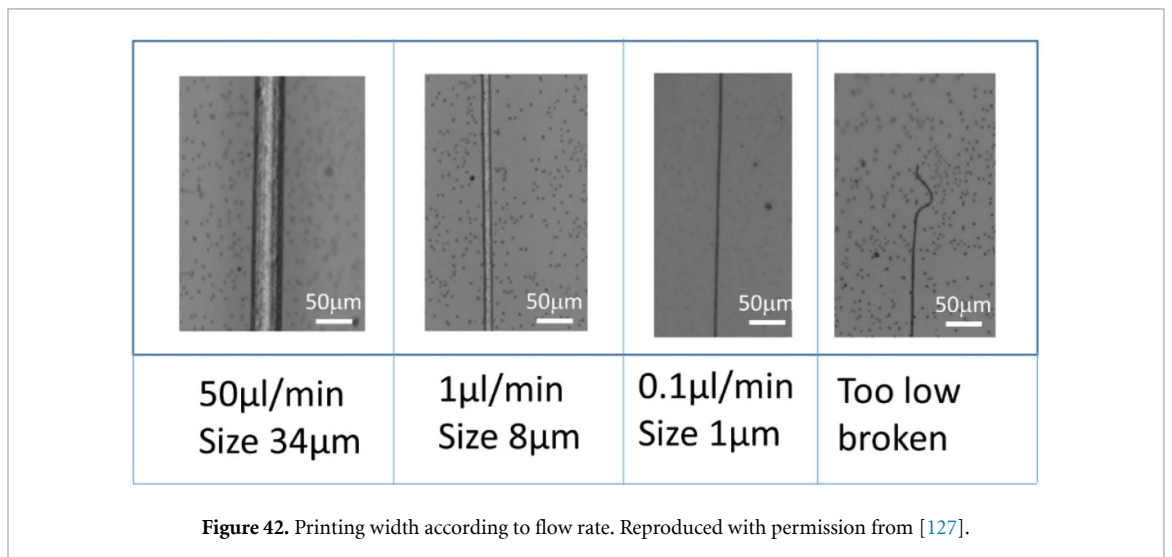
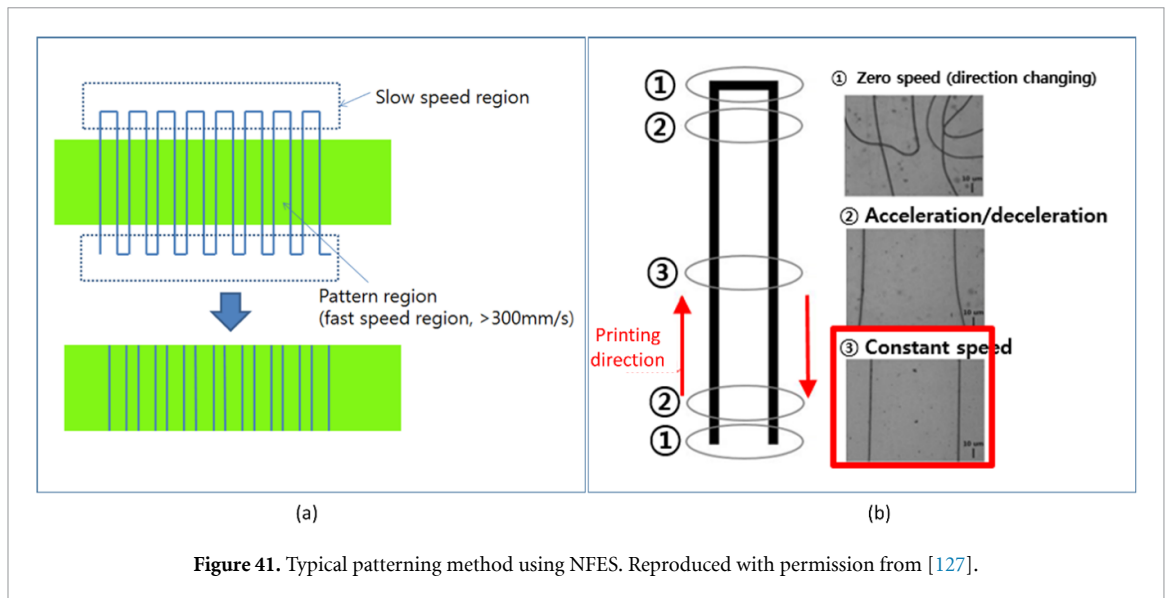
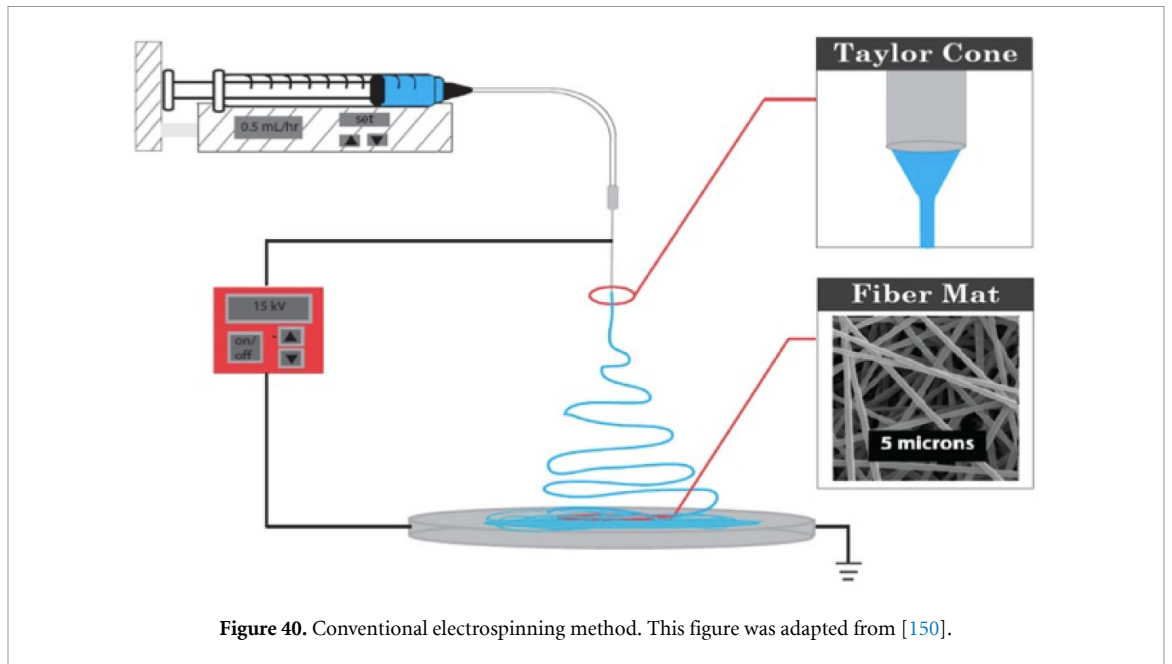
The classifications of EHD methods as NFES and DOD EHD are based on the most recent implementations. Different approaches can be used in order to enhance the printing process. For example, hybrid methods are proposed to use the advantages of each method [129].

It should be noted that EHD jetting performance is highly dependent on substrate conductivity. In case of highly insulating substrates, such as (Teflon $\sim 10^{-25} \text{ Sm}^{-1}$ and polyethylene terephthalate (PET)

film $\sim 10^{-21} \text{ Sm}^{-1}$ etc), proper droplet deposition may be difficult [151, 152] since the charge decay rate on such insulating substrates is very slow. The residual charge on a substrate will change the electrostatic field distribution and may interrupt the subsequent jetting. To solve this issue, methods for neutralizing charges on the substrate were proposed in order to generate alternating charged droplets via a sinusoidal AC voltage [130, 153].

3.5. Tonejet—multi-nozzle implementation of DOD EHD jet printing

Although the DOD EHD-jet printing process offers various advantages of fine pattern printing, most of its implementations are limited to research purposes. The low throughput has been the main reason for limited industry applications because of single nozzle implementation with very low printing speed (1 mm s^{-1}) [147, 154]. In order to overcome this problem, printing using multi-nozzle print-heads still remains as one of the important industry challenges. A multi-nozzle implementation has been proposed but most previous studies are limited to research purposes because of low nozzle density [155, 156]. Note that the nozzle to nozzle distance should be more than 2 mm to avoid cross-talk during multi-nozzle printing [157]. Despite this, using a method similar to DOD EHD jet, Tonejet have commercialized multi-nozzle print-head for electrostatic jet. By using the electrostatic jet print-heads, graphic images have been printed on non-flat surfaces such as beverage cans [158, 159]. From their print-heads, droplet volume 0.4–2.0 pl equivalent to approximately 20–30 μm dot size can be generated [160]. The droplet size is comparable to that of conventional inkjet droplets. In Tonejet print-heads, the nozzle size is big enough to insert an electrode. The electrode extends beyond the nozzle opening and the charge is concentrated near the electrode tip before jetting. The ejected droplets have a concentration of particles up to 20



times greater than the bulk ink [160, 161]. With their higher solids loading and relatively low solvent carry over, these concentrated droplets are highly viscous when ejected. Therefore, by ejecting drops with the higher density of particles as shown in figure 43(a), the printed pattern could have higher aspect ratios. Figure 43(b) illustrates the multi-nozzle electrostatic jets, which could be potentially useful for printed electronics applications due to the multi-nozzle features and higher solid loading features.

4. Printing algorithm for printed electronics

Most digital printing methods use bitmap images as printing information. Bitmap image printing is suitable for complicated patterns based on DOD or dot-based printing. In the case of graphics printing, the grey scale or color bitmap image should be converted into binary images for printing. Most graphic printing uses raster image processing algorithm to obtain half-tone binary images [162, 163]. However, graphics printing focuses on visual representation of images whereas printed electronics requires connectivity of dots, lines or areas for signal or electrical current pathways. As a result, the bitmap image requirement for printed electronics should be different from that of graphics printing. Note that the dimension and precision requirements for droplet placement are also much higher than those of graphics applications. For this purpose, it is recommended to use CAD software to generate patterns with exact dimension and location. Then, CAD information can be used for two different printing modes: (a) conversion of CAD information into bitmap image for raster printing; (b) the direct use of the CAD information for vector printing [164]. Note that vector printing is directly based on CAD coordinate information to move XY stages. Here, printing is performed via jetting control based on constant frequency or constant distance [164]. Figure 44 shows the printing process of using CAD software for two different printing modes [163].

4.1. Raster printing for printed electronics

The physical dimensions of printing patterns are related to the physical distance of the pixels in the binary image, or the printing resolution. In case of printing applications, one pixel in a bitmap image means one droplet (dot) placement. In general, the pixel spacing in the X and Y direction has the equal value in graphics applications. However, in printed electronics patterns, the X and Y pixel spacing might be different according to the directions. Note that the X direction image pixels are intended to be matched with nozzle spacing of multi-nozzle printing head. In case of commercial inkjet head, nozzle spacing has the unit of dpi. So, the bitmap image with resolution

defined by dpi are commonly used for graphics printing. However, in case of printed electronics applications, the required dot spacing may not be related to nozzle spacing. For non-matching nozzle spacing and image dot spacing, unmatched nozzles should not be used for jetting, which is an inefficient use of most nozzles. One simple method to solve this problem is to use tilted print-head with respect to the moving direction. In this way, the projected nozzle spacing could be matched with the bitmap pixel distance as shown in (figure 45).

CAD information can be converted to bitmap images with the right size and information [162]. Most CAD software has a capability of converting drawing information into bitmap images. The number of pixels of converted bitmap images will be different according to physical size of the patterns and one-pixel distance. Figure 46 illustrates the image size in relation to drop (pixel) interval distance. For example, the 2 mm line in the CAD will be converted to 20 pixels in case of defining one-pixel distance as 100 μm while it will be 200 pixels in case of defining one-pixel distance as 10 μm .

Since the bitmap image itself does not have any physical dimension information, printing software needs the pixel distance to be determined in order to define jetting triggering location and printing location movement. The pixel distance (droplet spacing) should be determined based on the deposited dot size, which is related to nozzle size of inkjet print-head, driving voltage and substrate condition. In general, when dot size is given as d_{dot} , dot spacing should be $d_{\text{dot}}/\sqrt{2}$ to form a connected area or line.

To understand bitmap image conversion effects in relation to pixel distance, an example of CAD information having ten lines with spacing 100 μm was converted to bitmap images by varying pixel distance of 25, 50, 75 and 100 μm . As shown in figure 46(b), the converted image is far from the original intended patterns in case of 75 and 100 μm . It has been discussed in [162] that the image resolution (pixel distance) should be at least two times better (smaller) than that of the density of lines or patterns in order to represent the pattern shape in the bitmap image.

Even though bitmap images represent patterns, the printed results can be different according to the droplet size and substrate conditions (surface energy and heating conditions). For example, figure 46(c) shows the printed results of four bitmap images when the dot size on the substrate was about 60 μm . As shown in figure 48(c), the printed results are quite different from the bitmap images. For example, in case of image resolution of 25 μm , the droplets are deposited with spacing of 25 μm . In such case, too much deposition will cause overflow to the adjacent lines. However, if the pixel distance (drop interval) becomes longer than the dot size, the drop will not be connected properly. In case of using 60 μm dot size, the dot spacing for connected lines (areas) would

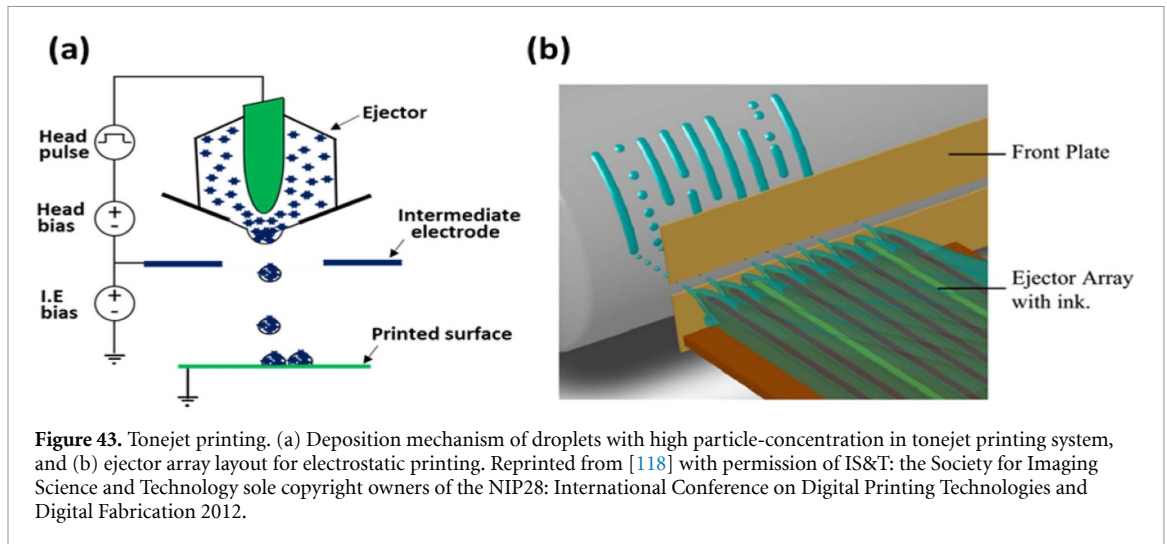


Figure 43. Tonejet printing. (a) Deposition mechanism of droplets with high particle-concentration in tonejet printing system, and (b) ejector array layout for electrostatic printing. Reprinted from [118] with permission of IS&T: the Society for Imaging Science and Technology sole copyright owners of the NIP28: International Conference on Digital Printing Technologies and Digital Fabrication 2012.

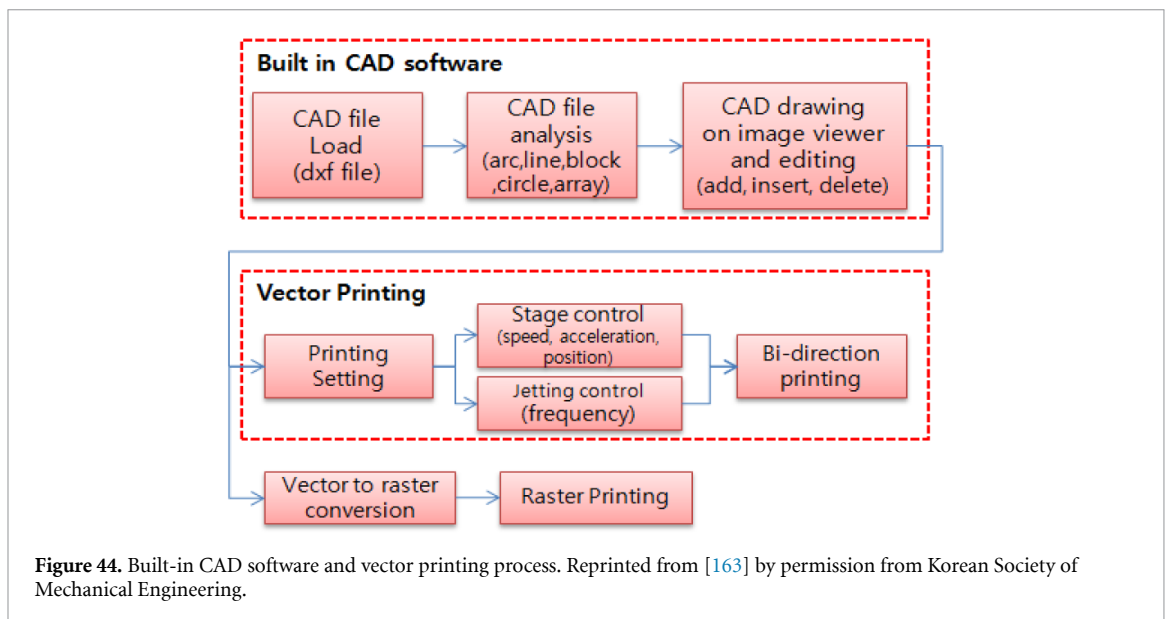


Figure 44. Built-in CAD software and vector printing process. Reprinted from [163] by permission from Korean Society of Mechanical Engineering.

be about $d_{\text{dot}}/\sqrt{2} = 42 \mu\text{m}$. Note that the requirement of drop interval is based on assumptions about the dried drops on the substrate. If un-dried droplets can be deposited, the droplets could be merged and connected to form lines or areas. So, the droplet spacing should consider various conditions unless deposited droplets are dried or cured prior to deposition of other droplets. For example, a line was well-connected using a spacing of $50 \mu\text{m}$ without overflow into the adjacent lines as shown in figure 46(c). On the other hand, in the case of droplet spacing (pixel distance) larger than the droplet size, the dot will be separated and the bitmap pattern cannot be used as a conduction line for electrical current pathway, as shown in figure 46(c).

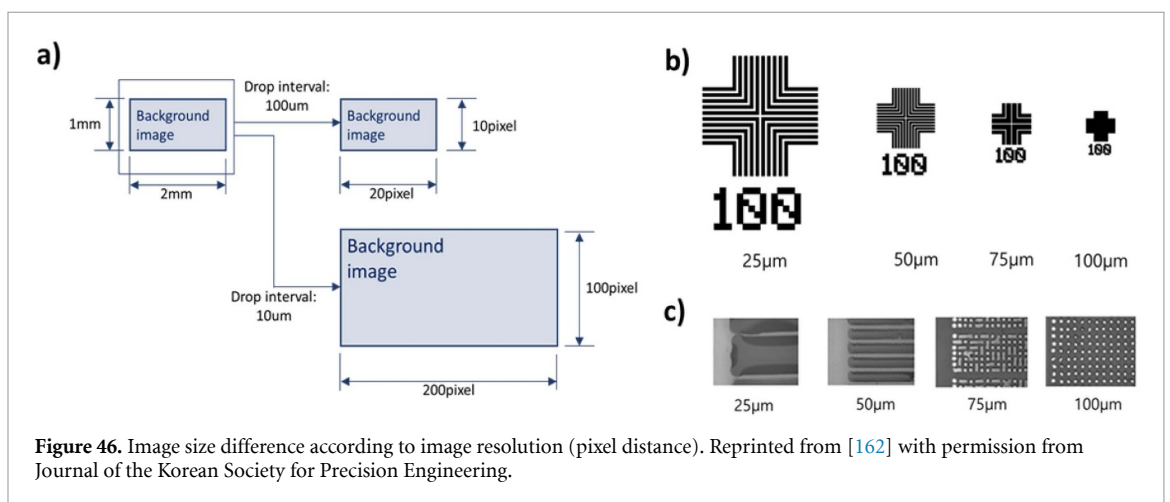
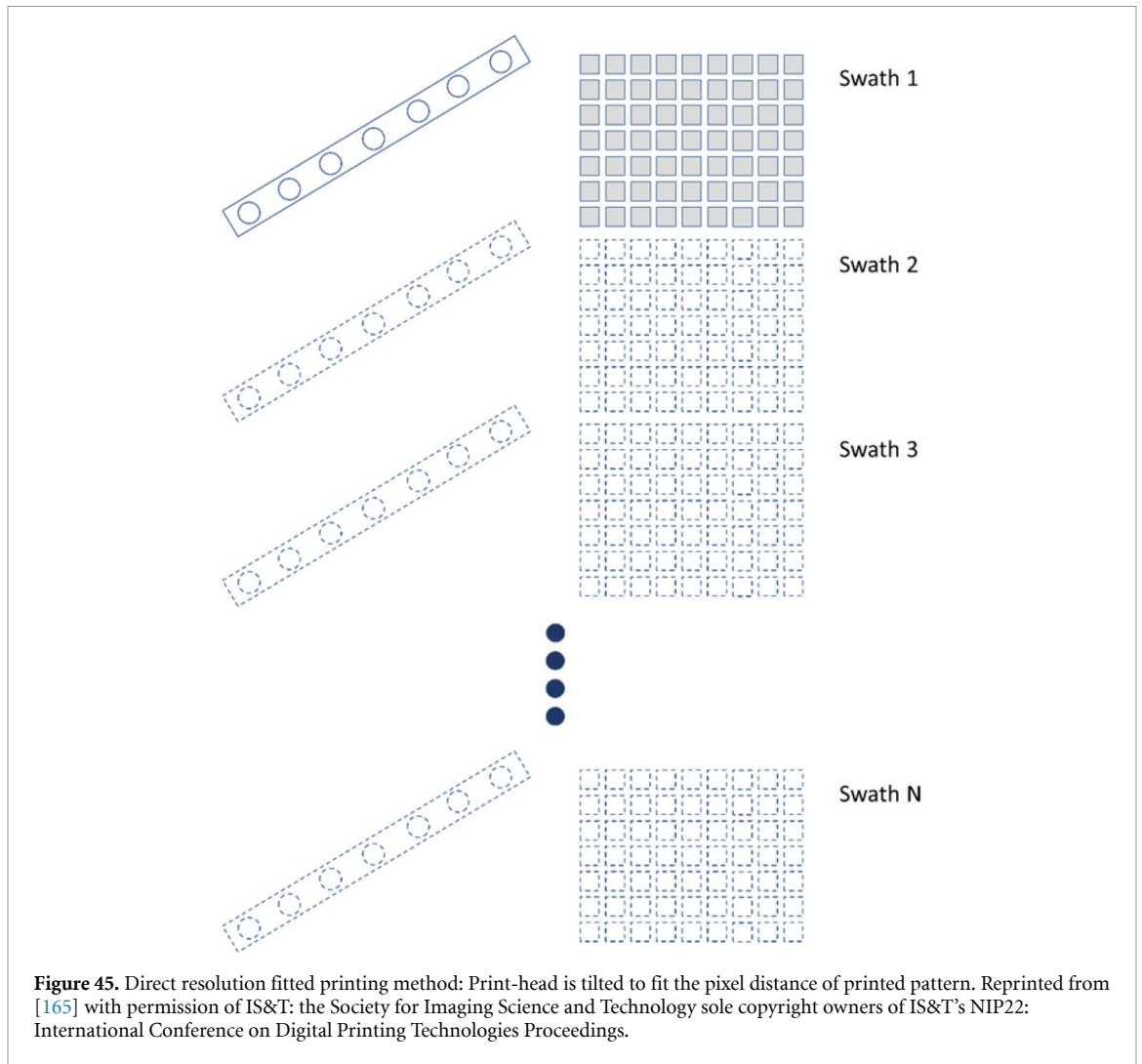
During bitmap image conversion and printing, some of the information could be lost or modified. To maintain printing quality, the converted patterns may need correction or modification. Chiu *et al* proposed a trimming method to enhance printing quality for inkjet printing circuits as shown in figure 47 [4]. The

method includes pattern trimming, smoothing the printed edge by canceling printed dots, compensating the boundary of filter image, and lengthening the printing trigger according to substrate thermal expansion.

4.2. Vector printing for printed electronics

In the case of single nozzle printing, vector printing method can be effective. The vector information can be easily generated by CAD and does not require any conversion of the data. For this reason, most of the single nozzle systems including EHD, aerosol jet, dispenser and Sonoplot micro-plotter rely on the vector printing method. In the case of two-dimensional (2D) vector printing, the XY simultaneous motion information is generated according to CAD coordinate information, just like XY plotter. The jetting or printing signal is applied during the movement of XY stages.

Most 2D printing systems can get the printing information from Drawing Exchange Format



or Gerber file format from CAD while 3D printing software uses G-code generated from stereolithography file.

Since most vector printing methods are based on single nozzle printing, the printing process could be slower than that of using multi-nozzle print-heads. Therefore, it is important to increase the vector printing speed. However, there are many limitations for

increasing printing speed. For example, jetting frequency could be less than 1 kHz in case of EHD jet printing, which could result in typical printing speed of less than 1 mm s⁻¹. As a result, the fine patterning methods could be limited to research purpose or specific applications, which do not require fast printing process. Recently, fast jetting mechanism of hybrid EHD method using the merits of DOD and NFES was

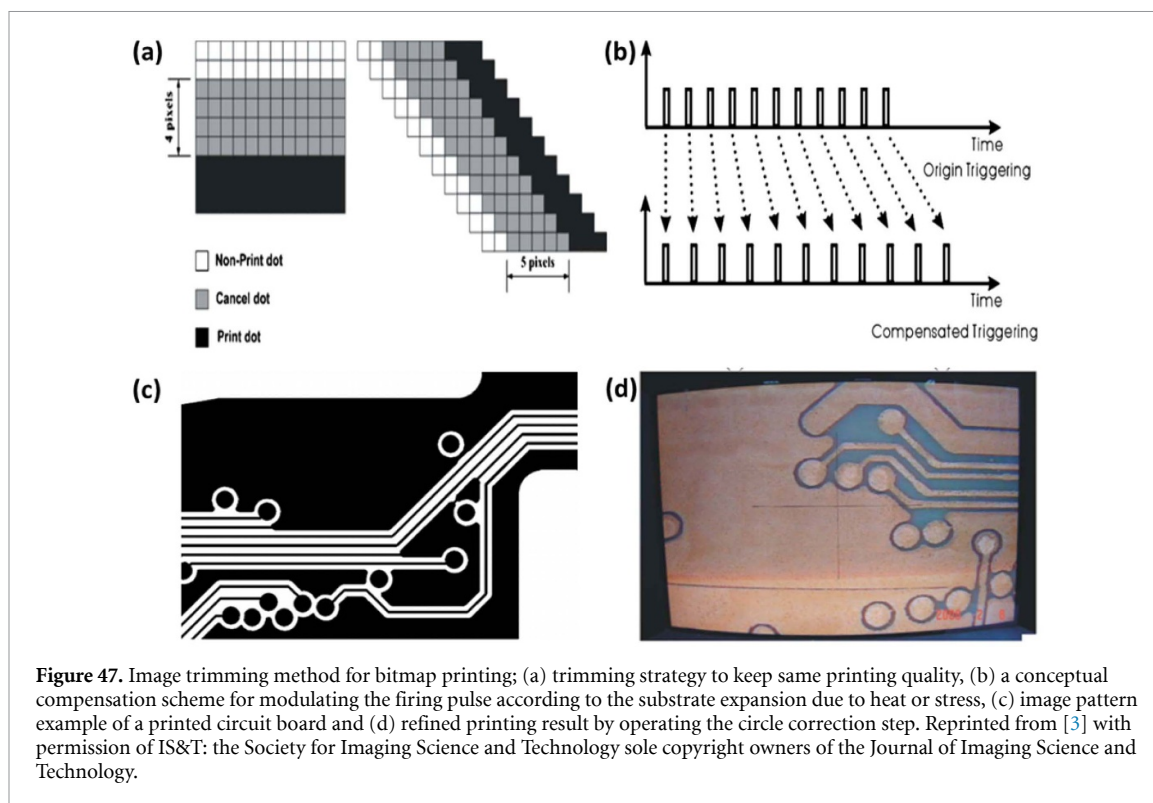


Figure 47. Image trimming method for bitmap printing: (a) trimming strategy to keep same printing quality, (b) a conceptual compensation scheme for modulating the firing pulse according to the substrate expansion due to heat or stress, (c) image pattern example of a printed circuit board and (d) refined printing result by operating the circle correction step. Reprinted from [3] with permission of IS&T: the Society for Imaging Science and Technology sole copyright owners of the Journal of Imaging Science and Technology.

proposed [129]. Another issue of high speed vector printing is that the end point of the lines is affected with greater deposition than elsewhere [164]. To solve this issue, the use of both X and Y encoder signals was proposed to generate jetting trigger signals based on equally spaced moving distance [164]. Due to such efforts, printing speed can be significantly increased up to 50 mm s^{-1} as shown in figure 48.

Panreck *et al* [166] reported the comparative study of vector printing process by using two different fine patterning technologies of aerosol jet-printing and micropipette-dispensing (Sonoplot or Microplotter) as shown in figure 49. Note that both vector printing processes could produce patterns with continuous features (in contrast to what can be achieved with droplets during inkjet printing). Even though the printed results looked similar, aspect ratios and printed characteristics might be different according to printing methods [166].

5. Inkjet printing for display applications

In this section, as a non-graphics application, recent inkjet printing applications for displays such as liquid crystal display (LCD) and organic LED (OLED) [2] are presented. The reason why inkjet printing technology is applied to display manufacturing technology is that manufacturing cost could be significantly reduced by replacing expensive photolithography and processes requiring high vacuum technology. In addition to reducing material costs, inkjet printing technology can easily be scaled up to large-area substrates of 8th generation or more.

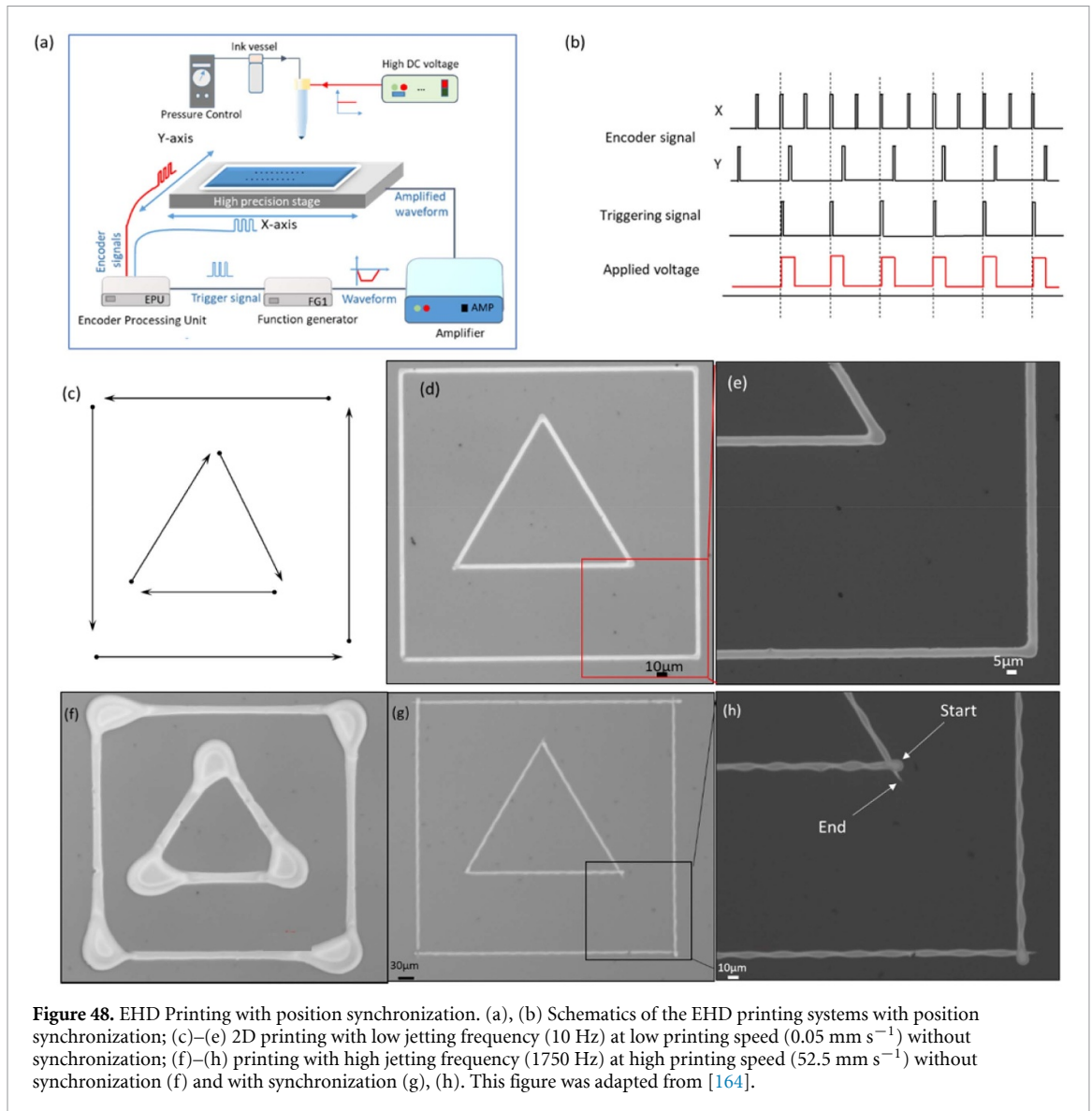
Figure 50 compares the structure of LCD and OLED displays. In case of LCD display, the inkjet process technology has been used for manufacturing color filter and polyimide (PI) film for liquid crystal alignment. On the hand, in case of OLED displays, the first inkjet implementation was an encapsulation film process for protecting organic pixels and cathode electrodes from oxygen and moisture. As a next-generation OLED pixel process technology, efforts are being actively made to make common layers and RGB light emitting layers by the inkjet printing method.

5.1. LCD color filter inkjet printing

As a first inkjet application, many display companies and research institutes developed inkjet printing technology for fabricating the color filter in LCD displays [167–170]. The commercial LCD products with inkjet-printed color filters were introduced by Samsung and Sharp companies.

The composition of the color filter ink consists of a color pigment, an acrylic binding polymer, a thermosetting resin, and a thermosetting agent, as shown in the following figure 51(a). To increase inkjet jettability and jetting reliability, high boiling point solvents were used for the color filter ink. In addition, substrate treatment was required in order to suppress printing defects. For example, hydrophobic BM (Black Matrix) with strong liquid-repellent properties was often used to prevent ink overflowing out of the BM.

Printing stains (mura) caused by the difference in the quantity of ink dropped on each adjacent pixel must be controlled because it degrades the color filter



characteristics. The DPN technique has been used for minimizing the deviation of the amount of ink droplet ejected among the print-head nozzles as discussed in figure 8 (section 2.3).

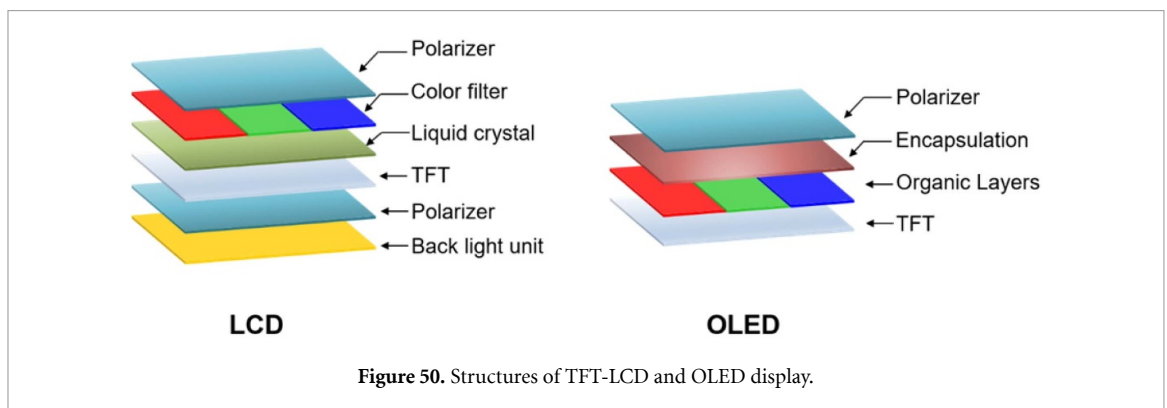
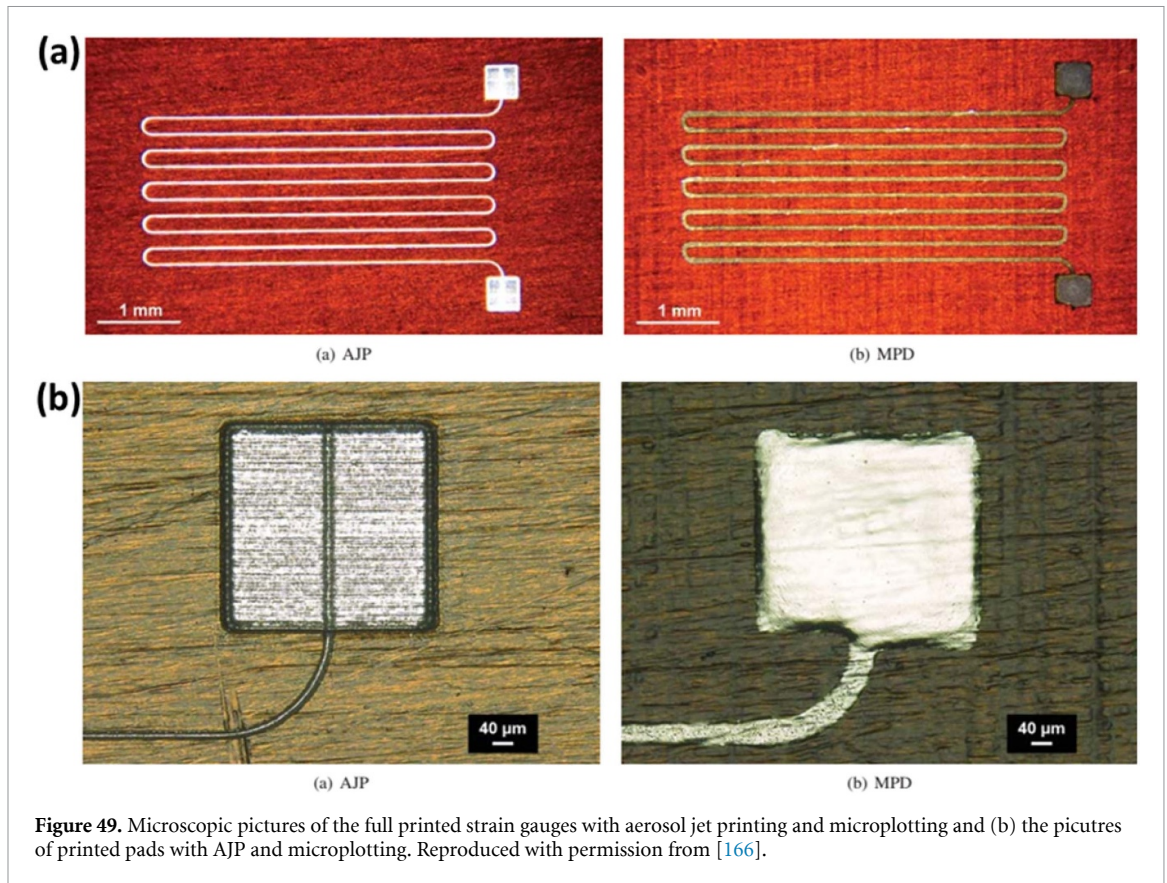
In order to implement DPN technology, the amount of droplet ejected from each nozzle should be measured accurately. For this purpose, various methods have been used including weighing ink using a scale, measuring the volume of ink using a vision camera, measuring the area of ink dropped on a paper substrate, or measuring the transmittance of a printed film. If the printing stains are persistent even with the DPN technology, a printing algorithm such as nozzle grouping has been used as a secondary method, as shown in figure 52 [167]. The printing algorithm have led to significant reduction in print stain due to the droplet amount averaging effects among nozzles.

5.2. PI printing in LCD application

The liquid crystal alignment layer is placed on the surface of the ITO (Indium Tin Oxide) anode and cathode. In the early stage of LCD technology, the

layer had been coated onto the glass substrate using a roll printing technique with a flexible relief plate as shown in figure 53(a). However, as the display substrate is enlarged, it is difficult to form an alignment film having uniform thickness over a large area. As a result, image quality has been seriously impaired. In order to overcome this drawback, a non-contact inkjet method has been developed for deposition of alignment film as shown in figure 53(b). Since the mid-2000s, PI coating process has been performed through the inkjet printing process.

Generally, PI is synthesized by pyrolysis reaction of polyamic acid made by reaction of pyromellitic dianhydride, an aromatic anhydride and aromatic diamine 4,4'-oxydianiline as shown in figure 54 [171]. Since PI has a very low solubility in a typical organic solvent, the synthesized polyamic acid is dissolved in a high polar solvent such as *N*-Methyl-2-pyrrolidone to make a PI ink for inkjet printing [172]. When the printed polyamic acid is heat-treated, a PI alignment layer is formed on the surface of the substrate through a dehydration reaction.



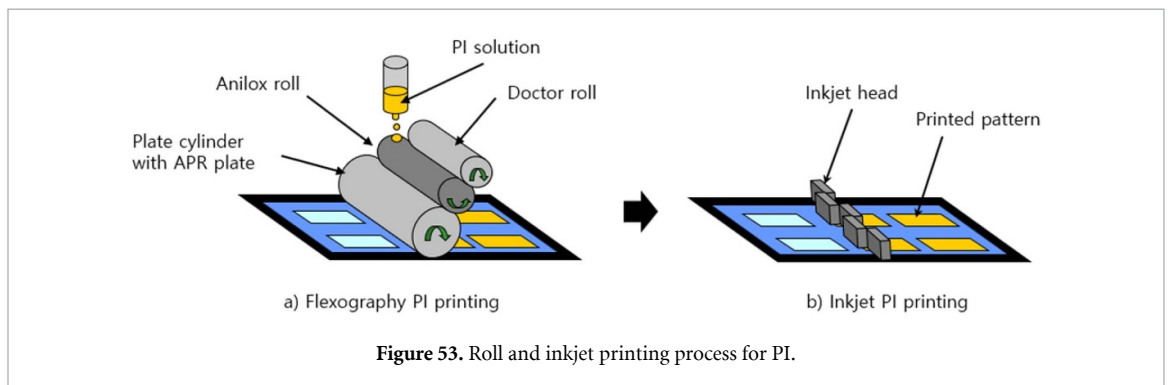
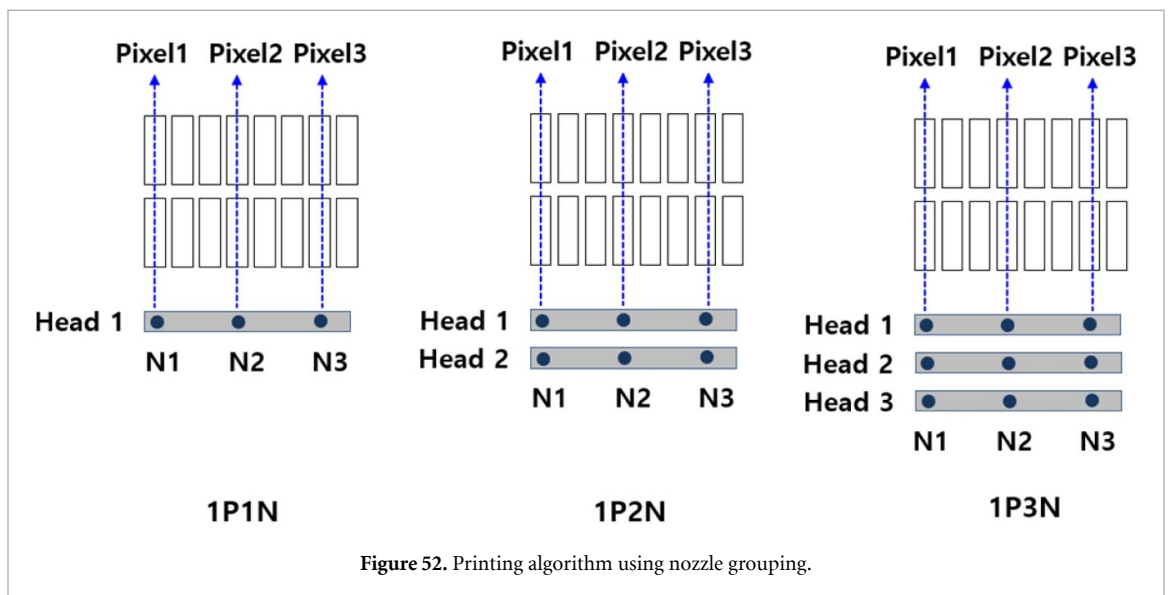
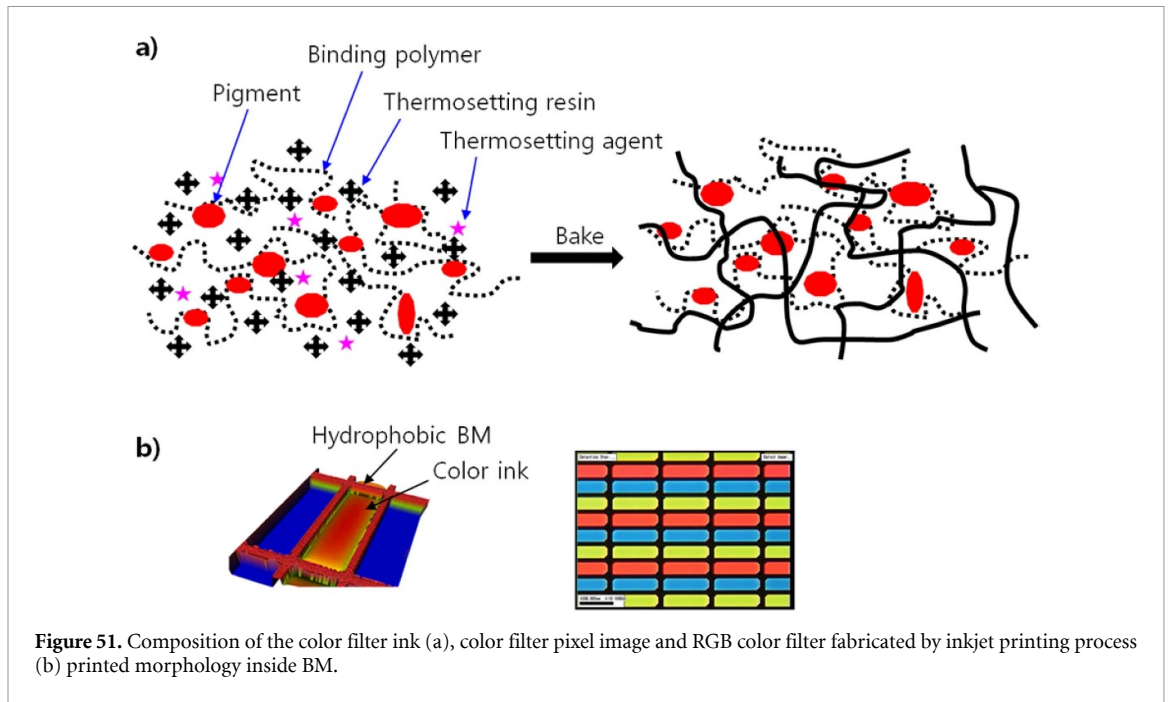
The printed PI thickness on the surface of ITO glass is less than 1000 nm, and the thickness deviation of glass should be controlled to less than 5%. Therefore, DPN technology has been required in PI inkjet printing process. To reduce printing stains caused by thickness variations, the surface of the ITO glass must have strong hydrophilic characteristics prior to inkjet printing process so that the printed PI liquid can evenly spread on the surface. Generally, oxygen atmospheric plasma has been used to obtain a hydrophilic surface.

5.3. OLED inkjet printing for the thin film encapsulation (TFE)

OLED devices are sensitive to humidity and oxygen and exposure to these environments could shorten operation lifetime of OLED display [173, 174].

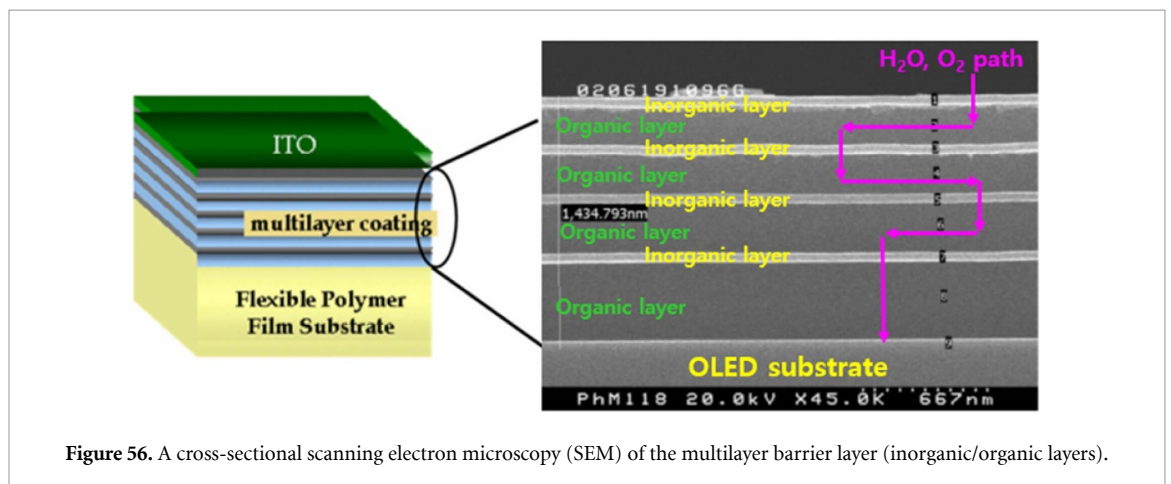
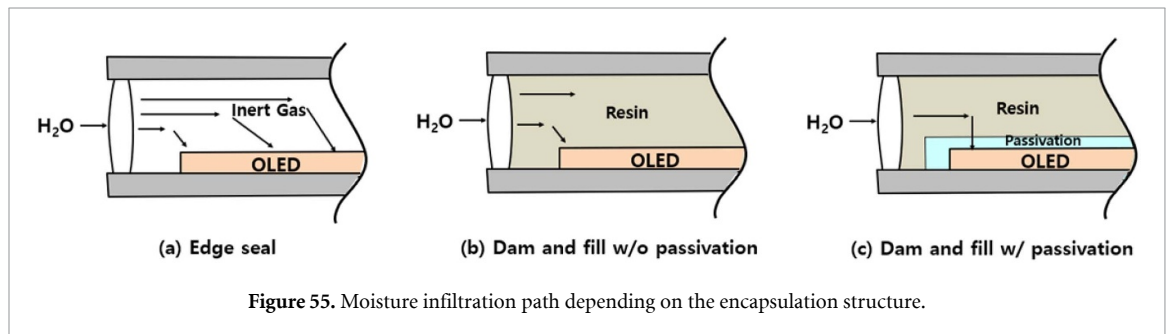
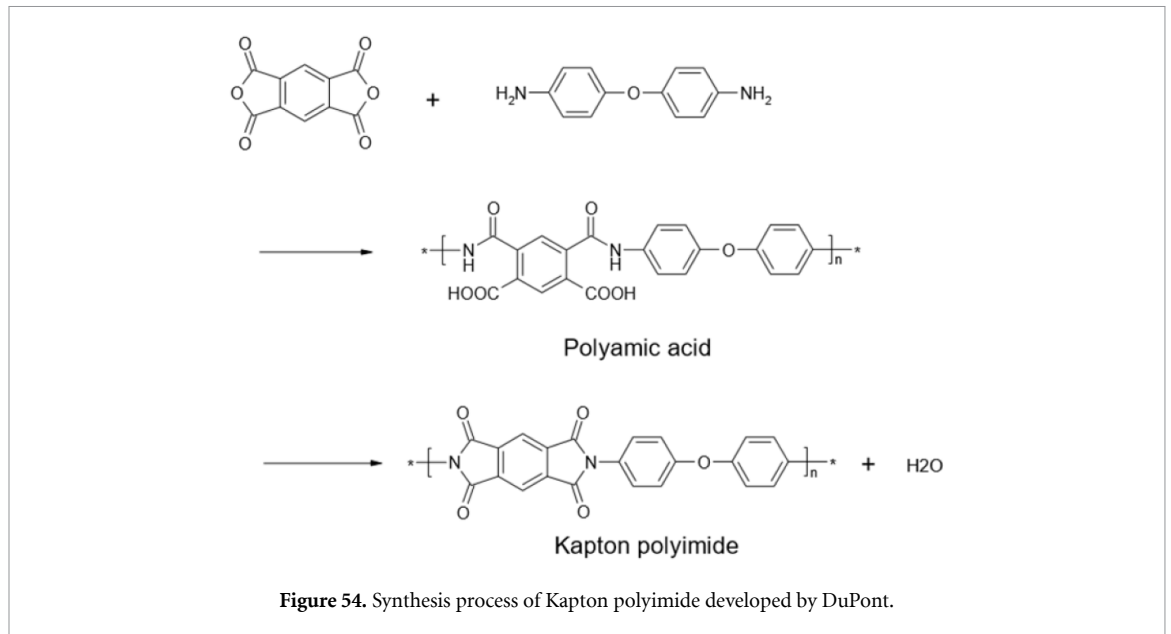
Hence, effective encapsulation technology has been developed to solve this problem [175–178]. In the early stage of the technology, OLED encapsulation is a combination of either epoxy resin and getter (edge seal) or of dam and stuffing resin (filling material) as shown in figure 55 [179]. However, since these methods do not ultimately guarantee the lifetime of OLED devices, frit seal technology using glass frit as an edge sealant has been used for encapsulation of small and medium sized rigid OLEDs [180].

For current and next-generation displays, OLEDs must be produced on thin, flexible large substrates. However, glass frit encapsulation technology cannot be used for these large OLED displays. Thus, as shown in figure 56, new encapsulation techniques, such as TFE alternating inorganic and organic layer pairs,



have been developed for flexible and large OLED displays [175, 181, 182]. The multilayer structure is able to slow down the moisture and oxygen diffusion due to the longer diffusion paths of permeants.

TFE is a structure formed by coating thin inorganic and organic materials on an OLED device. In the early stages of TFE development, the production yield was low due to the complex multilayer organic



and inorganic coating process. Recently, productivity has been improved significantly in terms of yield and cost. The inorganic layer is deposited by PECVD and the organic material (monomer) is coated by inkjet printing method and then cured through UV light or heat. The inorganic and organic materials used in the TFE encapsulation technology are trade secrets, so the details are not disclosed. Vitex System, a leader in TFE technology, has been known to use Al_2O_3 as the inorganic material and polyacrylate as the organic material.

5.4. OLED inkjet printing for the emitting layers

A thermal vacuum evaporation process technology using a fine metal mask (FMM) has been developed as an organic material deposition method for OLED devices. However, due to various problems caused by the high investment in expensive vacuum equipment and the increase in FMM size, inkjet printing technology has been actively developed as an alternative technology. As shown in figure 57, a typical OLED device structure is composed of five organic layers: four auxiliary layers and one RGB light emitting layer

between the anode and cathode electrodes. The HIL (hole injection layer), HTL (hole transport layer) and EML (emitting material layer) are fabricated by the inkjet printing process, and the electron transport layer and electron injection layer are vacuum deposited using the open mask. Note that the OLED inkjet printing process requires a hydrophobic PDL barrier to control ink overflow.

All the ink solutions used in the OLED inkjet printing method must have excellent jetability from inkjet head and printability on substrates. In addition to these process features, the ink materials should have excellent electrical properties in order to be used as the auxiliary layer and the light emitting layer.

The HOMO (highest occupied molecular orbital) energy level of the HIL material should be similar to the work function of the ITO anode electrode. PEDOT/PSS conductive polymer materials are well known as representative HIL materials, as shown in figure 58(a). It was reported that when Nafion (perfluorinated ionomer) was mixed with PEDOT: PSS for the HIL, the work function of the interface of the ITO/HIL and the device life were improved [183]. HTL materials should exhibit high hole mobility and HOMO energy levels of HTL materials should be similar to those of HIL. As a representative HTL material for an inkjet printing process, Poly[(9,9-dioctylfluorenyl-2,7-diyl)-co-(4,4'-(*N*-(4-sec-butylphenyl)diphenylamine)] in figure 58(b) has been used [184]. When an organosilicate polymer, *N,N'*-diphenyl-*N,N'*-bis(4-((*E*)-2-(triethoxysilyl)vinyl)phenyl)biphenyl-4,4'-diamine, was used as the hole injection/transport layers, significant device performance improvements were observed, such as low leakage current, low turn-on voltage, high brightness and higher current density as shown in figure 59 [185].

Light emitting materials for inkjet process can be classified into highly conjugated polymer materials and low molecular weight materials of relatively limited conjugate lengths. Conjugated polymer materials, as shown in figure 60, have delocalized π -electron systems inside the molecule whose size determines the emitting light wavelength. In the case of the polymer material, impurities are generated during the synthesis, and thus deterioration of device efficiency and stability occurs. Therefore, nowadays, the development of OLED light emitting materials for inkjet printing process is actively carried out mainly for low molecular weight materials.

Based on the light emitting mechanism, traditionally emitting materials can be divided into fluorescent and phosphorescent materials. Recently, new light emitting mechanisms such as thermally activated delayed fluorescence luminescent materials have been discovered [186].

Phosphorescent soluble materials for OLED device are actively developed because phosphorescent materials are highly efficient compared to fluorescent

materials. Phosphor materials used in OLED devices consist of a host material and dopant material. The host material is responsible for charge injection and transport while the dopant material is involved in luminescence. Figure 61 shows representative host and dopant materials used in OLED devices. To be suitable as a soluble material for the OLED inkjet process, the solubility of the host and dopant materials should be high enough. Therefore, efforts have been made to improve solubility by adding functional groups to the molecule itself in the case of the host [187] and to the ligand in the case of the dopant [188].

Since HIL, HTL, and EML organic thin films of OLED devices fabricated by inkjet printing are about 10 nm or less in thickness, it is very important to manage the amount of ink discharged from the inkjet head. For this purpose, DPN technology (figure 8) and various printing algorithms (figure 52) must be employed to control film thickness and printing stains of OLED displays.

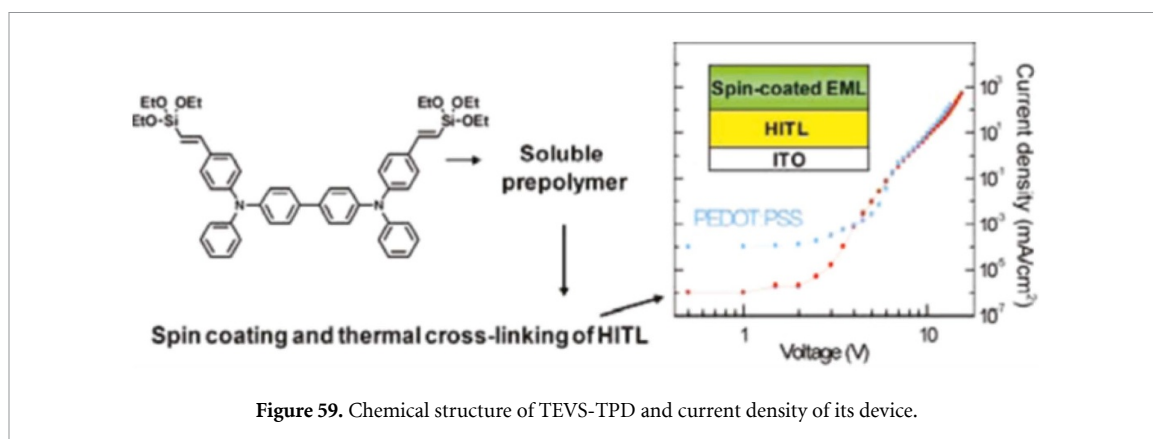
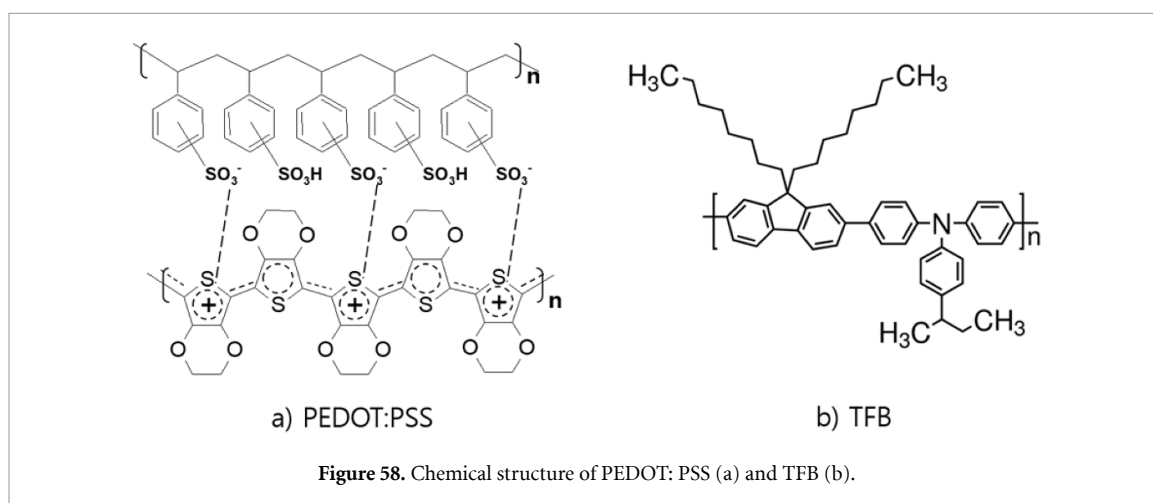
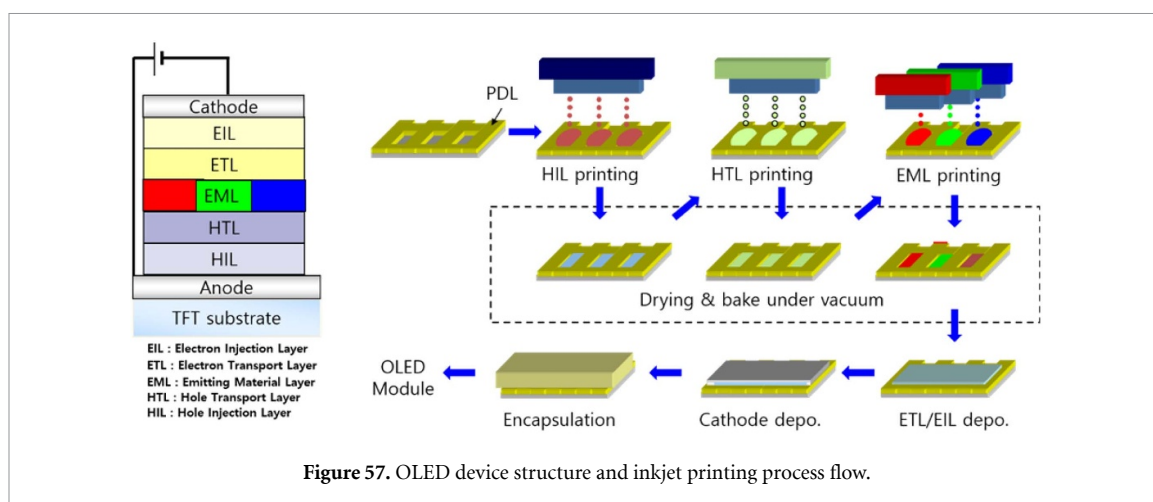
In recent years, intensive research on quantum dots (QDs), an inorganic compound semiconductor material, has been actively carried out because these materials can be used as light emitting materials for inkjet printed OLED devices [189–192]. The band gap energy that determines the emission wavelength of QDs is generally controlled by the size [192, 193]. The display device structure to which QD is inserted as a light emitting layer material is the same as the OLED device structure. As shown in figure 62, a QD consists of a core, a shell, and a ligand. Each part has its own role in making QD display devices. Quantum efficiency and emission color purity of QD are strongly dependent on the core and shell materials. Ligand, on the other hand, affects QD solubility in organic solvents.

As discussed in this section, display application, such as LCD color filter printing, OLED light emissive layer printing, PI printing and encapsulation, have been a good example of the successful application of inkjet printing process. Besides the display application, active or passive electrical component printing [195–197], sensors [166, 198, 199], and metal 3D printing [200–202] are also very active field of inkjet research.

6. Metal inks for printed electronics

6.1. Importance of conductive inks

Recently, metal ink printing technology has gained significant interest as a cost-effective manufacturing process for large area/flexible electronics. Chemical and physical properties of the conductive materials affect substantially electrical characteristics of the printed devices. As a result, a lot of research has been focused on a development of conductive materials. In this section a recent development in printable conductive materials is reviewed. A post-treatment

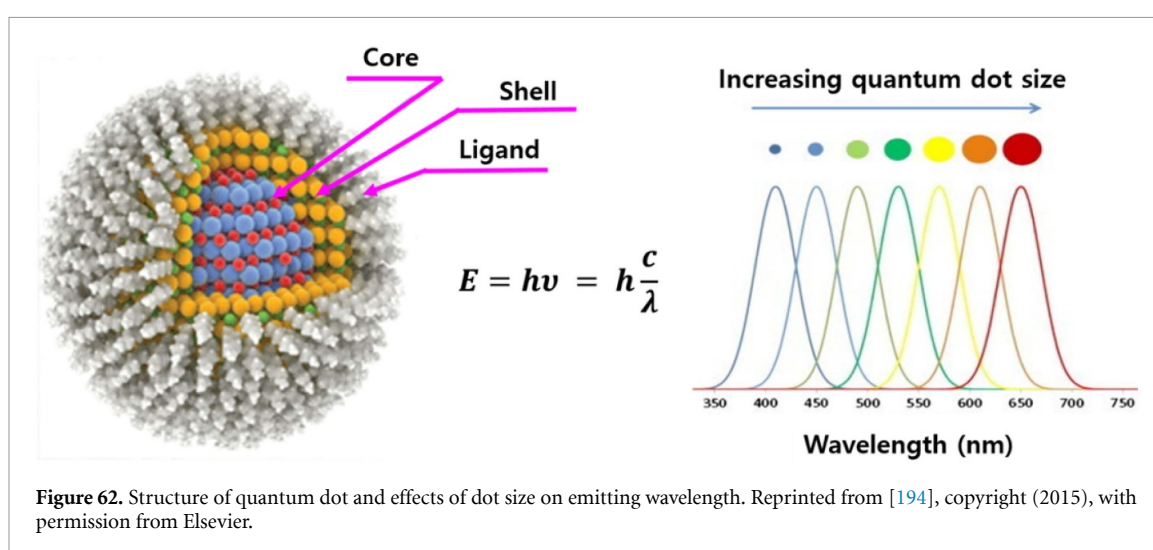
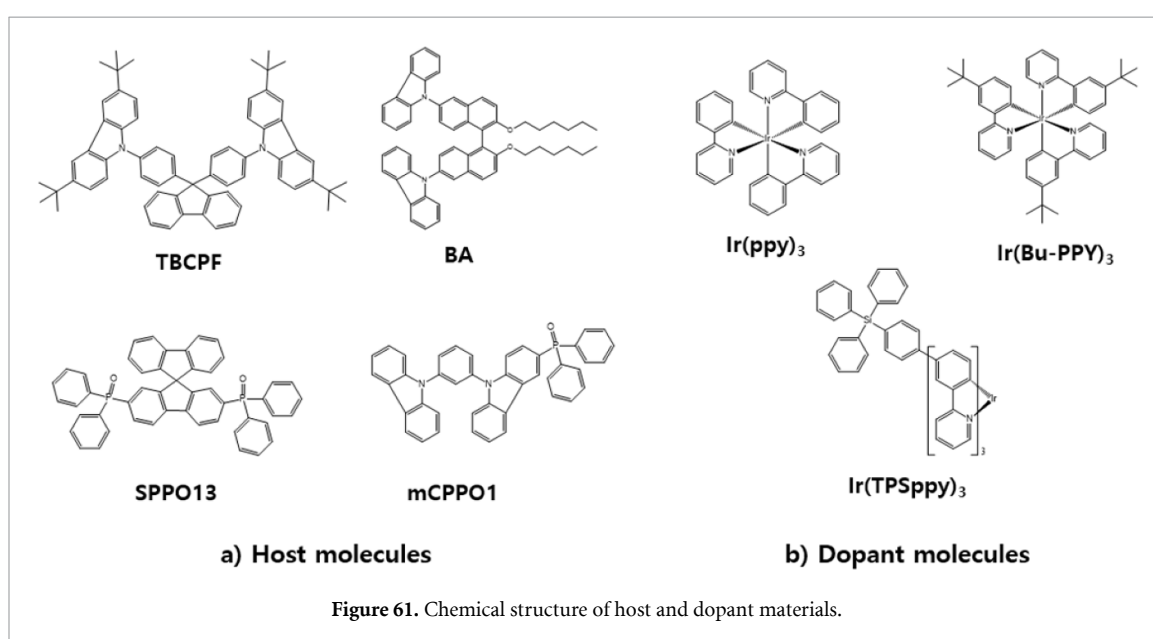
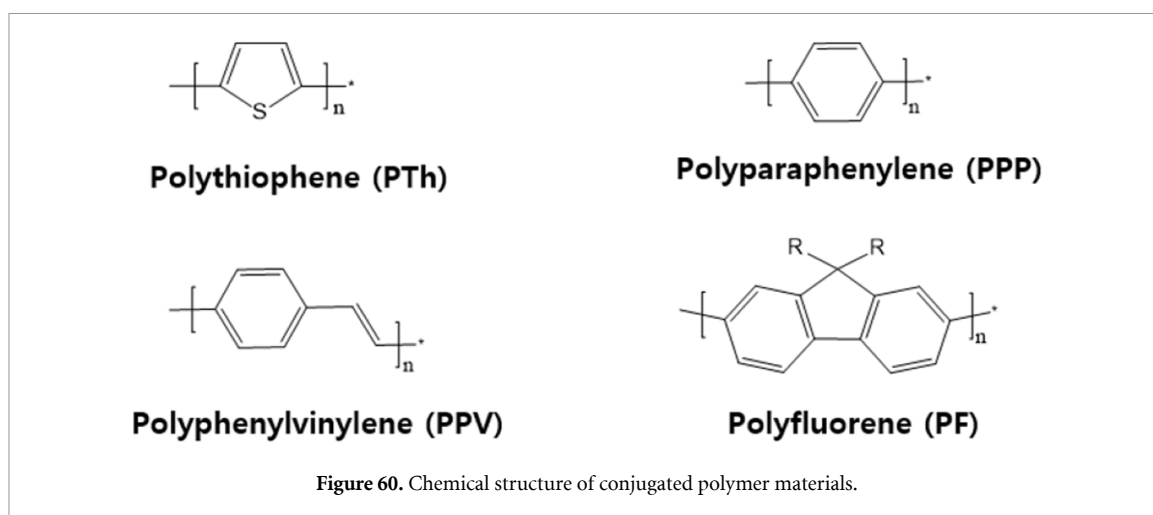


process is also discussed for improving the electrical characteristics of printed layers.

6.2. Metal nanoparticle inks

Nanomaterials for highly conductive electrodes are of paramount importance in the field of printed electronics. Electrodes are crucial components in electronic devices because they are used for interconnecting each active device or injecting the charge carriers into other functional layers. The printable nanomaterials for electrodes should meet the requirements of a high conductivity and a facile

processing capability [203, 204]. Conducting polymers can be easily prepared in the form of printable fluids as they are readily dispersed or dissolved in appropriate solvents, and the rheological properties of the prepared fluids are adjustable depending on the chemical/physical nature of the solvents used. However, conducting polymers have limited capability in bringing the electrical conductivity up to the level of pure metal conductors and also suffer from an environmental instability in certain applications. Alternatively, carbon materials such as CNTs and graphene derivatives have been suggested owing



to a characteristic advantage of environmental stability. Graphene oxides and exfoliated graphenes can be formulated into highly concentrated fluids.

The polar groups present on the surface of carbon materials could promote a protonation or deprotonation reaction depending on the pH of surrounding

medium; this enables production of a stable dispersion in solvent medium via specific chemical reactions with dispersants.

However, even with various chemical approaches, the conductivities of electrodes derived from highly concentrated graphene suspensions still remain below 10^3 S cm^{-1} [205, 206]. On the other hand, metallic nanowires have gained recent attention since they can be used for forming highly functioning, transparent/stretchable conductive films. However, an issue with patterning of nanowire-based films remains unresolved. In addition, the nanowire-based ink preparation in the form of printable fluid is demanding because of the rotational motion of one-dimensional wires in fluid during a printing process [207, 208].

Metal nanoparticles can be formulated as a printable ink by being dispersed in solvent, based on an inter-particle repulsion mechanism. The metal nanoparticles are stable in many different environments and have a high conductivity over 10^5 S cm^{-1} . At the early stage of metal nanoparticle ink development, Au nanoparticles were synthesized through a chemical reduction of Au ions in solvent at elevated temperatures. The metal nanoparticles form a multi-stacked particle assembly after a printing process. However, the charge carrier transport through particle assemblies relies on electrical junctions between neighboring metal nanoparticles. The morphological transformation into a dense film-like structure is generally triggered by annealing at temperatures approaching $0.8 \times T_m$, but the melting point (T_m) of bulk-phase Au is 1040°C . When the metal particle size decreases to the nanoscale, the effective T_m is reduced significantly, allowing for a low-temperature processing, even on plastic substrates. Such a thermally-activated reaction enables the formation of interconnections among neighboring nanoparticles, which improves drastically the electrical conduction. After such a thermal densification process, electrical conductivity over 10^5 S cm^{-1} can be easily achieved. However, because of the cost issue, Au nanoparticles have rarely used in practical applications.

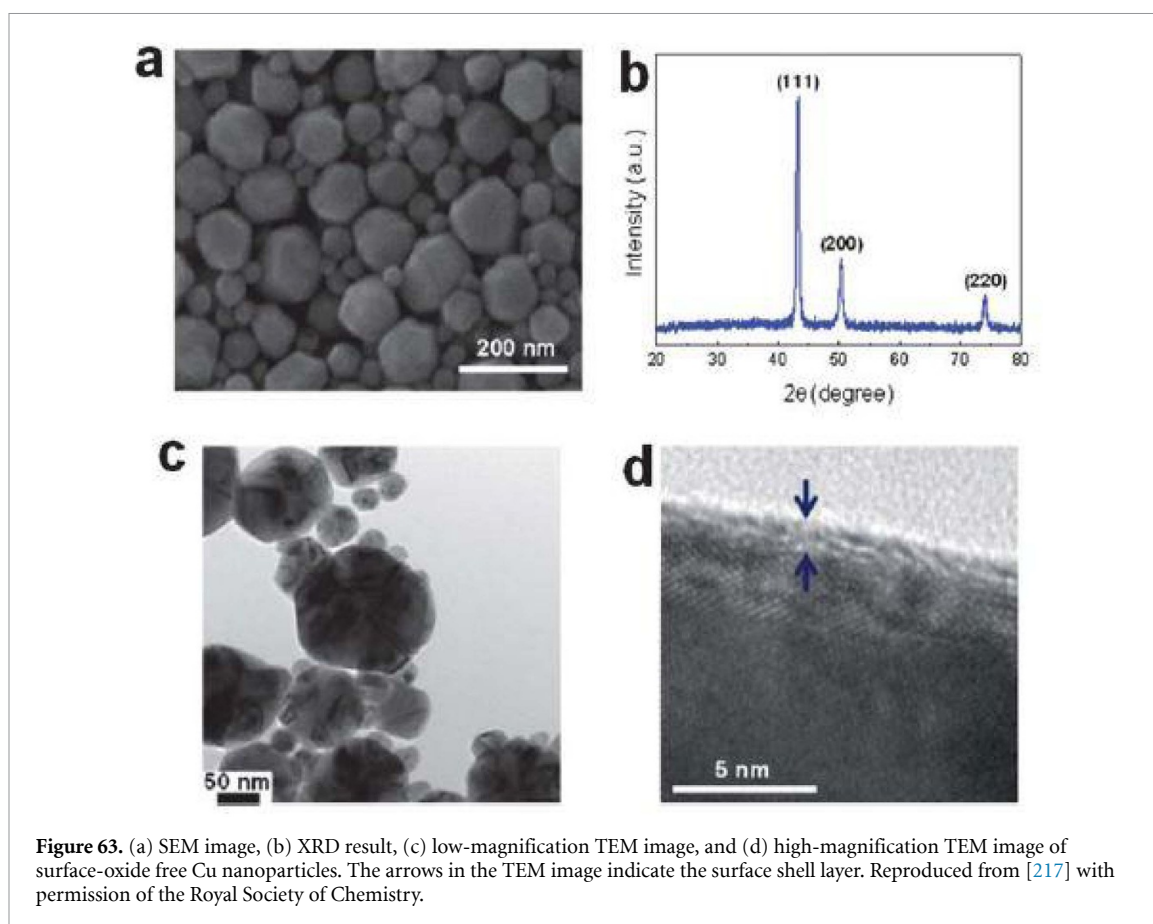
As an alternative to Au nanoparticles, Ag nanoparticles have gained significant attention. Similarly, Ag nanoparticles have been synthesized successfully via a variety of chemical methodologies. It has been reported that conductivities for Ag nanoparticle electrodes comparable to that for Au nanoparticles electrodes is achievable [209, 210]. To reduce further the cost of synthesizing metallic nanoparticles, Cu nanoparticle ink has been developed. The use of Cu is much more cost-effective, having comparable bulk conductivity to Ag [211, 212]. However, Cu tends to be easily oxidized, with a formation of a thermodynamically stable oxide layer on the surface of Cu nanoparticles. Consequently, thermal annealing should be carried out under an inert atmosphere, in order to prevent thermal oxidation at elevated temperatures.

The surface oxide layer is electrically insulating, and the value in T_m of Cu oxides is higher than that of the pure Cu phase, so surface oxide formation should be suppressed in order to form highly conductive electrodes from Cu nanoparticles [213]. Recently, as an alternative to easily oxidizable Cu nanoparticles, Ni nanoparticles have been suggested with a demonstration in practical applications [199, 214]. Despite the limitation of slightly inferior electrical conductivity in Ni nanoparticle-derived electrodes, the highly stable nature of these electrodes even under harsh environmental conditions has opened up new possibilities in printed electronics applications.

6.3. Unconventional post-treatment procedures

The surface oxide layer of Cu nanoparticles can be effectively eliminated by annealing under a chemically reactive atmosphere (e.g. formic acid and oxalic acid) [215]. However, the use of highly reactive gas can lead to undesirable chemical damage of other functional layers in integrated devices. Passivating the Cu surface with an air-stable Ag phase has been attempted to develop Cu-based, cost-effective metal nanoparticles that can be processed in air even during a thermal annealing process. However, the Ag shell layer tends to form surface localized aggregates at elevated temperatures, exposing the bare Cu surface [216]. Thus, an inert gas should be provided during a thermal annealing process, in order to prohibit the problematic oxidation reaction. Recently, it was reported that the inherent surface oxide formation could be suppressed by introducing an appropriate organic capping layer [210]. With the aid of densely packed organic molecules, the surface of Cu nanoparticles was effectively stabilized, suppressing the possibility of surface oxidation at room temperature in air [217]. As seen in figure 63, the phase-pure Cu nanoparticles were synthesized by passivating the exposed Cu atoms with oleic acid as a surface capping molecule. A shell layer as thin as a few nanometers, which is comprised of the surface oxide-free and organic capping layer, is clearly observed.

Nevertheless, the provision of an inert gas during thermal annealing remains necessary to obtain highly conductive properties in the resulting Cu electrodes. One alternative approach of using chemical energy was proposed, based on the activation of surface-charge-induced agglomeration [218, 219]. This chemical strategy requires a coupled-reaction between the charged ligands adsorbed to metal nanoparticles and additionally incorporated electrolytes. Other approaches, using microwave [220], plasma [221, 222], and microwave/plasma-based [223] densification processes, have been suggested for forming highly conductive electrodes at low temperatures at which substrate materials such as polycarbonate (PC), polyethylene naphthalate, and PET can be stable without mechanical deformation.



Alternatively, optical-energy-based sintering methodologies have been explored, based on a selective laser irradiation and an intensive visible light irradiation [224–226]. Laser is an optical energy source having a specific wavelength. When the wavelength of an irradiated laser couples to the surface plasmon behavior of metal nanoparticles in printed particular assemblies, the efficient absorption of optical energy leads to an inter-particle densification reaction [226]. One of the advantages in a laser-based sintering methodology is a localized provision of the optical energy, as the laser is primarily a point energy source. The particles in a region irradiated by a laser undergo the inter-particle agglomeration, whereas the particles in the non-irradiated region remain in the form of the original as-dried pristine morphology. With a successive washing step using solvents, the densified bulk-like particle assemblies in the irradiated region maintain their structure, while the particles in the non-irradiated region are entirely removed. This phenomenon enables formation of patterned structures along with a generation of highly conductive, interconnected particle frameworks (figure 64).

As shown in figure 64, the particle films can be converted into conductive electrodes with a patterned geometry on demand without a printing process. The pattern resolution is achievable even down to a level of 10 μm , and thermally vulnerable

polymeric substrates can be used because of the limited transport of optical/thermal energy to the underlying substrates. Furthermore, with a combination of an appropriate reducing agent, the optical/chemical reduction of copper oxide phase can be achieved even in CuO nanoparticle films [227].

A limitation of the laser-based sintering methodology is a low production throughput, as a large number of scan steps are required to generate electrodes over a large area. Alternatively, an intense lamp-type source can be utilized with an irradiation of visible light ranging from 300 nm to 800 nm in wavelength, which is called a photonic sintering process. The photonic sintering process can be easily implemented in a web-based continuous process. In general, an irradiation of intensive photons is performed on the timescale of 10^{-3} s. Highly energetic photons are absorbed within metal nanoparticle assemblies, and then a lattice vibration in metal nanoparticles can be converted into thermal energy. This converted thermal energy activates the inter-particle densification reaction. Note that only a part of the energy transfers to the underlying substrates, enabling limited thermal impact on the substrates. For conventional thermal annealing processes, thermal energy must be supplied for a prolonged time, longer than at least 10 min, to trigger sufficient mass transport between neighboring nanoparticles. In web-based continuous printing processes, the heat-treatment

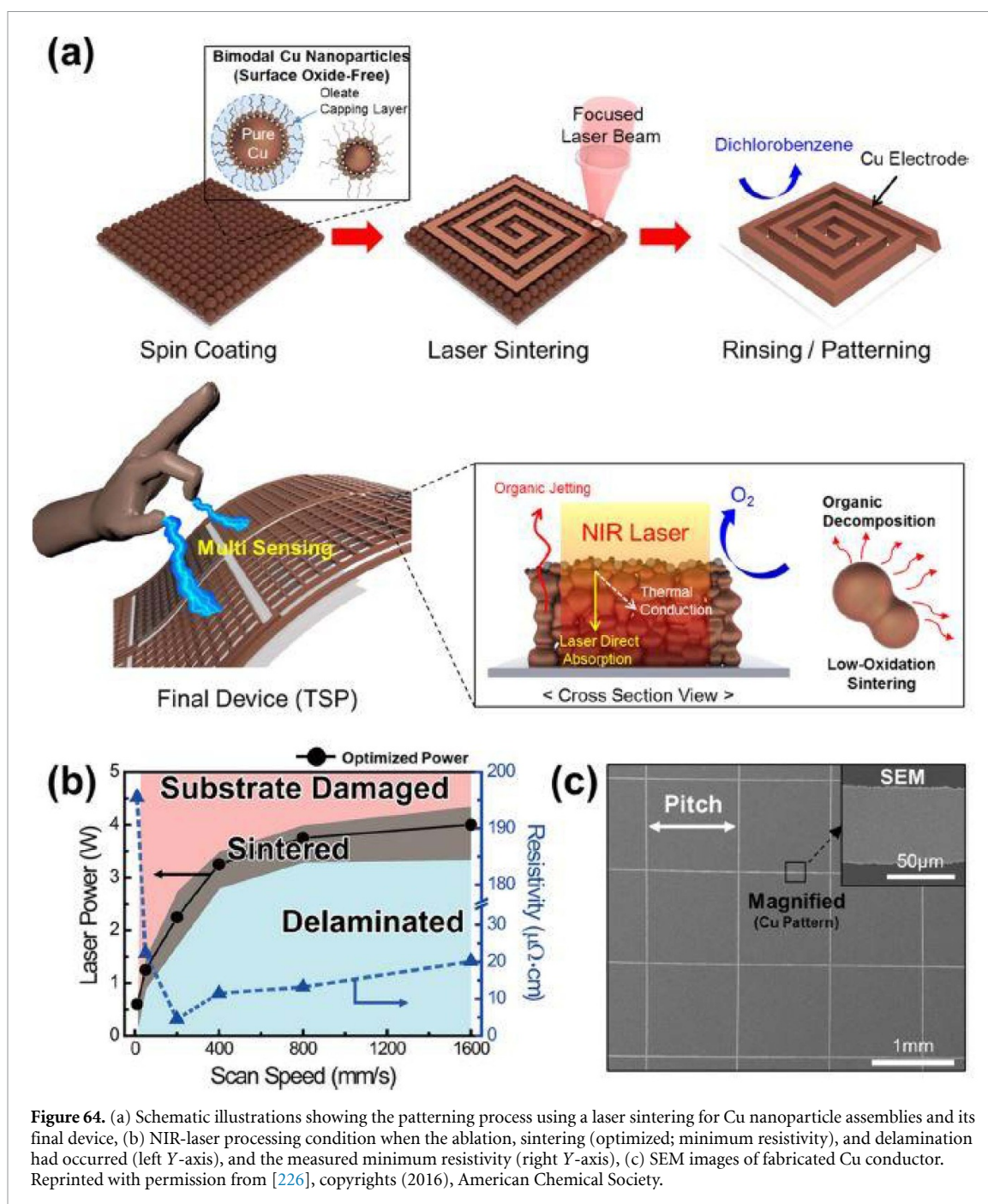


Figure 64. (a) Schematic illustrations showing the patterning process using a laser sintering for Cu nanoparticle assemblies and its final device, (b) NIR-laser processing condition when the ablation, sintering (optimized; minimum resistivity), and delamination had occurred (left Y-axis), and the measured minimum resistivity (right Y-axis), (c) SEM images of fabricated Cu conductor. Reprinted with permission from [226], copyrights (2016), American Chemical Society.

zone is equipped with a rapidly moving carrier stage; this requires a thermal zone to be long enough to produce an annealing effect of more than 10 min. In contrast, the photonic sintering process facilitates an (almost) instant, vigorous microstructural evolution from particulate assemblies to conductive dense frameworks. Highly conductive electrodes can be fabricated over a large area by a successive irradiation of the visible light along with a synchronized movement of the carrier stage [190, 228, 229].

Notably, the photonic sintering process enables a photo-chemical reduction of oxide phases in air as long as a particulate film includes a polymer (for instance, polyvinylpyrrolidone) that can act as a reducing agent for Cu oxides [230]. After completion

of photonic sintering processes, the incorporated polymers are decomposed, as the electrically insulating polymers hinder efficient charge transport in nanoparticle-derived electrodes. In some cases, the excessive amount of polymer leaves behind microstructural voids after completion of the sintering process, which results in a reduction in electrical conductivity. Use of oxide-free Cu nanoparticles can simplify this complicated photonic sintering process, as the photo-chemical reduction reaction is not necessary. In such a case, the primary reaction is only a microstructural transformation into a bulk-like film structure [231–236]. As seen in figure 65, highly conductive electrodes were formed successfully from oxide-free Cu nanoparticles on various PI,

polyethersulfone, PET, and paper substrates, showing excellent stability during long-term bending tests.

6.4. Percolation mechanism-based conductive materials

Apart from the aforementioned densification mechanism for producing highly conductive electrodes from metallic nanoparticles, the percolation mechanism can also be applied to printable nanomaterials (CNTs, metallic flakes/nanowires) for electrodes [237–248]. When conductive fillers are mixed with a polymer matrix, the conductivity of the overall films is improved significantly, depending on the volumetric composition of conductive fillers. When the volumetric composition of conductive fillers exceeds a threshold, the electrically insulating composites start to be converted into highly conductive ones. The threshold composition is highly dependent on the morphology of the conductive fillers. The one-dimensional conductive fillers (representatively, a CNT) have a relatively a low threshold, and the 2D ones have a lower threshold, compared with spherical counterparts. In general, the CNTs are incorporated in a polymer matrix together with 2D metal flakes. If the incorporated polymer has a stretchable rubber characteristic, the resulting composites can be used as stretchable conductors. It was reported that a carbon-based composite conductor exhibited a conductivity of 6 S cm^{-1} [247], while Ag flake-included composites were much more conductive, with a value in conductivity close to 5000 S cm^{-1} and a stretchability over 100% [248]. Ionic liquids were also considered as additives for composite electrodes, as they play a critical role in uniformly dispersing CNTs. However, there are critical criteria in preparing ionic liquid-based CNT/polymer mixtures: (a) an appropriate mixing ratio of ionic liquid and CNTs, (b) chemical compatibility between the ionic liquid and polymer, (c) use of extremely-high-aspect-ratio CNTs, and (d) a sophisticatedly controlled mixing procedure for dispersing the CNTs without a morphological degradation. Recently, it was reported that the conductivity of $41\,245 \text{ S cm}^{-1}$ was achieved by mixing nanostructured flower-like Ag particles with polyurethane as a polymer [240]. This result indicates that the nano-structured design of conductive metallic fillers is of paramount importance in preparing highly functioning, percolation-based, conductor materials.

For metal nanoparticle inks, since the polymeric substances should be decomposed during a post-treatment procedure, a limited loading of polymeric ingredients could be allowed in the printable fluid. High viscosity fluid can be produced by increasing the metal nanoparticle content, which could result in undesirable formation of agglomerates in the fluid. The range of ink viscosity in representative printing processes, namely ink-jet printing and a dispensing printing, is 1–30 mPas and

10 000–50 000 mPas, respectively. Metal nanoparticle inks can be formulated to meet such rheological requirements, but sophisticatedly controlled dispersion stability requirements for the ink preparations should be taken into consideration, in particular for the dispensing process. On the contrary, for percolation conduction-based composite inks, relatively more polymeric substances can be incorporated, which makes it easier to prepare viscous fluids. Thus, in general, composite inks are more appropriate for a dispensing printing process. Ink rheological properties are adjustable in a certain degree, depending on surface characteristics of metal fillers and the composition of printable fluids. Thus, the chemical design of metallic nanoparticles/fillers and compositional fluids are of paramount importance in facilitating the various printing processes.

7. Concluding remarks

In this review, recent development in printing methods, jetting materials, printing technologies and applications are discussed with emphasis on their jet mechanism. For printed electronics applications, all printing components including ink, jet mechanism, jet process, and equipment needs optimization via a proper understanding of each component. For example, the appropriate dispensing method should be determined based on the ink viscosity or vice versa. Ink viscosity is often related to the loading of functional materials in the ink and the electronics functionality is likely to increase with more solid contents in the ink.

Among other printing methods, piezo-driven inkjet methods have been regarded as mature technology since it has been widely used in the field of graphics applications for more than several decades. Recently, inkjet print-heads with a high density of nozzles and large numbers of nozzles have been used for fast single pass printing. The proven inkjet technology in graphics applications has been in successful transition stages from graphics printing to printed electronics. For example, the inkjet dispensing hardware for graphics applications, such as inkjet print-head, driver and fluidic system, can be used in printed electronics application. The recent methods for graphics printing can be suitable for manufacturing of electronics devices. However, in case of printed electronics, the functionality of electronics is more important than graphical representation for human perception. The development of suitable material for inkjet processes still remains one of the key issues in printed electronics applications. As a mass production industrial application, recent inkjet materials and other inkjet issues for the production of LCD and OLED are discussed.

Due to the diversity of printed electronics applications, various dispensing materials are being used. Recently, there are increasing demands for high

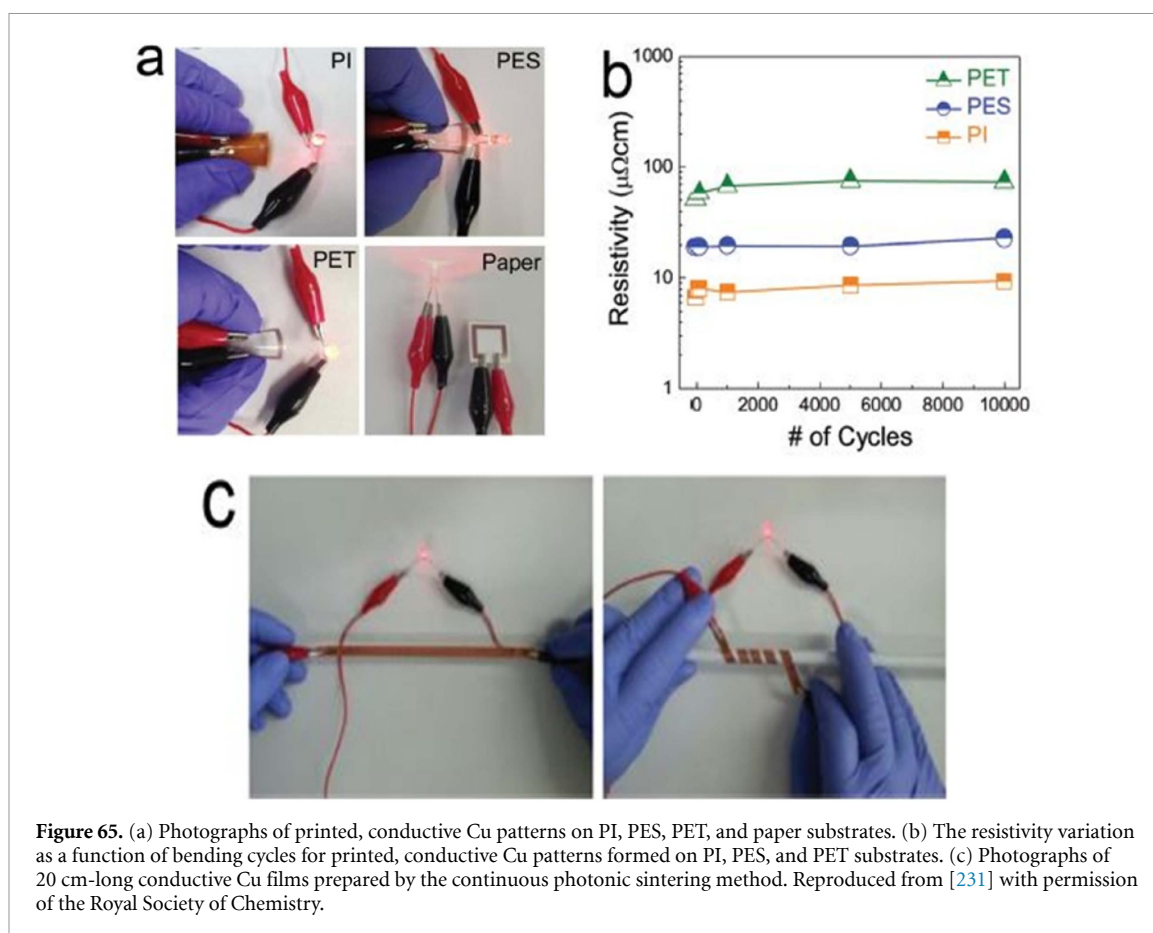


Figure 65. (a) Photographs of printed, conductive Cu patterns on PI, PES, PET, and paper substrates. (b) The resistivity variation as a function of bending cycles for printed, conductive Cu patterns formed on PI, PES, and PET substrates. (c) Photographs of 20 cm-long conductive Cu films prepared by the continuous photonic sintering method. Reproduced from [231] with permission of the Royal Society of Chemistry.

resolution printing of high viscosity ink, which is beyond the capability of conventional inkjet processes. For dispensing high viscosity ink, the nozzle inner diameter should be enlarged accordingly. Thus, dispensing of high viscosity ink could result in large printed features. As methods for overcoming the conventional jetting limitations, new jet mechanisms for fine patterns, using electrical field, ultrasonic vibration or focused atomized jet, have been developed. For example, AJP methods convert ink into aerosol (spray) and focus it via sheath gas to make fine patterns. Sonoplot micro-plotter uses ultrasonic vibration to push high viscosity ink through a nozzle tip with inner diameter of a few micrometers. Near field electrospinning uses an electrical field to extract a thin jet stream from the nozzle with larger inner diameter. These fine printing mechanisms could overcome the limitations of inkjet printing processes and the methods are successfully used in many applications. However, print-heads with a high density of nozzles for fine patterning are not yet commercially available for production printing.

Lastly, metal based conductive ink for printed electronics applications is reviewed. In the last decade various printable conductive materials have been suggested, having significant enhancements in material properties and electrical characteristics of the resulting printed layers. To date, a variety of organic, inorganic, hybrid, and carbon materials have been developed to satisfy chemical/physical requirements.

With the use of newly developed post-treatment procedures, performances of printed materials have been improved dramatically, approaching the level required for practical low-cost, large-area and flexible electronics applications. Note that such progress has not been achievable by conventional vacuum-deposition processes and photolithographic patterning processes. It is highly anticipated that further extensive work on novel functional materials in combination with well-designed digital printing techniques will open up new possibilities in the field of printed electronics.

Acknowledgments

This research was supported by the Basic Science Research Program through the National Research Foundation of Korea (NRF), funded by the Ministry of Education (2016R1D1A1B01006801). It was also partially supported by the Soonchunhyang University Research Fund. Professor Kye-Si Kwon gratefully acknowledge the useful discussion and comments from Dr Jurgen Daniel, Professor Tse Nga Ng and Mr Steven Ready for improvement of the paper.

ORCID iD

Kye-Si Kwon  <https://orcid.org/0000-0001-7041-5656>

References

- [1] Chung S, Cho K and Lee T 2019 Recent progress in inkjet-printed thin-film transistors *Adv. Sci.* **6** 1–27
- [2] Alamán J, Alicante R, Peña J I and Sánchez-Somolinos C 2016 Inkjet printing of functional materials for optical and photonic applications *Materials* **9** 910
- [3] Chiu C, Chiu W W W, Yang M, Wang C, Lin C and Cheng K 2007 Novel image trimming algorithm for use with ink jet printing fabrication *J. Imaging Sci. Technol.* **51** 514–9
- [4] Bracke P 2001 High throughput industrial digital printing *NIP17: Int. Conf. on Digital Printing Technologies High* pp 28–32
- [5] Mills R N, Gates G D and Santana S 2006 Drop placement error analysis for ink jet deposition *Digital Fabrication 2006 (Society for Imaging Science and Technology)* pp 124–7
- [6] Chunjiang J, Guangxue C, Xiaozhou L and Qifeng C 2011 Research on ink droplet shape on moving substrate *NIP 27 and Digital Fabrication vol 7 (Minneapolis, MN: Society for Imaging Science and Technology)* pp 300–3
- [7] Fujii M 2018 *Imaging Society of Japan (ISJ 60th Anniversary) for inkjet Printing system 27.07.2018 Japan Inkjet (Imaging Society of Japan (ISJ 60th Anniversary)) (Japan: ISJ) ([http://www.isj-imaging.org/isj\(e\).html](http://www.isj-imaging.org/isj(e).html))*
- [8] Kwon K S, Shin S J and Kim S J The opportunity of printing technology for display manufacturing process *Proc. of colloquium on micro/nano thermal engineering (Seoul National University)*
- [9] Borman D, Jahanshah F, Dehghani A A, King T and Gaskell P 2002 On-line vision system for ink-jet printed media *IS and T's NIP18: Int. Conf. On Digital Printing Technologies (Leeds)* pp 562–7
- [10] Kwon K S, Jang M H, Park H Y and Ko H S 2014 An inkjet vision measurement technique for high-frequency jetting *Rev. Sci. Instrum.* **85** 065101
- [11] Ungureanu G, Reinhold I, Sander I and Zapka W 2013 Parallel software design enabling high-speed reliability testing of inkjet printheads *NIP 29 and Digital Fabrication (Society for Imaging Science and Technology)* pp 60–65
- [12] Barnett D and McDonald M 2014 Evaluation and reduction of elevated height printing defects *NIP30 Technical Program (Society for Imaging Science and Technology)* pp 38–43
- [13] Kwon K S 2010 Experimental analysis of waveform effects on satellite and ligament behavior via in situ measurement of the drop-on-demand drop formation curve and the instantaneous jetting speed curve *J. Micromech. Microeng.* **20** 14
- [14] International Electrotechnical Commission 2017 International standard for printed electronics—part 302–1: equipment—inkjet—imaging based measurement of jetting speed (IEC 62899–302-1:2017)
- [15] Zapka W, Pausch S, Rapp H and Ab X 2008 Improved reliability in industrial inkjet printing *NIP24 and Digital Fabrication (Järfälla: Society for Imaging Science and Technology)* pp 865–8
- [16] Kwon K-S, Yu J and Phung T H 2017 Real-time jet failure detection of inkjet heads with 1024 ejectors *J. Imaging Sci. Technol.* **61** 050401
- [17] Mishra S, Barton K and Alleyne A 2010 Control of high-resolution electrohydrodynamic jet printing *2010 American Control Conf. June 30-July 02, 2010 (Marriott Waterfront, Baltimore, MD, USA: IEEE)* pp 6537–42
- [18] Mishra S, Barton K, Alleyne A, Mishra S, Alleyne A, Ferreira P and Rogers J 2010 Control of high-resolution electrohydrodynamic jet printing *Control Engineering Practice vol 19 (Marriott Waterfront, Baltimore, MD, USA: IEEE)* pp 1266–73
- [19] Lu S, Liu Y, Yao Y, Sun L and Zhong M 2014 Bond-graph model of a piezostack driven jetting dispenser *Simul. Model. Pract. Theory* **49** 193–202
- [20] Chen T, Huang C, Liu T, Chen F, Lee J, Shang K, Lee E and Cheng K 2007 Robust, reliable and repairable inkjet print head with dynamic drop modulation feedback for printable display applications *NIP 23 and Digital Fabrication (Society for Imaging Science and Technology)* pp 336–9
- [21] Cruz S M F, Rocha L A and Viana J C 2018 Printing Technologies on Flexible Substrates for Printed Electronics *Flexible Electron.* (London, UK: IntechOpen) **13**
- [22] Mei J, Lovell M R and Mickle M H 2005 Formulation and processing of novel conductive solution inks in continuous inkjet printing of 3-D electric circuits *IEEE Trans. Electron. Packag. Manuf.* **28** 265–73
- [23] Magdassi S 2010 Inkjet printing technologies *Chemistry of Inkjet Inks* (Singapore: World Scientific) pp 3–18
- [24] Bane J 2008 Advances in technologies for wide web single pass printing with piezoelectric inkjet *NIP24 Digit. Fabr.* pp 121–4
- [25] Abello L, Co H and Diego S 2010 The scalable pipeline architecture behind HP 's T300 color inkjet web press *NIP26 and Digital Fabrication (Society for Imaging Science and Technology)* pp 336–9
- [26] Reinhold I et al 2010 Inkjet printing of phase-change materials with Xaar1001 printheads *Int. Conf. Digit. Print. Technol.* pp 319–22
- [27] Mawatari K, Shimomura A, Matsuo T, Ishibashi D and Kobayashi H 2018 Newly developed MEMS print heads for industrial inkjet applications *2018 Society for Imaging Science and Technology vol 2018 (Society for Imaging Science and Technology)* pp 127–30
- [28] Mawatari K, Sameshima K, Miyai M, Matsuda S and Minolta K 2014 Development of new inkjet head applying MEMS technology and thin film actuator. *NIP30 Technical Program vol 12 (Society for Imaging Science and Technology)* pp 11–14
- [29] Konica Minolta inkjet print head 2019 (Nov.) (available at: www.konicaminolta.com/inkjet/inkjethead/index.html)
- [30] Fujifilm inkjet print head, USA 2019 (Nov.) (available at: www.fujifilmusa.com/products)
- [31] Trident Industrial Inkjet print head 2019 (Nov.) (available at: www.trident-itw.com/)
- [32] Global Kyocera inkjet print head 2019 (Nov.) (available at: <https://global.kyocera.com/prdct/printing-devices/inkjet-printheads/>)
- [33] Xaar inkjet print head 2019 (Nov.) (available at: www.xaar.com/en/products/xaar-printheads/xaar-5601/)
- [34] Kholghi Eshkalak S, Chinnappan A, Jayathilaka W A D M, Khatibzadeh M, Kowsari E and Ramakrishna S 2017 A review on inkjet printing of CNT composites for smart applications *Appl. Mater. Today* **9** 372–86
- [35] Ravasio C S, Hoath S D, Martin G D, Boltryk P and Dorrestijn M 2016 Meniscus motion inside a DoD inkjet print-head nozzle *Int. Conf. Digit. Print. Technol.* pp 348–52
- [36] Kwon K S 2009 Waveform design methods for piezo inkjet dispensers based on measured meniscus motion *J. Microelectromech. Syst.* **18** 1118–25
- [37] Kwon K S, Zhang D and Go H S 2015 Jetting frequency and evaporation effects on the measurement accuracy of inkjet droplet amount *Int. Conf. Digit. Print. Technol.* **59** 20401-1-20401-10
- [38] Magdassi S 2010 *The Chemistry of Inkjet Ink* (Singapore: World Scientific Publishing Co. Pte. Ltd.) (<https://doi.org/10.1142/6869>)
- [39] Wang X, Hu J, Wang Y, Jin H, Wang S and Cao Q 2015 A design for ink-supply circulation system based on advanced PID control *2015 Int. Conf. on Computational Science and Engineering Applications* pp 411–6
- [40] Hirakata S, Ishiyama T and Morita N 2015 Printing stabilization resulting from the ink circulation path installed inside the print head and the jetting phenomenon during nozzle drying *J. Imaging Sci. Technol.* **58** 505031–7

- [41] Kwon K-S, Kim H-S and Choi M 2016 Measurement of inkjet first-drop behavior using a high-speed camera *Rev. Sci. Instrum.* **87** 035101
- [42] Domae Y, Yamamura Y, Horiguchi S, Tachibana M and Printek S I I 2014 New print head technology for high productivity and stability *Digital Fabrication and Digital Printing: NIP30 Technical Program and Proc. (Society for Imaging Science and Technology)* pp 15–19
- [43] Crankshaw M, Rulman M, Zarezadeh H, Douaire M, Condie A and Uk X 2016 Ink recirculation—Xaar TF technology: a study of the benefits *NIP32 Printing for Fabrication vol 2016 (Society for Imaging Science and Technology)* pp 207–11
- [44] Power Electronics News Driving piezoelectric actuators in industrial inkjet printers 2019 Nov. (available at: www.powerelectronicsnews.com/technology/driving-piezoelectric-actuators-in-industrial-inkjet-printers)
- [45] Meteor develops and supplies electronics, software, tools and services for industrial inkjet systems 2019 Nov. (available at: www.meteorinkjet.com/)
- [46] Global Inkjet Systems for industrial inkjet software drive electronics components and services 2019 Nov. (available at: www.globalinkjetsystems.com/)
- [47] Kwon K S 2009 Speed measurement of ink droplet by using edge detection techniques *Meas. J. Int. Meas. Confed.* **42** 44–50
- [48] Kwon K-S 2012 Vision monitoring *Inkjet-Based Micromanufacturing*, ed P D J G Korvink, D P J Smith and D D Shin (Wiley-VCH Verlag GmbH & Co. KGaA) (<https://onlinelibrary.wiley.com/doi/pdf/10.1002/9783527647101.ch9>)
- [49] Kwon K S and Kim W 2007 A waveform design method for high-speed inkjet printing based on self-sensing measurement *Sensors Actuators A* **140** 75–83
- [50] Yoshioka Y and Jabbour G E 2006 Inkjet printing of oxidants for patterning of nanometer-thick conducting polymer electrodes *Adv. Mater.* **18** 1307–12
- [51] Yoshioka Y, Calvert P D and Jabbour G E 2005 Simple modification of sheet resistivity of conducting polymeric anodes via combinatorial ink-jet printing techniques *Macromol. Rapid Commun.* **26** 238–46
- [52] Peng X, Liu T, Zhang Q, Shang C, Bai Q W and Wang H 2017 Surface patterning of hydrogels for programmable and complex shape deformations by ion inkjet printing *Adv. Funct. Mater.* **27** 1–8
- [53] Typical multi-pulse waveforms in a greyscale printhead 2019 (available at: www.fujifilm.com/products/graphic_systems/inkjet_technology/pdf/index/inkjet_technology_catalog.pdf)
- [54] International Electrotechnical Commission 2018 International standard for Printed electronics—Part 302–2: equipment—Inkjet—Imaging-based measurement of droplet volume (IEC 62899–302-2:2018)
- [55] International Electrotechnical Commission 2019 International standard for Printed Electronics—Part 302–3: equipment—Inkjet—Imaging-based measurement of drop direction (IEC 62899–302-3:2019)
- [56] International Electrotechnical Commission PWI 119–14 ED1 Future IEC 62899–302-4 ED1: equipment—Measurement of drop placement
- [57] Mizes H, Spencer S, Sjolander C and Yeh A 2009 Active alignment of print heads *NIP25 and Digital Fabrication 2009 (Society for Imaging Science and Technology)* pp 711–4
- [58] Snyder T, Mizes H, Darling D and Brookfield J 2013 System-level inkjet performance and reliability—Customer needs and innovations from xerox *NIP 29 and Digital Fabrication (Society for Imaging Science and Technology)* pp 538–44
- [59] Klino M and York N 2000 Automated inkjet print-head quality analysis *IS&Ts NIP16 (IS&T)* pp 400–2
- [60] Kwon K S 2009 Methods for detecting air bubble in piezo inkjet dispensers *Sensors Actuators A* **153** 50–56
- [61] Kwon K S, Choi Y S, Lee D Y, Kim J S and Kim D S 2012 Low-cost and high speed monitoring system for a multi-nozzle piezo inkjet head *Sensors Actuators A* **180** 154–65
- [62] Kwon K S, Choi Y S and Go J K 2013 Inkjet jet failures and their detection using piezo self-sensing *Sensors Actuators A* **201** 335–41
- [63] Edwards C, Bennett R, Lee J, Jueng-G Lee and Silz K Precision industrial ink jet printing technology for full color PLED display manufacturing *2nd Internat. Meeting on Inf. Display (Daegu, Korea)*
- [64] Hsiao W-K, Hoath S D, Martin G D and Hutchings I M 2012 Aerodynamic effects in ink-jet printing on a moving web *NIP 28 and Digital Fabrication (Society for Imaging Science and Technology)* pp 412–5
- [65] Drury P, Morris A, Reinhold I, Tuladhar T, Voit W, Zapka W and Plc X 2010 Approaches to high speed inkjet printing *NIP 26 and Digital Fabrication (Society for Imaging Science and Technology)* pp 332–5
- [66] Chiu W W W, Wang C Y, Chiu C H, Yang M H and Cheng K 2006 The dawn of ink-jet fabrication in reel-to-reel system *Digital Fabrication 2006, Final Program and Proc. (Society for Imaging Science and Technology)* pp 140–3
- [67] Soltman D and Subramanian V 2008 Inkjet-printed line morphologies and temperature control of the coffee ring effect *Langmuir* **24** 2224–31
- [68] Lacombe J and Soulié-Ziakovic C 2017 Controlling self-patterning of acrylate films by photopolymerization *Polym. Chem.* **8** 1129–37
- [69] Hamad E M, Bilatto S E R, Adly N Y, Correa D S, Wolfrum B, Schöning M J, Offenhäusser A and Yakushenko A 2016 Inkjet printing of UV-curable adhesive and dielectric inks for microfluidic devices *Lab Chip* **16** 70–74
- [70] Saleh E et al 2017 3D inkjet-printed UV-curable inks for multi-functional electromagnetic applications *Addit. Manuf.* **13** 143–8
- [71] Deegan R D, Bakajin O, Dupont T F, Huber G, Nagel S R and Witten T A 1997 Capillary flow as the cause of ring stains from dried liquid drops *Nature* **389** 827–9
- [72] Fischer B J 2002 Particle convection in an evaporating colloidal droplet *Langmuir* **18** 60–67
- [73] Hu H and Larson R G 2002 Evaporation of a sessile droplet on a substrate *J. Phys. Chem. B* **106** 1334–44
- [74] Hu H and Larson R G 2006 Marangoni effect reverses coffee-ring depositions *J. Phys. Chem. B* **110** 7090–4
- [75] He P and Derby B 2017 Controlling coffee ring formation during drying of inkjet printed 2D inks *Adv. Mater. Interfaces* **4** 2–7
- [76] Al-Milaji K N, Secondo R R, Ng T N, Kinsey N and Zhao H 2018 Interfacial self-assembly of colloidal nanoparticles in dual-droplet inkjet printing *Adv. Mater. Interfaces* **5** 1–11
- [77] Shen X, Ho C M and Wong T S 2010 Minimal size of coffee ring structure *J. Phys. Chem. B* **114** 5269–74
- [78] Chung J, Ko S, Grigoropoulos C P, Bieri N R, Dockendorf C and Poulidakos D 2005 Damage-free low temperature pulsed laser printing of gold nanoinks on polymers *J. Heat Transfer* **127** 724–32
- [79] Lim T, Han S, Chung J, Chung J T, Ko S and Grigoropoulos C P 2009 Experimental study on spreading and evaporation of inkjet printed pico-liter droplet on a heated substrate *Int. J. Heat Mass Transf.* **52** 431–41
- [80] Kim Y H, Kim K H, Oh M S, Kim H J, Han J I, Han M K and Park S K 2010 Ink-jet-printed zinc-tin-oxide thin-film transistors and circuits with rapid thermal annealing process *IEEE Electron Device Lett.* **31** 836–8
- [81] Hong S J, Chou T H, Chan S H, Sheng Y J and Tsao H K 2012 Droplet compression and relaxation by a

- superhydrophobic surface: contact angle hysteresis *Langmuir* **28** 5606–13
- [82] Li Y, Lan L, Xiao P, Sun S, Lin Z, Song W, Song E, Gao P, Wu W and Peng J 2016 Coffee-ring defined short channels for inkjet-printed metal oxide thin-film transistors *ACS Appl. Mater. Interfaces* **8** 19643–8
- [83] Lin S Y, Yang K C and Chen L J 2015 Effect of surface hydrophobicity on critical pinning concentration of nanoparticles to trigger the coffee ring formation during the evaporation process of sessile drops of nanofluids *J. Phys. Chem. C* **119** 3050–9
- [84] Li Y F, Sheng Y J and Tsao H K 2013 Evaporation stains: suppressing the coffee-ring effect by contact angle hysteresis *Langmuir* **29** 7802–11
- [85] Mampallil D and Eral H B 2018 A review on suppression and utilization of the coffee-ring effect *Adv. Colloid Interface Sci.* **252** 38–54
- [86] Lim J A, Lee W H, Lee H S, Lee J H, Park Y D and Cho K 2008 Self-organization of ink-jet-printed triisopropylsilylethynyl pentacene via evaporation-induced flows in a drying droplet *Adv. Funct. Mater.* **18** 229–34
- [87] Still T, Yunker P J and Yodh A G 2012 Surfactant-induced Marangoni eddies alter the coffee-rings of evaporating colloidal drops *Langmuir* **28** 4984–8
- [88] Kajiya T, Kobayashi W and Okuzono T 2009 Controlling the drying and film formation processes of polymer solution droplets with addition of small amount of surfactants *J. Phys. Chem. B* **113** 15460–6
- [89] Majumder M et al 2012 Overcoming the “coffee-stain” effect by compositional Marangoni-flow-assisted drop-drying *J. Phys. Chem. B* **116** 6536–42
- [90] Goto O, Tomiya S, Murakami Y, Shinozaki A, Toda A, Kasahara J and Hobara D 2012 Organic single-crystal arrays from solution-phase growth using micropattern with nucleation control region *Adv. Mater.* **24** 1117–22
- [91] Yunker P J, Still T, Lohr M A and Yodh A G 2011 Suppression of the coffee-ring effect by shape-dependent capillary interactions *Nature* **476** 308–11
- [92] Minemawari H, Yamada T, Matsui H, Tsutsumi J Y, Haas S, Chiba R, Kumai R and Hasegawa T 2011 Inkjet printing of single-crystal films *Nature* **475** 364–7
- [93] Layani M, Gruchko M, Milo O, Balberg I, Azulay D and Magdassi S 2009 Transparent conductive coatings by printing coffee ring arrays obtained at room temperature *ACS Nano* **3** 3537–42
- [94] Li J and Deng G 2004 Technology development and basic theory study of fluid dispensing—a review *Proc. Sixth IEEE CPMT Conf. High Density Microsyst. Des. Packag. Compon. Fail. Anal. HDP'04* pp 198–205 ([https://www3.uic.com/wcms/images2.nsf/\(GraphicLib\)/Practical_Issues_Concerning_Dispensng_End_Effectors.PDF/](https://www3.uic.com/wcms/images2.nsf/(GraphicLib)/Practical_Issues_Concerning_Dispensng_End_Effectors.PDF/))
- [95] Chen X B and Kai J 2000 Modeling of time-pressure fluid dispensing processes *IEEE Trans. Electron. Packag. Manuf.* **27** 157–63
- [96] Chen X B 2009 Modeling and control of fluid dispensing processes: a state-of-the-art review *Int. J. Adv. Manuf. Technol.* **43** 276–86
- [97] Dixon B D, Kazalski J, Murch F and Marongelli S 1997 Practical issues concerning dispensing end effectors *Circuits Assem.* (Binghamton, New York, USA 36–40) ([https://www3.uic.com/wcms/images2.nsf/\(GraphicLib\)/Practical_Issues_Concerning_Dispensng_End_Effectors.PDF/File/Practical_Issues_Concerning_Dispensng_End_Effectors.PDF](https://www3.uic.com/wcms/images2.nsf/(GraphicLib)/Practical_Issues_Concerning_Dispensng_End_Effectors.PDF/File/Practical_Issues_Concerning_Dispensng_End_Effectors.PDF))
- [98] Wang F, Mao P and He H 2016 Dispensing of high concentration Ag nano-particles ink for ultra-low resistivity paper-based writing electronics *Sci. Rep.* **6** 1–8
- [99] Chen X B and Kai J 2004 Modeling of positive-displacement fluid dispensing processes *IEEE Trans. Electron. Packag. Manuf.* **27** 157–63
- [100] Godlinski D, Zichner R, Zöllmer V and Baumann R R 2017 Printing technologies for the manufacturing of passive microwave components: antennas *IET Microwaves, Antennas Propag.* **11** 2010–5
- [101] Nordson EFD fluid dispensing system (available at: www.nordson.com/en/divisions/efd)
- [102] Poly Dispensing Systems Precifluid Easy (available at: <https://polydispensing.com>)
- [103] Fisher Scientific lab equipment for high viscous ink jetting (available at: www.fishersci.ca/)
- [104] Epak Electronics dispensing system for microdispensing nozzles (available at: www.epakelectronics.com/spt_dispensingmdn.htm)
- [105] Wang L, Du J, Luo Z, Du X, Li Y, Liu J and Sun D 2013 Design and experiment of a jetting dispenser driven by piezostack actuator *IEEE Trans. Components, Packag. Manuf. Technol.* **3** 147–56
- [106] Zhou C, Duan J A and Deng G 2015 Giant magnetostrictive material based jetting dispenser *Optik* **126** 5859–60
- [107] Zhu P, Xu Z, Wang X, Zheng Y, Xu X and Wang L 2018 Influence of initial distance between needle tip and substrate on contact dispensing of high-viscosity adhesive *Int. J. Adhes. Adhes.* **85** 23–28
- [108] Sun J, Ng J H, Fuh Y H, Wong Y S, Loh H T and Xu Q 2009 Comparison of micro-dispensing performance between micro-valve and piezoelectric printhead *Microsyst. Technol.* **15** 1437–48
- [109] Zhou C, Du P, Feng Z, Cui W and Deng G 2018 Influence of Bi-piezoelectric micro-valve's parameters on jet performance *Optik* **167** 129–35
- [110] Phung T H and Kwon K S 2019 How to manipulate droplet jetting from needle type jet dispensers *Sci. Rep.* **9** 1–12
- [111] Lu S, Yao Y, Liu Y and Zhao Y 2015 Design and experiment of a needle-type piezostack-driven jetting dispenser based on lumped parameter method *J. Adhes. Sci. Technol.* **29** 716–30
- [112] Zhou C, Li J H, Duan J A and Deng G L 2015 The principle and physical models of novel jetting dispenser with giant magnetostrictive and a magnifier *Sci. Rep.* **5** 1–13
- [113] Sohn J W and Choi S B 2018 Identification of operating parameters most strongly influencing the jetting performance in a piezoelectric actuator-driven dispenser *Appl. Sci.* **8** 243
- [114] Yang Y, Gu S, Lv Q, Liu J, Yang Z, Li C and Tian H 2019 Influence of needle impact velocity on the jetting effect of a piezoelectric needle-collision jetting dispenser *AIP Adv.* **9** 045302–8
- [115] Zapka W 2018 *Handbook of Industrial Inkjet Printing* (Germany: Wiley-VCH Verlag GmbH & Co. KGaA) (<http://doi.org/10.1002/9783527687169>)
- [116] Time pressure dispensing tutorial for adhesive dispensing Ltd. 2019 (available at: www.adhesivedispensing.net/kb_results.asp?ID=146)
- [117] Lewis A and Babiarz A 1999 Conductive adhesive dispensing process considerations *National Electronic Packaging and Production Conf.-Proc. of the Technical Program (West and East)* **1** pp 335–49
- [118] Creative Automation True Volume™ Piston Positive Displacement Pump Digital Dispensing System 2019 (<http://www.creativedispensing.com/SP-2/SP2.html>)
- [119] Tsai H L, Hwang W S, Wang J K, Peng W C and Chen S H 2015 Fabrication of microdots using piezoelectric dispensing technique for viscous fluids *Materials* **8** 7006–16
- [120] Ashley D and Adamson S J 2008 Advancements in solder paste dispensing *SMT Surf. Mt. Technol. Mag.* **22** 10–15
- [121] Quinones H 2013 Jetting fine lines for high viscosity fluids onto 2D and 3D electronic packages *Pan Pacific Symp.* pp 3–6
- [122] Nguyen Q H, Han Y M, Choi S B and Hong S M 2008 Design of a new mechanism for jetting dispenser featuring piezoactuator *Proc. Inst. Mech. Eng. C* **222** 711–22
- [123] Larson B J, Gillmor S D and Lagally M G 2004 Controlled deposition of picoliter amounts of fluid using an ultrasonically driven micropipette *Rev. Sci. Instrum.* **75** 832–6

- [124] Zang Z, Tang X, Liu X, Lei X and Chen W 2014 Fabrication of high quality and low cost microlenses on a glass substrate by direct printing technique *Appl. Opt.* **53** 7868
- [125] Gupta A A, Bolduc A, Cloutier S G and Izquierdo R 2016 Aerosol jet printing for printed electronics rapid prototyping 2016 *IEEE International Symposium on Circuits and Systems (ISCAS) 22-25 May 2016 Montreal, QC, Canada Proc.—IEEE Int. Symp. Circuits Syst.* (New York, USA: IEEE) 866–9 (<https://ieeexplore.ieee.org/document/7527378>)
- [126] Hoey J M, Lutfurakhmanov A, Schulz D L and Akhatov I S 2012 A review on aerosol-based direct-write and its applications for microelectronics *J. Nanotechnol.* **2012** 1–22
- [127] Phung T H, Oh S and Kwon K S 2018 High-resolution patterning using two modes of electrohydrodynamic jet: drop on demand and near-field electrospinning *J. Vis. Exp.* e57846 (<https://pubmed.ncbi.nlm.nih.gov/30059021/>)
- [128] Onses M S, Sutanto E, Ferreira P M, Alleyne A G and Rogers J A 2015 Mechanisms, capabilities, and applications of high-resolution electrohydrodynamic jet printing *Small* **11** 4237–66
- [129] Phung T H, Kim S and Kwon K S 2017 A high speed electrohydrodynamic (EHD) jet printing method for line printing *J. Micromech. Microeng.* **27** 8pp
- [130] Qin H, Dong J and Lee Y S 2017 AC-pulse modulated electrohydrodynamic jet printing and electroless copper deposition for conductive microscale patterning on flexible insulating substrates *Robot. Comput. Integr. Manuf.* **43** 179–87
- [131] Sonoplot Printed Electronics system (available at: www.sonoplot.com/printed-electronics)
- [132] Microplotter system based on Desktop Manual 53562 (available at: <https://static1.squarespace.com/static/MicroplotterDesktopManual.pdf>)
- [133] Cheun H, Rugheimer P P, Larson B J, Gopalan P, Lagally M G and Winokur M J 2006 Polymer light emitting diodes and poly(di-*n*-octylfluorene) thin films as fabricated with a microfluidics applicator *J. Appl. Phys.* **100** 1–7
- [134] Lee S J, Kim Y J, Yeo S Y, Lee E, Lim H S, Kim M, Song Y W, Cho J and Lim J A 2015 Centro-apical self-organization of organic semiconductors in a line-printed organic semiconductor: polymer blend for one-step printing fabrication of organic field-effect transistors *Sci. Rep.* **5** 1–13
- [135] King B and Renn M 2008 Aerosol jet direct write printing for mil-aero electronic applications (Albuquerque, NM 87109, USA: Optomec) (https://www.optomec.com/wp-content/uploads/2014/04/Optomec_Aerosol_Jet_Direct_Write_Printing_for_Mil_Aero_Electronic_Apps.pdf)
- [136] Deiner L J and Reitz T L 2017 Inkjet and aerosol jet printing of electrochemical devices for energy conversion and storage *Adv. Eng. Mater.* **19** 1–18
- [137] Secor E B 2019 Principles of aerosol jet printing *Flex. Print. Electron. Accept.* **3** 035002
- [138] Optomec 2012 Additive manufacturing videos Optomec Aerosol Jet Technology. *Adding Electronics Functionality to RP/RM* (Berlin) (available at: <https://optomec.com/resources/3d-printing-application-videos/>)
- [139] Mahajan A, Frisbie C D and Francis L F 2013 Optimization of aerosol jet printing for high-resolution, high-aspect ratio silver lines *ACS Appl. Mater. Interfaces* **5** 4856–64
- [140] Secor E B 2018 Guided ink and process design for aerosol jet printing based on annular drying effects *Flex. Print. Electron.* **3** 035007
- [141] Smith M, Choi Y S, Boughey C and Kar-Narayan S 2017 Controlling and assessing the quality of aerosol jet printed features for large area and flexible electronics *Flex. Print. Electron.* **2** 015004
- [142] Cai F, Pavlidis S, Papapolymerou J, Chang Y H, Wang K, Zhang C and Wang B 2014 Aerosol jet printing for 3-D multilayer passive microwave circuitry *Proc. 44th European Microwave Conf.* (Italy: European Microwave Association) pp 512–5
- [143] Khorramdel B, Torkkeli A and Mäntysalo M 2018 Electrical contacts in SOI MEMS using aerosol jet printing *IEEE J. Electron Devices Soc.* **6** 34–40
- [144] Ou C, Sangle A L, Chalklen T, Jing Q, Narayan V and Kar-Narayan S 2018 Enhanced thermoelectric properties of flexible aerosol-jet printed carbon nanotube-based nanocomposites *APL Mater.* **6** 096101
- [145] Seifert T, Sowade E, Roscher F, Wiemer M, Gessner T and Baumann R R 2015 Additive manufacturing technologies compared: morphology of deposits of silver ink using inkjet and aerosol jet printing *Ind. Eng. Chem. Res.* **54** 769–79
- [146] Reiser A et al 2019 Metals by micro-scale additive manufacturing: comparison of microstructure and mechanical properties *Adv. Funct. Mater.* **1910491** 1–20
- [147] Gao D and Zhou J 2018 Designs and applications of electrohydrodynamic 3D printing *Int. J. Bioprinting* **5** 1–11
- [148] Kien Nguyen T, Nguyen V D, Seong B, Hoang N, Park J and Byun D 2014 Control and improvement of jet stability by monitoring liquid meniscus in electrospray and electrohydrodynamic jet *J. Aerosol Sci.* **71** 29–39
- [149] Pan Y and Zeng L 2019 Simulation and validation of droplet generation process for revealing three design constraints in electrohydrodynamic jet printing *Micromachines* **10** 94
- [150] Drahansky M, Paridah M, Moradbak A, Mohamed A, Owolabi F A T, Asniza M and Abdul K S H 2016 Recent trends in electrospinning of polymer nanofibers and their applications as templates for metal oxide nanofibers preparation *Electrospinning - Material, Techniques, and Biomedical Applications* (London, UK: IntechOpen) (<https://www.intechopen.com/books/electrospinning-material-techniques-and-biomedical-applications/recent-trends-in-electrospinning-of-polymer-nanofibers-and-their-applications-as-templates-for-metal>) (<https://doi.org/10.5772/65900>)
- [151] Kim B, Kim I, S W J and Lim G 2009 Electrohydrodynamic repulsion of droplets falling on an insulating substrate in an electric field *Appl. Phys. Lett.* **95** 204106
- [152] Park J and Hwang J 2014 Fabrication of a flexible Ag-grid transparent electrode using ac based electrohydrodynamic Jet printing *J. Phys. D: Appl. Phys.* **47** 405102
- [153] Wei C, Qin H, Ramirez-Iglesias N A, Chiu C P, Lee Y S and Dong J 2014 High-resolution ac-pulse modulated electrohydrodynamic jet printing on highly insulating substrates *J. Micromech. Microeng.* **24** 045010
- [154] Khan A, Rahman K, Kim D S and Choi K H 2012 Direct printing of copper conductive micro-tracks by multi-nozzle electrohydrodynamic inkjet printing process *J. Mater. Process. Technol.* **212** 700–6
- [155] Lee S, Kim Y, Sin J, Son S, An K, Choi J, Lee W H, Wijesundara M and Stephanou H E 2011 Array-nozzle EHD print head and its drop-on-demand experimentation School of Information and Communication Engineering, Sungkyunkwan University, Korea, Automation & Robotics Research Institute, The University of Texas at Arlington, USA *Design* **2** 516–9
- [156] Theron S A, Yarin A L, Zussman E and Kroll E 2005 Multiple jets in electrospinning: experiment and modeling *Polymer* **46** 2889–99
- [157] Khan A, Rahman K, Hyun M T, Kim D S and Choi K H 2011 Multi-nozzle electrohydrodynamic inkjet printing of silver colloidal solution for the fabrication of electrically functional microstructures *Appl. Phys. A* **104** 1113–20
- [158] Clippingdale A and Uk T L 2011 Meeting the challenges of digitally printing cans *NIP 27 and Digital Fabrication 2011* (Cambridge: Society for Imaging Science and Technology) pp 540–3
- [159] Mace D 2012 Digital printing of packaging—the Tonejet solution *NIP28 and Digital Fabrication* pp 404–7
- [160] Teape J, Taylor P, Crees O, Nicholls S and Emerton N 2002 ToneJet: a new standard in digital printing *NIP Digit. Fabr. Conf. 2002 Int. Conf. Digit. Print. Technol.* pp 145–147(3)

- [161] Digital Printing System of Tonejet Printing 2019 (available at: www.tonejet.com/)
- [162] Kim H S and Kwon K 2015 Using CAD-converted bitmap images for inkjet printing *Korean Soc. Precis. Eng.* **32** 833–40
- [163] Kwon K-S, Go J-K and Kim J-W 2010 Development of inkjet printing system for printed electronics *Trans. Korean Soc. Mech. Eng.* **A34** 1537–42
- [164] Phung T H, Nguyen L and Kwon K-S 2018 A vector printing method for high-speed electrohydrodynamic (EHD) jet printing based on encoder position sensors *Appl. Sci.* **8** 351
- [165] Chang C, Lin C and Cheng K 2006 Dynamic management for multiple rotation printheads with interlace printing : part II : patterning algorithm *22nd Int. Conf. on digital Printing Technologies Final Program (Society for Imaging Science and Technology)* pp 122–6
- [166] Panreck B and Hild M 2018 Fully printed strain gauges: a comparison of aerosoljet-printing and micropipette-dispensing *Int. Sch. Sci. Res. Innov.* **12** 678–84
- [167] Souk J H and Kim B J 2008 Inkjet Technology for large size color filter plates *SID Symp. Dig. Tech. Pap.* **39** 429
- [168] Chen C T, Wu K H, Lu C F and Shieh F 2010 An inkjet printed stripe-type color filter of liquid crystal display *J. Micromech. Microeng.* **20** 055004
- [169] Shin D Y and Smith P J 2008 Theoretical investigation of the influence of nozzle diameter variation on the fabrication of thin film transistor liquid crystal display color filters *J. Appl. Phys.* **103** 1–11
- [170] Moon K S, Choi J H, Choi D J, Kim S H, Ha M H, Nam H J and Kim M S 2008 A new method for analyzing the refill process and fabrication of a piezoelectric inkjet printing head for LCD color filter manufacturing *J. Micromech. Microeng.* **18** 125011
- [171] Tsai C L, Yen H J and Liou G S 2016 Highly transparent polyimide hybrids for optoelectronic applications *React. Funct. Polym.* **108** 2–30
- [172] Jung D-K Y J-M 2005 Characterization of polyimimide: application of hydrolysis and reactive-pyrolysis for composition analysis *Polym. Sci. Technol.* **16** 93–100
- [173] Aziz H and Popovic Z D 2004 Degradation phenomena in small-molecule organic light-emitting devices *Chem. Mater.* **16** 4522–32
- [174] Liew Y F, Aziz H, Hu N X, Chan H S O, Xu G and Popovic Z 2000 Investigation of the sites of dark spots in organic light-emitting devices *Appl. Phys. Lett.* **77** 2650–2
- [175] Park J S, Chae H, Chung H K and Lee S I 2011 Thin film encapsulation for flexible AM-OLED: a review *Semicond. Sci. Technol.* **26** 034001
- [176] Li C Y, Wei B, Hua Z K, Zhang H, Li X F and Zhang J H 2008 Thin film encapsulation of OLED displays with organic-inorganic composite film *Proc.—Electron. Components Technol. Conf.* pp 1819–24
- [177] Ewald KMG and Auch MDJ 2007 Encapsulation for OLED devices 1 US 7,255,823 B1 USA US 7,255,823 B1 (<https://patents.google.com/patent/US7255823B1/en>)
- [178] Park J, Seth J, Cho S and Sung M M 2020 Hybrid multilayered films comprising organic monolayers and inorganic nanolayers for excellent flexible encapsulation films *Appl. Surf. Sci.* **502** 144109
- [179] Souk J, Morozumi S and Luo I B F-C 2018 *Flat Panel Display Manufacturing* (New York: Wiley)
- [180] Choi D-S, Park J-W and Kim T-S 2013 Organic light emitting display with frit seal 2 US 7,545,094 B2 USA (<https://patents.google.com/patent/US7545094>)
- [181] Majeed M 2011 Multilayer film for encapsulating oxygen and/or moisture sensitive electronic devices 1 2010–2 CN102057750B China (<https://patents.google.com/patent/CN102057750B/en>)
- [182] Visser R 2006 *Barix Multilayers: A Water and Oxygen Barrier for Flexible Organic Electronics* (MIT-Stanford-UC Berkeley Nano Forum: Vitex Systems Inc.) (http://www.mitstanfordberkeleynano.org/events_past/0504%20-%20Organic%20Electronics/5%20-%20Nanoforum050422a.pdf)
- [183] Lee T W, Chung Y, Kwon O and Park J J 2007 Self-organized gradient hole injection to improve the performance of polymer electroluminescent devices *Adv. Funct. Mater.* **17** 390–6
- [184] Choulis S A, Choong V E, Mathai M K and So F 2005 The effect of interfacial layer on the performance of organic light-emitting diodes *Appl. Phys. Lett.* **87** 1–4
- [185] Lim Y, Park Y S, Kang Y, Jang D Y, Kim J H, Kim J J, Sellinger A and Yoon D Y 2011 Hole injection/transport materials derived from heck and sol-gel chemistry for application in solution-processed organic electronic devices *J. Am. Chem. Soc.* **133** 1375–82
- [186] Yang Z, Mao Z, Xie Z, Zhang Y, Liu S, Zhao J, Xu J, Chi Z and Aldred M P 2017 Recent advances in organic thermally activated delayed fluorescence materials *Chem. Soc. Rev.* **46** 915–1016
- [187] Yook K S and Lee J Y 2014 Small molecule host materials for solution processed phosphorescent organic light-emitting diodes *Adv. Mater.* **562** 608–11
- [188] Giridhar T, Cho W, Park J, Park J S, Gal Y S, Kang S, Lee J Y and Jin S H 2013 Facile synthesis and characterization of iridium (III) complexes containing an N-ethylcarbazole-thiazole main ligand using a tandem reaction for solution processed phosphorescent organic light-emitting diodes *J. Mater. Chem. C* **1** 2368–78
- [189] Shirasaki Y, Supran G J, Bawendi M G and Bulović V 2013 Emergence of colloidal quantum-dot light-emitting technologies *Nat. Photon.* **7** 13–23
- [190] Kim T H et al 2011 Full-colour quantum dot displays fabricated by transfer printing *Nat. Photon.* **5** 176–82
- [191] Choi M K, Yang J, Hyeon T and Kim D-H 2018 Flexible quantum dot light-emitting diodes for next-generation displays *Npj Flex. Electron.* **2** 1–14
- [192] Zlateva G, Zhelev Z, Bakalova R and Kanno I 2007 Precise size control and synchronized synthesis of six colors of CdSe quantum dots in a slow-increasing temperature gradient *Inorg. Chem.* **46** 6212–4
- [193] Capek R K, Yanover D and Lifshitz E 2015 Size control by rate control in colloidal PbSe quantum dot synthesis *Nanoscale* **7** 5299–310
- [194] Vasudevan D, Gaddam R R, Trinchi A and Cole I 2015 Core-shell quantum dots: properties and applications *J. Alloys Compd.* **636** 395–404
- [195] Khim D, Lee W H, Baeg K J, Kim D Y, Kang I N and Noh Y Y 2012 Highly stable printed polymer field-effect transistors and inverters via polyselenophene conjugated polymers *J. Mater. Chem.* **22** 12774–83
- [196] Ko S H, Pan H, Grigoropoulos C P, Luscombe C K, Fréchet J M J and Poulidakos D 2007 All-inkjet-printed flexible electronics fabrication on a polymer substrate by low-temperature high-resolution selective laser sintering of metal nanoparticles *Nanotechnology* **18**
- [197] Ko S H, Pan H, Grigoropoulos C P, Fréchet J M J, Luscombe C K and Poulidakos D 2008 Lithography-free high-resolution organic transistor arrays on polymer substrate by low energy selective laser ablation of inkjet-printed nanoparticle film *Appl. Phys. A* **92** 579–87
- [198] Kwon J, Hong S, Lee H, Yeo J, Lee S S and Ko S H 2013 Direct selective growth of ZnO nanowire arrays from inkjet-printed zinc acetate precursor on a heated substrate *Nanoscale Res. Lett.* **8** 1–6
- [199] Shin J et al 2020 Sensitive wearable temperature sensor with seamless monolithic integration *Adv. Mater.* **32** 1–9
- [200] Fuller S B, Wilhelm E J and Jacobson J M 2002 Ink-jet printed nanoparticle microelectromechanical systems *J. Microelectromech. Syst.* **11** 54–60
- [201] Ko S H, Chung J, Hotz N, Nam K H and Grigoropoulos C P 2010 Metal nanoparticle direct inkjet printing for

- low-temperature 3D micro metal structure fabrication *J. Micromech. Microeng.* **20**
- [202] Kullmann C, Schirmer N C, Lee M T, Ko S H, Hotz N, Grigoropoulos C P and Poulidakos D 2012 3D micro-structures by piezoelectric inkjet printing of gold nanofluids *J. Micromech. Microeng.* **22**
- [203] Yang C, Wong C P and Yuen M M F 2013 Printed electrically conductive composites: conductive filler designs and surface engineering *J. Mater. Chem. C* **1** 4052–69
- [204] Kamyshny A and Magdassi S 2014 Conductive nanomaterials for printed electronics *Small* **10** 3515–35
- [205] Han J T et al 2013 Dispersant-free conducting pastes for flexible and printed nanocarbon electrodes *Nat. Commun.* **4**
- [206] Secor E B, Ahn B Y, Gao T Z, Lewis J A and Hersam M C 2015 Rapid and versatile photonic annealing of graphene inks for flexible printed electronics *Adv. Mater.* **27** 6683–8
- [207] Lee P, Lee J, Lee H, Yeo J, Hong S, Nam K H, Lee D, Lee S S and Ko S H 2012 Highly stretchable and highly conductive metal electrode by very long metal nanowire percolation network *Adv. Mater.* **24** 3326–32
- [208] Ravi Kumar D V, Woo K and Moon J 2015 Promising wet chemical strategies to synthesize Cu nanowires for emerging electronic applications *Nanoscale* **7** 17195–210
- [209] Kim D, Jeong S and Moon J 2006 Synthesis of silver nanoparticles using the polyol process and the influence of precursor injection *Nanotechnology* **17** 4019–24
- [210] Kim D and Moon J 2005 Highly conductive ink jet printed films of nanosilver particles for printable electronics *Electrochem. Solid-State Lett.* **8** 45–48
- [211] Park B K, Kim D, Jeong S, Moon J and Kim J S 2007 Direct writing of copper conductive patterns by ink-jet printing *Thin Solid Films* **515** 7706–11
- [212] Jeong S, Song H C, Lee W W, Lee S S, Choi Y, Son W, Kim E D, Paik C H, Oh S H and Ryu B H 2011 Stable aqueous based Cu nanoparticle ink for printing well-defined highly conductive features on a plastic substrate *Langmuir* **27** 3144–9
- [213] Jeong S, Woo K, Kim D, Lim S, Kim J S, Shin H, Xia Y and Moon J 2008 Controlling the thickness of the surface oxide layer on Cu nanoparticles for the fabrication of conductive structures by ink-jet printing *Adv. Funct. Mater.* **18** 679–86
- [214] Nam V B, Shin J, Yoon Y, Giang T T, Kwon J, Suh Y D, Yeo J, Hong S, Ko S H and Lee D 2019 Highly stable Ni-based flexible transparent conducting panels fabricated by laser digital patterning *Adv. Funct. Mater.* **29** 1–10
- [215] Woo K, Kim Y, Lee B, Kim J and Moon J 2011 Effect of carboxylic acid on sintering of inkjet-printed copper nanoparticulate films *ACS Appl. Mater. Interfaces* **3** 2377–82
- [216] Grouchko M, Kamyshny A and Magdassi S 2009 Formation of air-stable copper-silver core-shell nanoparticles for inkjet printing *J. Mater. Chem.* **19** 3057–62
- [217] Jeong S et al 2013 Air-stable, surface-oxide free Cu nanoparticles for highly conductive Cu ink and their application to printed graphene transistors *J. Mater. Chem. C* **1** 2704–10
- [218] Grouchko M, Kamyshny A, Mihailescu C F, Anghel D F and Magdassi S 2011 Conductive inks with a “built-in” mechanism that enables sintering at room temperature *ACS Nano* **5** 3354–9
- [219] Layani M, Grouchko M, Shemesh S and Magdassi S 2012 Conductive patterns on plastic substrates by sequential inkjet printing of silver nanoparticles and electrolyte sintering solutions *J. Mater. Chem.* **22** 14349–52
- [220] Perelaer J, Klokkenburg M, Hendriks C E and Schubert U S 2009 Microwave flash sintering of inkjet-printed silver tracks on polymer substrates *Adv. Mater.* **21** 4830–4
- [221] Reinhold I, Hendriks C E, Eckardt R, Kranenburg J M, Perelaer J, Baumann R R and Schubert U S 2009 Argon plasma sintering of inkjet printed silver tracks on polymer substrates *J. Mater. Chem.* **19** 3384–8
- [222] Wunscher S, Stumpf S, Perelaer J and Schubert U S 2014 Towards single-pass plasma sintering: temperature influence of atmospheric pressure plasma sintering of silver nanoparticle ink *J. Mater. Chem. C* **2** 1642–9
- [223] Perelaer J, Jani R, Grouchko M, Kamyshny A, Magdassi S and Schubert U S 2012 Plasma and microwave flash sintering of a tailored silver nanoparticle ink, yielding 60% bulk conductivity on cost-effective polymer foils *Adv. Mater.* **24** 3993–8
- [224] Park J H et al 2017 Plasmonic-tuned flash Cu nanowelding with ultrafast photochemical-reducing and interlocking on flexible plastics *Adv. Funct. Mater.* **27** 1–11
- [225] Jung J et al 2019 Moiré-free imperceptible and flexible random metal grid electrodes with large figure-of-merit by photonic sintering control of copper nanoparticles *ACS Appl. Mater. Interfaces* **11** 15773–80
- [226] Park J H, Jeong S, Lee E J, Lee S S, Seok J Y, Yang M, Choi Y and Kang B 2016 Transversally extended laser plasmonic welding for oxidation-free copper fabrication toward high-fidelity optoelectronics *Chem. Mater.* **28** 4151–9
- [227] Kang B, Han S, Kim J, Ko S and Yang M 2011 One-step fabrication of copper electrode by laser-induced direct local reduction and agglomeration of copper oxide nanoparticle *J. Phys. Chem. C* **115** 23664–70
- [228] Galagan Y, Coenen E W C, Abbel R, Van Lammeren T J, Sabik S, Barink M, Meinders E R, Andriessen R and Blom P W M 2013 Photonic sintering of inkjet printed current collecting grids for organic solar cell applications *Org. Electron.* **14** 38–46
- [229] Chung W H, Hwang H J, Lee S H and Kim H S 2013 In situ monitoring of a flash light sintering process using silver nano-ink for producing flexible electronics *Nanotechnology* **24**
- [230] Han W S, Hong J M, Kim H S and Song Y W 2011 Multi-pulsed white light sintering of printed Cu nanoinks *Nanotechnology* **22**
- [231] Oh S J et al 2015 Ambient atmosphere-processable, printable Cu electrodes for flexible device applications: structural welding on a millisecond timescale of surface oxide-free Cu nanoparticles *Nanoscale* **7** 3997–4004
- [232] Park H J, Jo Y, Lee S S, Lee S Y, Choi Y and Jeong S 2019 Printable thick copper conductors from optically modulated multidimensional particle mixtures *ACS Appl. Mater. Interfaces* **11** 20134–42
- [233] Kim T G, Park H J, Woo K, Jeong S, Choi Y and Lee S Y 2018 Enhanced oxidation-resistant Cu@Ni core-shell nanoparticles for printed flexible electrodes *ACS Appl. Mater. Interfaces* **10** 1059–66
- [234] Park H J, Jo Y, Cho M K, Young Woo J, Kim D, Lee S Y, Choi Y and Jeong S 2018 Highly durable Cu-based electrodes from a printable nanoparticle mixture ink: flash-light-sintered, kinetically-controlled microstructure *Nanoscale* **10** 5047–53
- [235] Park H J, Cho M K, Jeong Y W, Kim D, Lee S Y, Choi Y and Jeong S 2017 Ultrathin plasmonic optical/thermal barrier: flashlight-sintered copper electrodes compatible with polyethylene terephthalate plastic substrates *ACS Appl. Mater. Interfaces* **9** 43814–21
- [236] Oh S J, Kim T G, Kim S Y, Jo Y, Lee S S, Kim K, Ryu B H, Park J U, Choi Y and Jeong S 2016 Newly designed Cu/Cu₁₀Sn₃ core/shell nanoparticles for liquid phase-photonic sintered copper electrodes: large-area, low-cost transparent flexible electronics *Chem. Mater.* **28** 4714–23
- [237] Han S et al 2014 Fast plasmonic laser nanowelding for a Cu-nanowire percolation network for flexible transparent conductors and stretchable electronics *Adv. Mater.* **26** 5808–14
- [238] Hong S, Lee H, Lee J, Kwon J, Han S, Suh Y D, Cho H, Shin J, Yeo J and Ko S H 2015 Highly stretchable and transparent metal nanowire heater for wearable electronics applications *Adv. Mater.* **27** 4744–51

- [239] Park M, Park J and Jeong U 2014 Design of conductive composite elastomers for stretchable electronics *Nano Today* **9** 244–60
- [240] Ma R, Kang B, Cho S, Choi M and Baik S 2015 Extraordinarily high conductivity of stretchable fibers of polyurethane and silver nanoflowers *ACS Nano* **9** 10876–86
- [241] Kang J H, Kim J Y, Jo Y, Kim H S, Jung S M, Lee S Y, Choi Y and Jeong S 2019 Three-dimensionally printed pressure sensor arrays from hysteresis-less stretchable piezoresistive composites *RSC Adv.* **9** 39993–40002
- [242] Lee H S, Jo Y, Joo J H, Woo K, Zhong Z, Jung S, Lee S Y, Choi Y and Jeong S 2019 Three-dimensionally printed stretchable conductors from surfactant-mediated composite pastes *ACS Appl. Mater. Interfaces* **11** 12622–31
- [243] Jo Y, Jeong D W, Lee J O, Choi Y and Jeong S 2018 3D-printed origami electronics using percolative conductors *RSC Adv.* **8** 22755–62
- [244] Jo Y, Kim J Y, Jung S, Ahn B Y, Lewis J A, Choi Y and Jeong S 2017 3D polymer objects with electronic components interconnected: via conformally printed electrodes *Nanoscale* **9** 14798–803
- [245] Kim J Y, Ji S, Jung S, Ryu B H, Kim H S, Lee S S, Choi Y and Jeong S 2017 3D printable composite dough for stretchable, ultrasensitive and body-patchable strain sensors *Nanoscale* **9** 11035–46
- [246] Jo Y *et al* 2017 3D-printable, highly conductive hybrid composites employing chemically-reinforced, complex dimensional fillers and thermoplastic triblock copolymers *Nanoscale* **9** 5072–84
- [247] Chae C, Seo Y H, Jo Y, Kim K W, Song W, An K S, Choi S, Choi Y, Lee S S and Jeong S 2015 3D-stacked carbon composites employing networked electrical intra-pathways for direct-printable, extremely stretchable conductors *ACS Appl. Mater. Interfaces* **7** 4109–17
- [248] Chun K Y, Oh Y, Rho J, Ahn J H, Kim Y J, Choi H R and Baik S 2010 Highly conductive, printable and stretchable composite films of carbon nanotubes and silver *Nat. Nanotechnol.* **5** 853–7